5G MM-WAVE BAND BASE STATION ANTENNA DESIGN

by
Hilmi Öztürk

Submitted to Graduate School of Natural and Applied Sciences
in Partial Fulfillment of the Requirements
for the Degree of Doctor of Philosophy in
Electrical and Electronics Engineering

Yeditepe University
2022

5G MM-WAVE BAND BASE STATION ANTENNA DESIGN

APPROVED BY:

Prof. Dr. Korkut Yeğin ....
(Thesis Supervisor)
(Ege University)

Prof. Dr. Duygun Erol Barkana ....
(Yeditepe University)

Prof. Dr. Serkan Topaloğlu ....
(Yeditepe University)

Prof. Dr. Serkan Aksoy ....
(Gebze Technical University)

Prof. Dr. Mansur İsgenderoğlu ....
(Gebze Technical University)

DATE OF APPROVAL: ..../..../20..

I hereby declare that this thesis is my own work and that all information in this thesis has been obtained and presented in accordance with academic rules and ethical conduct. I have fully cited and referenced all material and results as required by these rules and conduct, and this thesis study does not contain any plagiarism. If any material used in the thesis requires copyright, the necessary permissions have been obtained. No material from this thesis has been used for the award of another degree.

I accept all kinds of legal liability that may arise in case contrary to these situations.

Name, Last name ....

Signature ....

ACKNOWLEDGEMENTS

I acknowledge my Professor Prof. Dr. Korkut Yeğin's support and assistance with great gratitude.

I would like to thank my friend Dr. Yavuz Aşcı, who gave significant support and assistance in the completion of my thesis and my friend Dağhan Doğan who shared his knowledge and experience in mechanical design with me, my friend Hüseyin Yiğit, who helped with the measurements, and Servet Ayok, who provided material and moral support at every stage of the thesis.

Finally, I would like to thank to my wife and son , Dr. Hülya Öztürk, and Efe Öztürk, for their unlimited support, which has made everything even more wonderful.

ABSTRACT

5G MM-WAVE BAND BASE STATION ANTENNA DESIGN

5G mobile communication is an indispensable technology due to immense usage scenarios it provides. Unlike other generations, the 5G communication network utilizes a wide variety of operating frequencies. In 5G base stations, there is a requirement for an ultra-wide band antenna that covers all of the operating frequency bands n257, n258, n261 (24.25-29.5 GHz). In this study, 45° linear slant polarized antenna design is aimed. Antenna is radiating from the slots with a cavity structure behind. The unit antenna gain is over 14 dBi with gain variation ±0.5 dB throughout the band. Impedance match $|S_{11}|$ is less than -15 dB.

Firstly, +45° linear slant polarized 2×2 aperture, cavity-back, air-gap waveguide fed unit antenna was designed. In order to improve the antenna's gain, groove and stub have been applied to the surface of the antenna. Instead of using a rectangular feed aperture, which is the traditional method in the transition from the waveguide to the cavity, ian hourglass sturcture is used to improve imedance match. Waveguide dimensions at the feed part of the antenna are designed to be the same as the WR34 standard waveguide. The WR34 adapter is externally attached to the antenna. In the second and third antennas, two unit antennas are combined and the polarization windows are adjusted to be 2×4 apertures with linear slant polarization of +45° and -45°. The power divider structure has been designed and optimized for a perfectly compatible transition so that the unit antennas can be fed in equal amplitude and in-phase. Antennas are produced in parts from Aluminum material in CNC.

To be placed on the base station, the second and third antennas were combined on a single structure and the fourth antenna structure with ±45° slant polarization was designed.
All antennas have $|S_{11}| < -15$ dB value, ±0.5 dB gain variation, ±2.5° half power beam width deviation value in 5G mmWave operating region. As a result, the antenna structures developed are appropriate for usage in 5G base stations.

ÖZET

5G MM-DALGA BANDI BAZ İSTASYONU TASARIMI

5G mobil iletişim, sunduğu geniş kullanım senaryoları nedeniyle vazgeçilmez bir teknolojidir. Diğer nesillerin aksine, 5G iletişim ağı çok çeşitli çalışma frekanslarını kullanır. 5G baz istasyonlarında, n257, n258, n261 (24.25-29.5 GHz) tüm çalışma frekans bantlarını kapsayan ultra geniş bantlı bir anten gereksinimi vardır. Bu çalışmada, 45° lineer eğik polarize anten tasarımı amaçlanmıştır. Anten, arkasında kative yapısı bulunan açıklıklardan ışıma yapmaktadır. Birim anten kazancı, bant boyunca ±0.5 dB kazanç değişimi ile 14 dBi'nin üzerindedir. Empedans uyumu $|S_{11}|$ -15 dB'den azdır.

İlk olarak +45° lineer eğik polarize 2×2 açıklıklı arkası kaviteli, hava boşluklu dalga kılavuzu beslemeli birim anten tasarlanmıştır. Antenlerin kazancını arttırmak için antenin yüzeyine oluk ve kütük yapıları uygulanmıştır. Dalga kılavuzundan kaviteye geçişte geleneksel yöntem olan dikdörtgen besleme açıklığı yerine, emedans uyumunu iyileştirmek için kum saati yapısı kullanılmıştır. Antenin besleme kısmındaki dalga kılavuzu boyutları, WR34 standart dalga kılavuzu ile aynı olacak şekilde tasarlanmıştır. WR34 adaptör antene harici olarak takılmıştır. İkinci ve üçüncü antenlerde, iki birim anten birleştirilmiş ve polarizasyon pencereleri +45° ve -45° lineer eğik polarizasyon ile 2×4 açıklık olacak şekilde ayarlanmıştır. Güç bölücü yapısı, ünite antenlerinin eşit genlikte ve aynı fazda beslenebilmesi için mükemmel uyumlu bir geçiş için tasarlanmış ve optimize edilmiştir. Antenler CNC de Alüminyum malzemeden parçalar halinde üretilmektedir. Baz istasyonu üzerine yerleştirilmek üzere ikinci ve üçüncü antenler tek bir yapı üzerinde birleştirilmiş ve ±45° eğik polarizasyonlu dördüncü anten yapısı tasarlanmıştır.

Tüm antenler 5G mmDalga çalışma bölgesinde, $|S_{11}| < -15\,\text{dB}$ değerine, ±0.5 dB kazanç değişimine, ±2.5° yarım güç ışıma genişliğinde sapma değerine sahiptir. Sonuç olarak, geliştirilen anten yapıları 5G baz istasyonlarında kullanılmaya uygundur.

TABLE OF CONTENTS

LIST OF FIGURES

LIST OF TABLES

LIST OF SYMBOLS/ABBREVIATIONS

1G	First generatoion
2G	Second generation
3G	Third generation
4G	Forth genertion
5G	Fifth generation
BBU	Base station units
BFN	Beam forming network
β	Phase constant
CDMA	Code division multiple access
CNC	Computer numerical control
CST	Computer simulation technology
CTS	Continuous transverse stub
D	Directivity
dB	Decibel
E	Electric field
e	Efficiency
ε	Dielectric permittivity
EDM	Electrical discharge machine
ETSI	European Telecommunications Standards Institute
FBW	Fractional beam width
FCC	Federal Communications Commission
G	Gain
GB	Giga byte
GHz	Giga Hertz
GSM	Global system for mobile communications
H	Magnetic field
HPBW	Half power beam width
KBPS	Kilo byte per second
λ	Wavelength
ITU	International Telecommunication Unions

NR	New radio
MIMO	Multiple input multiple output
MBPS	Mega byte per second
MM	Millimeter
μ	Magnetic permeability
ω	Angular frequency
P	Power density
R	Radius
RGW	Ridge gap waveguide
RRU	Remote radio units
SIW	Substrate integrated waveguide
SLL	Side lobe level
Ω_A	Solid angle
TE	Transverse electric
TM	Transverse magnetic
TUBITAK	Scientific and Technological Research Council of Turkey
U	Radiation intensity
UE	Unit element
UHD	Ultra high definition
VSWR	Voltage standingwave ratio

1. INTRODUCTION

The first generation mobile communication network (1G) has been replaced every ten years since its inception in the 1980s. The evolution of network of mobile phones generation is depicted in Figure 1.1 below. Users of the 1st generation (1G) could only make voice calls through analog signals, with a maximum speed of 2.4 Kbps. Analog signals were replaced by digital signals in the 2nd generation (2G). This generation's primary goal is to create a secure and dependable communication connection. In this generation, CDMA and GSM principles have been incorporated. Small data service such as sms and mms started to be provided. Voice data has been transmitted using digital signals in 2G cellular communication, and the channel speed has increased to 64 kbps. For duplex communication, GSM uses two bands of frequencies: 890-915 MHz and 935-960 MHz. These band gaps were filled using 124 channels[1]. With the transition to the third generation, requirements for broadband communication, IP-based services, high-speed data transfer, and multimedia communication were developed. In 3rd generation (3G) systems, data transfer rates range from 125 Kbps to 5 Mbps. Data transfer rates have grown tenfold since the switch to the fourth generation. Effective spectrum usage, large network capacity, smooth transition to multiple generation networks, high-density multimedia support, and an entirely packet-based (IP) architecture are all available with 4th generation (4G) technology.

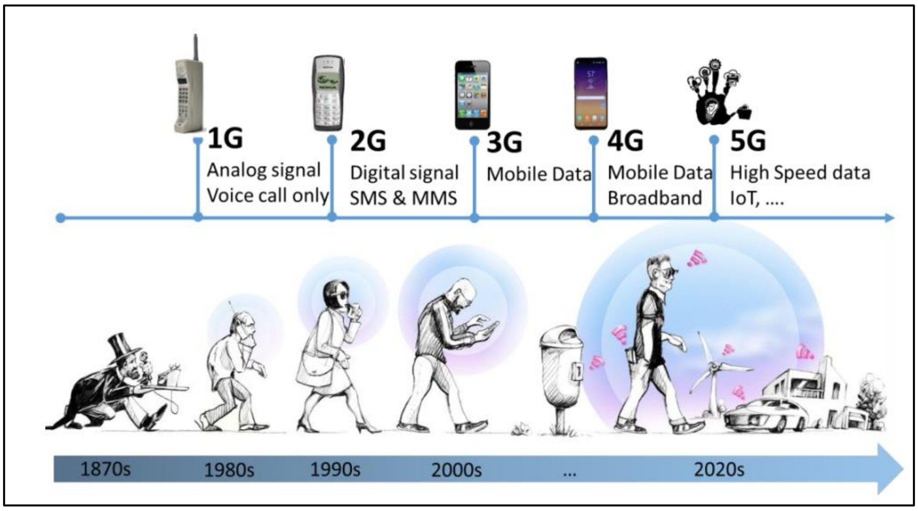

Figure 1.1. Evolution of mobile network generations [2]

One of the game changing technology is 5th Generation (5G) New Radio(NR) in mobile communication industry. 5G provides great conectivity between people and machine, between machine and machine. It brings low latency in order to be used at smart healthcare, connected vehicle, smart grid, factory automation, home broadband, UHD video, and smart city applications. In order to give better service quality, 5G networks require ten to hundred times faster data speeds and thousand times larger capacity. High data rates are expected, with no latency and reliable connectivity regardless of location.

However antennas are the key elements for 5G network. Considering 5G network properties and to support all bands, antennas must adopt application scenarios. 3G and 4G antennas have fixed patterns and directivity, however 5G antennas have beamforming ability in order to use time and frequency sources efficiently. High precision beamforming is critical for 5G antennas, because accurate coverage of network depends on it. Main beam should be focused on desired areas and radiation should be minimized in nondesired coverage areas. It is necessary for increasing spectral and spatial efficiency. Antenna should have low loss property, to increase coverage depth with the same radiated power. Possible 5G network structure is given in Figure 1.2 below.

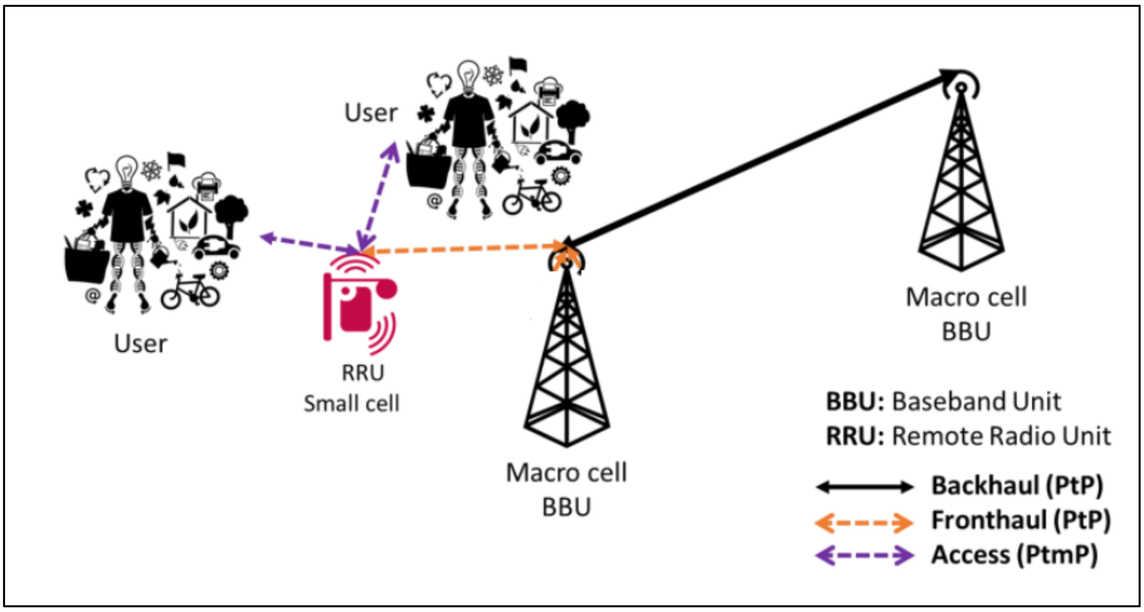

Figure 1.2. Possible 5G network connections [3]

Despite the International Telecommunication Unions' (ITU) World Radiocommunication Conference in 2015 defining frequency bands below 6 GHz for 5G, it was unclear until mid-2018 which millimeter frequency bands would be allocated for 5G backhaul links in order to meet 5G expectations where large bandwidths are required. Aside from the massive bandwidths, another advantage of mm-wave frequency bands is that some of them are unlicensed or minimally licensed, saving operators cost. Furthermore, mm-wave frequency bands have a higher rate of air attenuation than sub-millimeter wave frequency bands. Although this may appear to be a disadvantage, high attenuation allows for close frequency re-use while avoiding interferences, which is one of the mm-wave deployment choices for dense urban networks (small cells). The European Telecommunications Standards Institute (ETSI) and the Federal Communications Commission (FCC) have recently focused their attention on mm-wave frequency bands as possible solutions for 5G backhauling. These bands are main candidates for 5G mmWave frequencies: n257 (26.5 – 29.5 GHz), n258 (24.25 – 27.5 GHz), n260 (37-40 GHz), n261 (27.5 – 28.35 GHz), 42 GHz (40.5 – 43.5 GHz), V-Band (ETSI:57 - 66 GHz, FCC: 57-71 GHz) and E-Band (71-76 GHz & 81-86 GHz) [3]. The designs were primarily focused on the lowest mmWave frequency bands in this thesis. Because the purpose is to provide connection between the users and the base station, these bands have been targeted. As a result, the antenna to be developed is expected to have a high unit antenna gain. A high gain antenna also means a narrow beam radiation pattern, which allows the antenna to avoid interference. The antenna must have a small form factor and be affordable in order to meet client expectations.

1.1. GOALS OF THIS STUDY

Fifth-generation (5G) communication technologies and beyond have become critical to many applications as the demand for higher bandwidth and mobile connection grows. 5G systems that target millimeter wave (mm-wave) bands, in particular, have demanding base station antenna (BSA) requirements [4]. In the millimeter wave range covering 24.25GHz to 29.5GHz, the BSA must be beam steerable and beam programmable [5]. Wideband and high gain unit elements (UE's) with 45° linear slant polarization are required for such antennas [6-7]. Microstrip antennas on low-loss substrates with limited bandwidth and lower efficiency due to dielectric loss have been proposed to meet BSA standards [8-9]. The use of a substrate integrated waveguide (SIW) helps reduce feed network loss, however large bandwidth is challenging to achieve using SIW technology. Depending on the antenna design, traditional waveguides with air dielectric in the form of antenna feed and radiation element can overcome these challenges at the cost of increased size and manufacturing complexity [10-11]. The majority of BSAs are outdoor units, thus size isn't normally an issue. As a result, waveguide-fed antenna arrays may be an excellent match for these purposes. The use of sophisticated ridge waveguide technology to improve the bandwidth of a waveguide antenna array for the 5G millimeter wave spectrum was proposed in [12]. The described design was able to cover the intended 5G millimeter band with an impedance bandwidth of $|S_{11}| < -10$ dB. Most BSA systems, on the other hand, require at least a -14 dB impedance match to reduce reflected power and maximize overall system efficiency, when output power is just as important as bandwidth consumption [13].

To meet the coverage requirements of a typical mmwave 5G BSA, numerous small beams may be required at the antenna. Due to antenna efficiency, a separate beamforming network (BFN) with each antenna element connected to it through a short transmission line for proper phase and amplitude would be preferable to BFN integrated antenna arrays. To boost channel capacity and coverage, 5G uses multiple-input multiple-output (MIMO) technology in addition to beamforming. The purpose of this research is to develop a 2×2 slotted array UE that can be stacked vertically or horizontally to form an antenna array, with each UE controlled by BFN or operated independently in a MIMO environment. Then, using this unit element, it is aimed to design a 2×4 slotted array cavity backed waveguide dual antenna with +45° and -45° polarization. Finally, dual antennas with different polarizations were combined on a single structure and transformed into a transceiver BSA structure with polarization diversity. Due to separate BFN, we aim to maintain at least 14 dB match (VSWR $\leq$ 1.5) to minimize standing wave ratio between the BFN and the UE. The transition from waveguide to feed-cavity, cavity iris, slot orientations, and shapes have all been adjusted for optimal performance. The proposed antennas are manufactured and their performance have been measured.

1.2. OUTLINE OF THE THESIS

This thesis consists of five chapters.

In Chapter 1, the evolution and stages of mobile communication are explained. It is mentioned which frequency bands are included in the 5G frequency planning and their infrastructure. The purpose and characteristics of the mm wave antenna to be utilized in the base station are discussed in Section 1.1. It is mentioned that +45° slant polarized 2x2 slot cavity backed waveguide unit antenna is designed for 5G base station systems and +45° and -45° 2x4 slot cavity backed waveguide dual antenna is designed using this UE. In addition to these, the result values of these antennas are mentioned.

The antenna's functional mechanism and general characteristics are described in Chapter 2. The concepts of beamwidth, radiation patterns, beam area, radiation intensity, antenna efficiency, directivity, gain, near and far field, antenna polarization, antenna array and waveguide are examined.

In Chapter 3, the family of directly fed antenna arrays are examined.

In Chapter 4, antennas, which are the subject and purpose of this thesis, are explained. In Section 4.1, firstly, the design of the +45° slant polarized 2x2 slotted cavity backed waveguide antenna is explained in detail. The target criteria for this unit antenna are stated at the beginning. Then, the gain, reflection coefficient and HPBW results were compared with the values obtained in the measurements and simulations. A comparison with other researches is presented at the end of this section. At the end of this section, measurement and simulation graphs of copol and cross-pol graphs in azimuth and elevation planes between 22 – 31 GHz are given. In Section 4.2, two different dual array antenna structures with 2x4 slots +45° and -45° slant polarized are designed using UE. A power splitter structure is designed to combine two unit antennas and to feed the structure from the center. The signal is split equally in amplitude and phase and delivered to the antennas via the splitter. The results of measurement and simulation are compared, just as in the unit antenna. In section 4.3, polarization diversity is achieved by combining +45° and -45° slant polarized 2x4 dual antennas on a single metal surface, and a base station antenna with two ports that are well separated from one other is developed. Reflection coefficient, gain and HPBW values are given comparatively. Radiation patterns are extracted in the azimuth and elevation planes for +45° and -45° slant polarization values.

In Chapter 5 the results of the study are summarized. In Section 5.1, the image of the scenario to be established in the future is given. The antenna designed in Section 5.1 is radially distributed 360 degrees at 45° intervals. It is considered to strengthen or weaken in the desired directions by placing the BFN structure in the center of these eight antennas.

2. ANTENNA PARAMETERS

An antenna is a converter that converts electrical signals from wired to wireless and vice versa. Antennas can be used as both transmitter and receiver due to the equivalence principle. In two-way communication, one antenna can be used for both transmit and receive operations. Today, there are many types of antennas according to the purpose they are used for. The antenna studies that will be proposed in this thesis will be aimed at fulfilling the functions of 5G base station antennas in the mm-waveband.

Figure 2.1 depicts the transmitting and receiving antenna's radiation process. Time-varying electrical signals from the source proceed along the transmission line and reach the external environment after passing through the tapered transition structure. Planar waves in empty space coming from the far field are transmitted to the receiver structure by advancing along the transmission line by inducing current on the tapered transition structure in the figure.

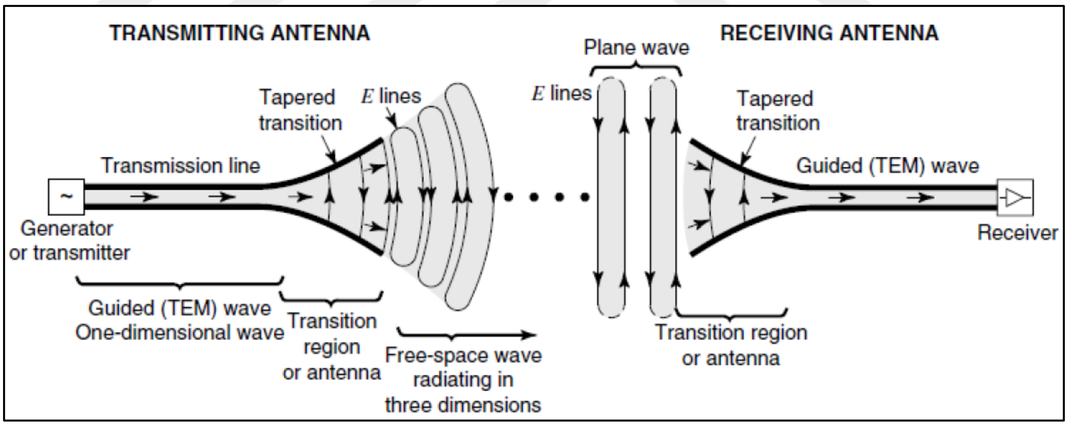

Figure 2.1. Radiation mechanism in the antenna [14]

The equivalent circuit of this structure can be expressed with resistors, inductors and capacitors.

2.1. BANDWIDTH

One of an antenna's most important properties is its bandwidth. An antenna's bandwidth refers to the frequency range it can cover. It meets certain criteria such as radiation pattern, directivity, gain, and VSWR. In most cases, bandwidth is measured in terms of VSWR. This bandwidth characteristic is known as impedance bandwidth. A 2:1 VSWR is typically used, which means that a VSWR of less than 2 is chosen for bandwidth operations. The values of antenna parameters can be changed based on the operating frequency in its bandwidth. Fractional Bandwidth is another way to describe an antenna (FBW). The Fractional Bandwidth is calculated by dividing the bandwidth by the center frequency.

2.2. RADIATION PATTERNS

A radiation pattern is a graphical representation of the antenna's radiating properties as a function of space coordinates. In general, the far field is where the radiation pattern is defined. Radiation characteristics include phase, polarization, directivity, radiation intensity, field strength, and power flux density. The three-dimensional spatial distribution of radiated power as a function of observer position along a path or surface of constant radius is the most necessary feature of radiation. Figure 2.2 shows the antenna analysis coordinate system.

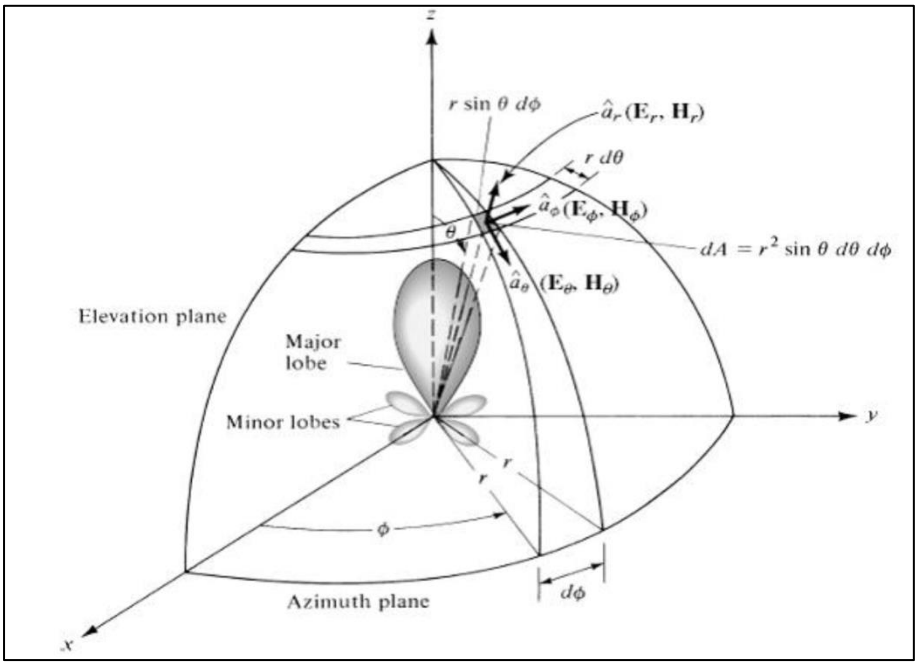

Figure 2.2. The coordinate system for antenna analysis [14]

A constant-radius trace of the electric field is the amplitude field pattern. An amplitude power pattern is a graph that illustrates the spatial fluctuation of the power density along a constant radius. Power and field patterns are typically standardized at their maximum value, resulting in power patterns and normalized field. Typically, the power pattern is represented on a logarithmic scale or in dB. We get a normalized or relative field pattern with dimensionless by dividing a field component by its greatest value

$$E_\theta(\theta,\phi)_n = \frac{E_\theta(\theta,\phi)}{E_\theta(\theta,\phi)_{\max}} \tag{2.1}$$

The field pattern shape is independent of distance at large distances. The patterns are mostly for far-field situation. The E- and H-plane patterns are commonly used to describe a linearly polarized antenna's performance. The E-plane contains the electric field vector and also the highest radiation direction, whereas the H-plane contains the magnetic field vector as well as the greatest radiation direction. Figure 2.3. depicts an illustration. The xoz plane (elevation plane; $\phi = 0$) is the main E-plane in this case, whereas the the xoy plane is the primary H-plane (azimuthal plane; $\theta = \pi/2$).

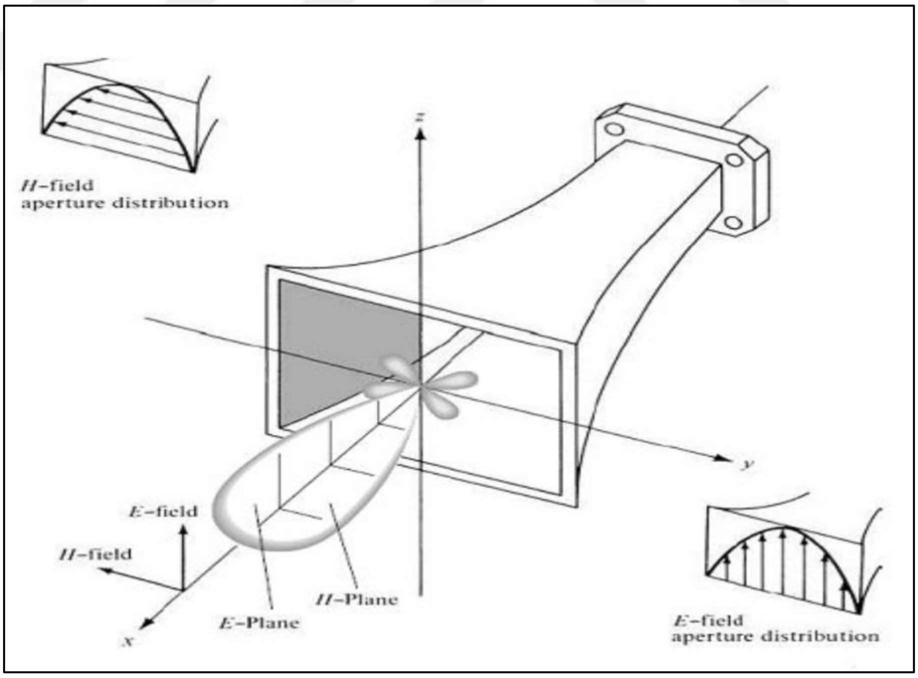

Figure 2.3. A pyramidal horn antenna’s main H and E plane patterns [14]

2.3. BEAM AREA

As illustrated in Figure 2.4, dA is an incremental area on the surface of a sphere in polar two-dimensional coordinates, $rd\theta$ is the product of the length in the θ direction (latitude) and $r\sin\theta d\phi$ in the ϕ direction (longitude). Hence $dA = (rd\theta)(r\sin\theta d\phi) = r^2 d\Omega$, where $d\Omega$ is the measurement of a solid angle in steradians (sr).

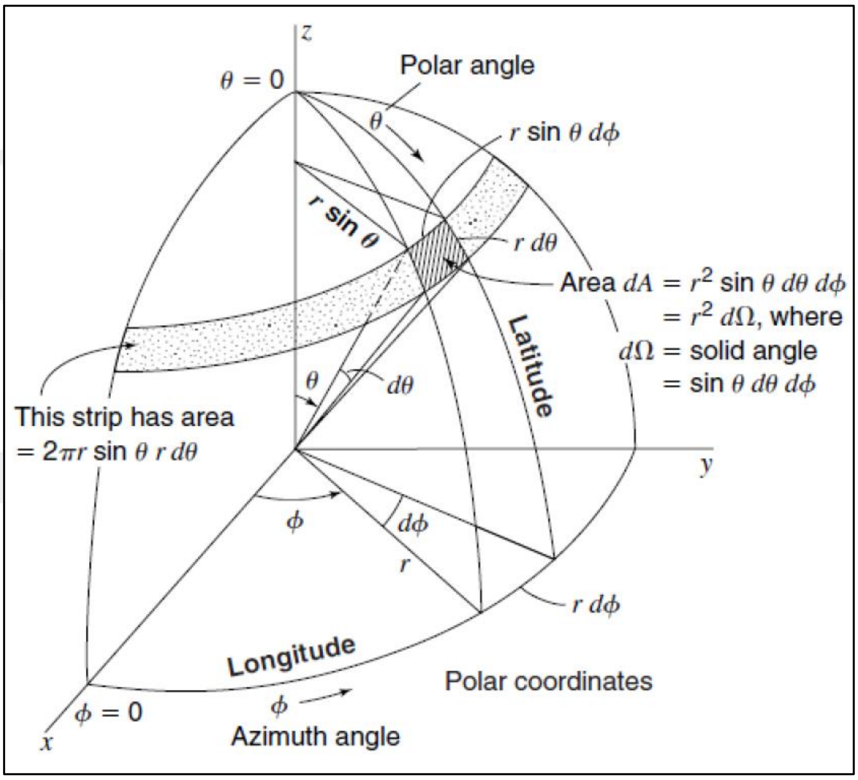

Figure 2.4. The beam area [14]

An antenna's beam area, also known as the beam solid angle or Ω_A, is the area of the antenna's beam. The summation of the normalized power pattern across a sphere(4π sr) yields Figure 2.5.

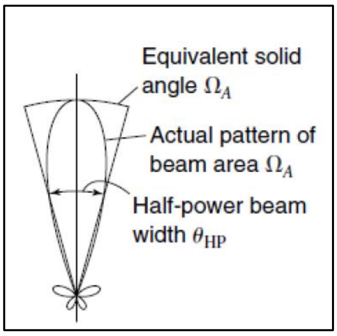

Figure 2.5. The normalized power pattern [14]

$$\Omega_A = \int_{\phi=0}^{\phi=2\pi} \int_{\theta=0}^{\theta=\pi} P_n(\theta,\phi) \sin\theta d\theta d\phi \tag{2.2}$$

And

$$\Omega_A = \iint_{4\pi} P_n(\theta,\phi) d\Omega \tag{2.3}$$

2.4. RADIATION INTENSITY

Radiation intensity is the amount of power radiated by an antenna per unit solid angle. The normalized power pattern is the ratio of the radiation intensity $U(\theta,\phi)$ as just a function of angle to its highest value. Thus,

$$P_n(\theta,\phi) = \frac{U(\theta,\phi)}{U(\theta,\phi)_{\max}} \tag{2.4}$$

The intensity of the radiation, U , is unaffected by distance.

2.5. ANTENNA EFFICIENCY

Losses at the input terminals and within the antenna construction must be taken into account. Reflections from mismatch and I^2R losses might create such losses.

$$e_0 = e_r e_c e_d \tag{2.5}$$

where e_0 represents overall efficiency, e_r represents reflection efficiency, e_c represents conduction efficiency, and e_d represents dielectric efficiency. They are all dimensionless.

2.6. DIRECTIVITY

The ratio of an antenna's highest power density $P(\theta,\phi)_{\max}$ (watts/m2) to its average value over a sphere as measured in the far field is known as its directivity. As a result, pattern directivity is

$$D = \frac{P(\theta,\phi)_{\max}}{P(\theta,\phi)_{av}} \tag{2.6}$$

The following formula is used to compute the average power density of a sphere,

$$P(\theta,\phi)_{av} = \frac{1}{4\pi} \int_{\phi=0}^{\phi=2\pi} \int_{\theta=0}^{\theta=\pi} P(\theta,\phi) \sin\theta d\theta d\phi \tag{2.7}$$

$$= \frac{1}{4\pi} \iint_{4\pi} P(\theta,\phi) d\Omega \tag{2.8}$$

As a result, the beam area's directivity

$$D = \frac{4\pi}{\iint_{4\pi} P_n(\theta,\phi) d\Omega} = \frac{4\pi}{\Omega_A} \tag{2.9}$$

2.7. GAIN

Because of the antenna's ohmic losses, an antenna's gain G is a real or realized value less than its directivity D. The antenna construction heats up as a result of these losses. A mismatch in the antenna's feed might also lower gain. The gain-to-directivity ratio is the antenna efficiency factor.

$$G = eD \tag{2.10}$$

In actuality, G is always smaller than D.

2.8. NEAR FIELD FAR FIELD

There are two primary zones in the fields surrounding an antenna: the near field (Fresnel zone), which is close to the antenna, and the far field (Fraunhofer zone), which is further away. The radius of the boundary between the two can be freely chosen

$$R = \frac{2L^2}{\lambda} \tag{2.11}$$

where L is the antenna's maximum dimension in meters and λ is the wavelength. In the far field, the field pattern's geometry is unaffected by distance. The longitudinal component of the electric field may be significant in the near or Fresnel zone, and the power flow isn't totally radial. The distance generally determines the form of the field pattern in the near field.

2.9. ANTENNA POLARIZATION

The antenna's polarization in a specific direction is defined as the polarization of the wave transmitted by the antenna in that direction. Polarization of a radiated wave is a feature of an electromagnetic wave that describes the time-varying direction and relative amplitude of the electric-field vector.

The three forms of polarization are linear, circular, and elliptical polarization. The field is said to be linearly polarized if the vector that characterizes the electric field as a function of time at a particular point in space is always orientated down a line.The electric field, in general, follows an ellipse and is referred to be elliptically polarized. Linear and circular polarizations are two types of elliptical polarizations that result from transforming an ellipse into a straight line or a circle, respectively. It is possible to track the electric field in either a clockwise or counterclockwise manner. The rotation of the electric-field vector clockwise is referred to as right-hand polarization, whereas the rotation clockwise is referred to as left-hand polarization.

2.10. ANTENNA ARRAY

An antenna array is a radiating system with several antennas placed correctly to produce greater field strength at a great distance from the radiating system by combining radiations from all of the antennas in the system at a single location. The vector sum of the fields produced by the array's individual antennas produces the total field produced by an antenna array at a considerable distance. The component elements of an antenna array are referred to as elements.

The elements of an antenna array are considered to be linear if they are equally spaced along a straight line. A uniform linear array is one in which all of the elements in a linear antenna array are supplied with the same amplitude current and have a uniform phase shift along the line.

Some of the most prevalent array types include End Fire Array, Broadside Array, Parasitic Array, and Collinear Array.

A broadside array is made up of a series of identical antennas arranged in a straight line. The axis of each antenna is perpendicular to this straight line. The axis of an antenna array is what it's called. As a result, each element is perpendicular to the antenna array's axis. Individual antennas are uniformly spaced along the axis of the antenna array.

The end fire array is fairly similar to the broadside array in terms of setup. However, the most significant distinction is in the direction of maximal radiation. In a broadside array, maximum radiation is perpendicular to the array's axis, whereas maximum radiation in an end fire array is parallel to the array's axis.

Thus, an end fire array can be described as one in which the highest radiation direction corresponds with the array's axis, resulting in unidirectional radiation.

Individual elements of the collinear array are supplied with identical-sized and phase currents. The broadside array is analogous to this condition. The maximum radiation direction in a collinear array is perpendicular to the array's axis. The collinear and broadside arrays have similar radiation patterns, however the collinear array's radiation pattern has circular symmetry, with the main lobe perpendicular to the primary axis everywhere. As a result, the omnidirectional or broadcast array is also known as a collinear array.

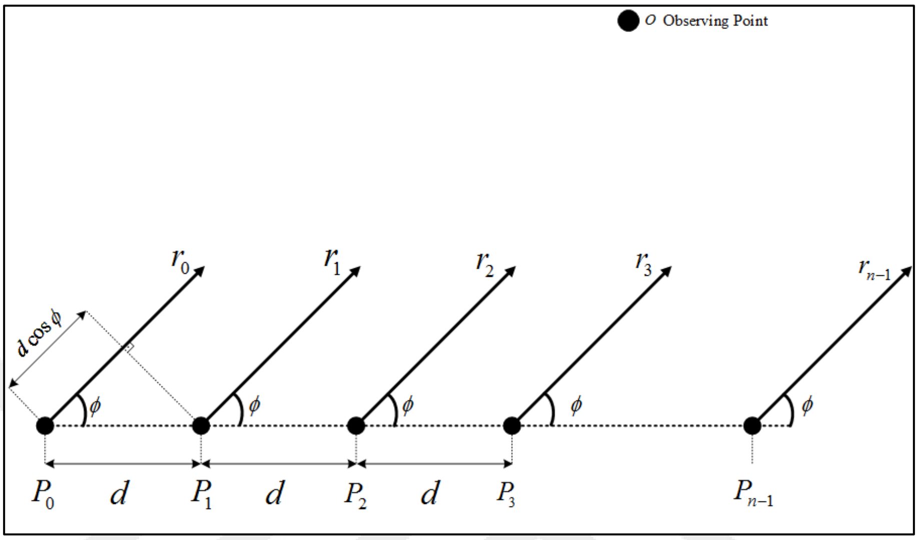

Figure 2.6. Array distribution [14]

The electric field produced by an element at a given point is given by,

$$E_0 = \frac{IdL\sin\theta}{4\pi\omega\varepsilon_0}\left[j\frac{\beta^2}{r_0} \right] e^{-j\beta r_0} \tag{2.12}$$

Since the separation distance d between any two array components is quite small compared to the radial distances between point O and point P_0, P_1, $...P_{n-1}$, we can assume r_0, r_1, r_{n-1} are approximately same.

Because r_0 and r_1 are not exactly the same, the electric field produced at point O by an element P_1 will differ. As a result, the electric field caused by P_1 is given by,

$$E_1 = \frac{IdL\sin\theta}{4\pi\omega\varepsilon_0}\left[j\frac{\beta^2}{r_1} \right] e^{-j\beta r_1} \tag{2.13}$$

$$r_1 = r_0 - d\cos\phi \tag{2.14}$$

Hence,

$$E_1 = \frac{IdL\sin\theta}{4\pi\omega\varepsilon_0}\left[j\frac{\beta^2}{r_0}\right]e^{-j\beta\left(r_0 - d\cos\phi\right)} \tag{2.15}$$

$$E_1 = E_0 e^{j\beta\cos\phi} \tag{2.16}$$

For similar line electric fields at O point,

$$\begin{gathered} E_2 = \frac{IdL\sin\theta}{4\pi\omega\varepsilon_0}\left[j\frac{\beta^2}{r_2}\right]e^{-j\beta r_2} \\ E_2 = \frac{IdL\sin\theta}{4\pi\omega\varepsilon_0}\left[j\frac{\beta^2}{r_1}\right]e^{-j\beta r\left(r_1 - d\cos\phi\right)} \end{gathered} \tag{2.17}$$

$$E_2 = E_1 e^{j\beta d\cos\phi} \tag{2.18}$$

By substituting E_0 the equation becomes

$$E_2 = E_0 e^{2j\beta d\cos\phi} \tag{2.19}$$

Similarly

$$E_{n-1} = E_0 e^{j(\mathrm{n}-1)\beta d\cos\phi} \tag{2.20}$$

The total electric field at O location is then calculated,

$$\begin{gathered} E_T = E_0 + E_1 + E_2 ... + E_{n-1} \\ E_T = E_0 + E_0 e^{j\beta d\cos\phi} + E_0 e^{2j\beta d\cos\phi} + ... + E_0 e^{j\left(n-1\right)\beta d\cos\phi} \end{gathered} \tag{2.21}$$

When the $\beta d\cos\phi = \psi$ is written, the above equation becomes,

$$E_T = E_0 + E_0 e^{j\psi} + E_0 e^{2j\psi} + ... + E_0 e^{j\left(n-1\right)\psi} \tag{2.22}$$

Considering the series by $p = 1 + r + r^2 + r^3 + ... + r^{n-1}$ Where $r = e^{j\psi}$ and by multiplying the following equation by $\left(1-r\right)$ on both sides and simplifying, we obtain

$$p = \frac{1-r^n}{1-r} \tag{2.23}$$

E_T becomes

$$E_T = E_0 \left[\frac{1 - e^{jn\psi}}{1 - e^{j\psi}} \right] \tag{2.24}$$

By simplifying

$$\frac{E_T}{E_0} = e^{j(n-1)\frac{\psi}{2}} \left[\frac{\sin\left(\frac{n\psi}{2}\right)}{\sin\left(\frac{\psi}{2}\right)} \right] \tag{2.25}$$

The phase shift, as well as the magnitudes of the electric fields, are represented by the exponential term in the equation above.

$$\left| \frac{E_T}{E_0} \right| = \frac{\sin\left(\frac{n\psi}{2}\right)}{\sin\left(\frac{\psi}{2}\right)} \tag{2.26}$$

In order to find minima, the above equation should be zero, then $\frac{n\psi}{2} = \pm m\pi$, in here $\psi = \beta d \cos\phi$, therefore

$$\begin{gathered} \frac{n}{2}\left(\frac{2\pi}{\lambda} d\right)\cos\phi_{\min} = \pm m\pi \\ \phi_{\min} = \cos^{-1}\left(\pm \frac{m\lambda}{nd}\right) \end{gathered} \tag{2.27}$$

2.11. WAVEGUIDE

Waveguides are metal pipes through which electromagnetic waves can travel above a certain frequency. Waveguides are used in satellite applications because of their advantages such as low loss, durability and carrying high power. It is not preferred much in low frequency applications due to its size. However, they are often used in the 6-140 GHz range as they are smaller in size. There are many different waveguide structures in the literature, the most commonly used are rectangular and circular waveguides. Figure 2.7

shows the standard rectangular waveguide structure. The waveguide's long side (a) and short side (b) determine the operating frequency of the waveguide. Depending on the frequency to be worked with, standard waveguides are produced commercially in the market.

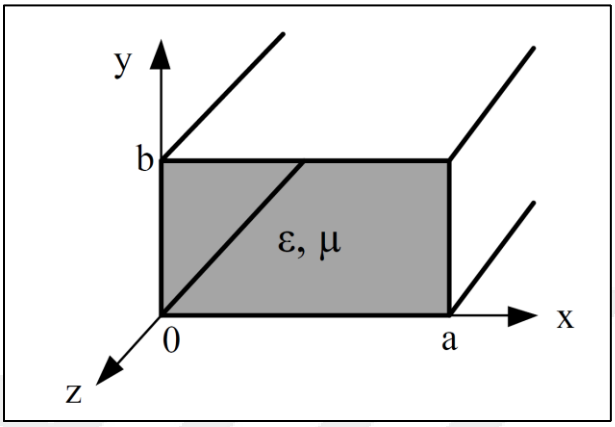

Figure 2.7. Rectangular waveguide [14]

The rectangular waveguide is the basic waveguide used to carry microwave signals. There are many waveguide components manufactured as standard. Examples of these are dampers, adapters, filters, insulators. In waveguides, electromagnetic waves can propagate in TEM, TM, and TE modes, but in rectangular waveguides, propagation in TEM mode is absent because the boundary conditions for this mode are not met. As a result, rectangular waveguides are used to propagate TE and TM modes.

2.11.1. Modes in a Rectangular Waveguide

In rectangular waveguides, only TE_{mn} and TM_{mn} modes can be excited. As seen in Figure 2.7, if the direction of the electromagnetic wave is considered as +*z* direction, there is no component of the electric field in the direction of progression for TE waves, Ez = 0. As a result, the electric field for TE waves is always perpendicular to the wave's propagation. It can be said that waveguides behave like a high pass filter.

2.11.2. Dominant Mode in a Rectangular Waveguide

The dominant mode in waveguides is the mode with the lowest cutoff frequency. The TE_{10} mode is the dominant mode in rectangular waveguides, with the condition a > b. The cutoff frequency and area expressions are as follows.

$$f_c = \frac{c}{2a\sqrt{\mu\varepsilon}} \tag{2.28}$$

$$E_x = 0 \tag{2.29}$$

$$E_y = -\frac{A_{10}}{\varepsilon}\frac{\pi}{a}\sin\left(\frac{\pi}{a}x\right)e^{-j\beta_z z} \tag{2.30}$$

$$E_z = 0 \tag{2.31}$$

$$H_x = -A_{10}\frac{\beta_z}{\omega\mu\varepsilon}\frac{\pi}{a}\sin\left(\frac{\pi}{a}x\right)e^{-j\beta_z z} \tag{2.32}$$

$$H_y = 0 \tag{2.33}$$

$$H_z = -j\frac{A_{10}}{\omega\mu\varepsilon}\left(\frac{\pi}{a}x\right)^2\cos\left(\frac{\pi}{a}x\right)e^{-j\beta_z z} \tag{2.34}$$

In a waveguide traveling in the +z direction and excited in the fundamental mode, the electric field has only *y* component.

Exciting more than one mode in waveguides causes the power to be divided into excited modes. Therefore, separate detectors are needed for each mode. Because this is difficult to achieve, waveguides are often used in a single mode.

2.12. WAVEGUIDE T JUNCTION

Waveguide T-junctions are used as power dividers or combiners in feeder network designs in many antenna applications. These structures are generally divided into two groups as H-plane and E-plane, as seen in Figure 2.8 [35].

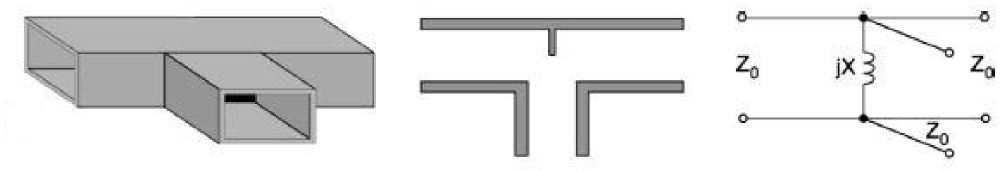

(a)

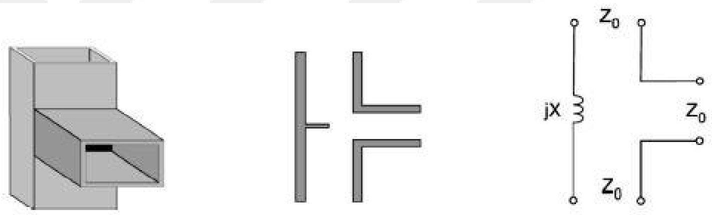

(b)

Figure 2.8. T junction and equivalent circuit (a) H-plane (b) E-plane [35]

3. DIRECTLY FED ANTENNA ARRAYS FOR MM-WAVES

There is no direct route between the feeding network and radiating elements in a directly fed antenna array, and they are generally connected or coupled to use an aperture coupled microstrip patch antenna or slotted arrays.Figure 3.1 illustrates the various types of directly fed antenna arrays for high gain applications.

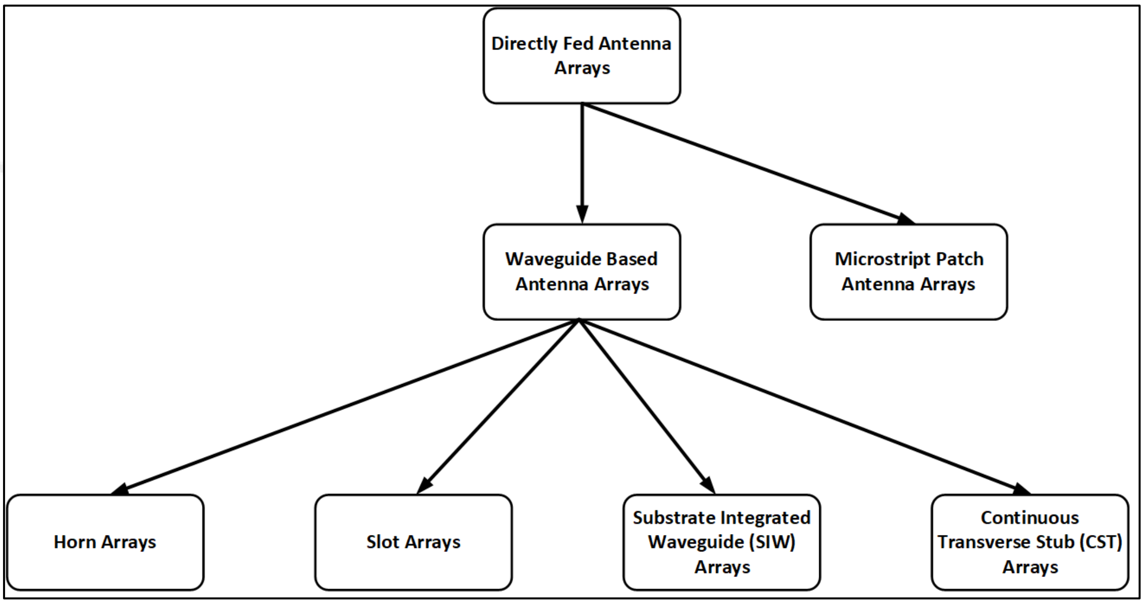

Figure 3.1. Different types of directly fed antenna arrays representation [3]

To create high gain antenna systems, several antenna technologies are used in the form of arrays. Microstrip arrays might appear appropriate for 5G communications at first because of their beam steering compatibility and ability to control side lobe level. However, because the antenna's working frequency range would be at mmWaves, these arrays will be difficult to use, owing to the large dielectric substrate loss, which affects the antenna's efficiency dramatically [17]. Another problem in microstrip antennas is that the surface wave on the microstrip line causes spurious radiation and leakage, thereby reducing the antenna gain and efficiency. As a result, waveguide-based antenna arrays are favoured in mmWave applications over microstrip antennas since they do not suffer from dielectric loss.

Waveguide-based antenna arrays are divided into groups such as slot arrays, horns arrays, Continuous Transverse Stub (CTS) arrays, and substrate integrated waveguide (SIW) arrays. High-frequency horn antenna arrays bring difficulties in manufacturing, as they have very complicated small dimensions in both the radiating element and the feeding network [18]. Therefore, such antenna arrays are challenging and costly. As with horn arrays, slot arrays have high efficiency since there is no dielectric. However, it has limited gain bandwidth due to its resonant nature. Center feed (parallel feeding) or End feed (serial feeding) structures are common in slot arrays. Due to the long-line effect in networks, serial feed has a limited gain bandwidth [19]. When compared to the end feed type, the center feed type reduces the long-line effect by placing the feed waveguide in the center of the array [20]. The corporate feeding network structure offers higher bandwidth than the series fed structure.

Full-corporate feed antenna with a wideband and high efficiency was published in V-band [21]. To eliminate grating lobes, this antenna is made up of two layers with element spacing less than one wavelength. The full-corporate feed network layout described here is also employed in a variety of different waveguide-based slot antenna arrays. Center feed waveguide slot array offers very wide bandwidth performances and good efficiency comparing to other waveguide slot array antennas. This antenna type, however, demands near-perfect electric contact between the radiating layers and feeding. In this study, to over come this problem, all antenna parts are plated with silver. The silver coating provides both good conductivity and solder retention, so even the smallest gaps can be closed with solder.

In literature instead of waveguide slot arrays, a solution based on gap waveguide was introduced [22]. The perfect electrical contact is no longer necessary in gap waveguide technology, but manufacturing process needs molding or diesink Electrical Discharge Machining (EDM) techniques. This method uses a parallel plate waveguide design with hard/soft boundary conditions to regulate wave propagation between the two plates in desired directions. During the manufacturing process, however, metallic multi-layer geometries of the arrays should be separated into various sections [23-24].

A multi-layer RGW slot array with corporate feed network for the 58-70 GHz frequency band was proposed in another study [25]. This structure consists of 16×16 slot array and has 80% efficiency and 18% as 1 dB gain bandwidth.

In another study on 2×2 cavity backed slot array has bandwidth with 15% $|S_{11}| < -10$ dB, and operating frequency of 3.6GHz to 4.31GHz and 13.4 dBi peak gain with total efficiency >95% , although a resonant-iris mod and ridges are used in the cavity [26].

In order to get high gain at mmWave frequencies, there is a gap waveguide technology. This method has the advantage of not requiring electrical contact between adjacent layers [27-28]. Another method is ridge gap waveguide technology, in [29] corporate-feed slot array antenna with RGW technology shows that antenna has a 21% FBW ($VSWR < 2$, 12-15 GHz) gain higher than 12.2 dBi.

In [30] fed with groove gap waveguide structure is proposed on single layer cavity backed 4×4 slot array. With this structure, the impedance bandwidth is increased and the radiation in the coaxial cavity slots is improved. The proposed antenna FBW is 6% $|S_{11}| < -10$ dB, and working frequency between 36.25 and 38.75GHz, maximum 23.4 dBi gain with efficiency 99.2%.

The study in [31] used a two-dimensional feeding network design instead of a three-dimensional feeding network design. Planar corporate waveguide feeding has been proposed due to its ease of production and design, however it has not been possible to feed each horn element structurally at a smaller distance than λ_0. The explanation for this is revealed to be $0.92\lambda_0$ of the waveguide's width. A design is proposed in which more than one array element is fed from a single slot, rather than one by one, in order to realize the corporate feeding network where the distance between the radiating elements is smaller than λ_0 [32]. Multi-part production of the feeding network in the design contributes to its flexibility. In the 60 GHz range, the waveguide has an impedance bandwidth of 4.8 GHz ($|S_{11}| < -14$, FBW = 8.3%), 32 dBi gain, 80% antenna efficiency, proves the freedom of design of the corporate feed antenna. 16x16 element high gain (33.7 dBi), high efficiency (85%) and 1.5 GHz (VSWR < 2, 11.45–12.95 GHz, FBW = 12%) impedance bandwidth antennas are designed [33]. In these designs, the distance between the elements in the E-plane is almost at wavelength in order to feed each element in equal phase, has been placed. The E-plane side lobe level is increased as a result of this (SLL > 8.8 dB).

In this study, iris structures are added and optimized within the cavity to increase the impedance bandwidth, and an hourglass structure is used from waveguide transition to cavity transition to improve the S parameter value. Thus, with this structure, the fractional bandwidth is over 28.94% for $|S_{11}| < -15$.Firstly, we introduce 2x2 slot broad band +45° slant polarize wr34 waveguide feed cavity back unit antenna geometry with simulated and measurement results of S parameters, gain radiation patterns are discussed. Then 2x4 slot broad band +45° slant polarize cavity back array antenna with perfectly match power splitter and the results are discussed. Finally, it is explained that 2x4 slot broad band +45° and -45° slant polarize cavity back array antennas are combined in a single body and work in harmony as a transmit and receive antenna pair.

4. ANTENNA DESIGN

In this study, waveguide cavity supported slot antennas with high gain and wideband are presented for fifth generation (5G) millimeter wave (mmWave) base station antenna applications. The unit element (UE) antenna has four slots arranged symmetrically with a polarizer to form +45° slant linear polarization. On the other hand, there are eight slots in the dual design made with the power combiner designed to be perfectly matched. Polarizers are designed separately to be ±45°. In addition to these, a separate model has been designed in which ±45° slant polarization is combined on a single structure. When compared to standard slotted waveguide antennas, the waveguide cavity backing provides increased bandwidth and gain. Grooves are also included to improve directivity and expand the impedance bandwidth. A beamforming network is a separate unit that consists of many antenna elements that are combined to make an array or a MIMO antenna. The unit antenna has a 31.2% fractional impedance bandwidth ($|S_{11}|$-14 dB, 22.6-31 GHz) and a 14.3 dBi average boresight gain, according to measurements. The UE antenna is suited for phased-array or massive MIMO base station applications, with +/-0.5 dB gain flatness and +/- 2.5° beamwidth variation throughout the entire 5G mm Wave range.

4.1. +45° SLANT POLARIZED 2X2 SLOT ARRAY CAVITY BACK WAVEGUIDE UNIT ANTENNA

Although BSA specifications for 5G mm-wave band applications are not fully standardized, the antenna must meet some important design criteria. Because the antenna controller circuit is considered independent of the radiating elements, the goal parameters are limited to the UE and are listed in Table 4.1. Unlike 2G/3G GSM BSAs, where array configuration is prevalent, 5G mmWave band antenna systems can be either array or MIMO, as shown in Figure 4.1. BSA requirements of earlier GSM systems are used to estimate target UE specifications [13,15]. To meet cell coverage requirements in urban areas, 2G/3G BSA HPBW is commonly set to 65°. However, we plan to have at least two antenna panels covering the same azimuth span, allowing for at least 2-Transmit 2-Receive (2T2R) MIMO.

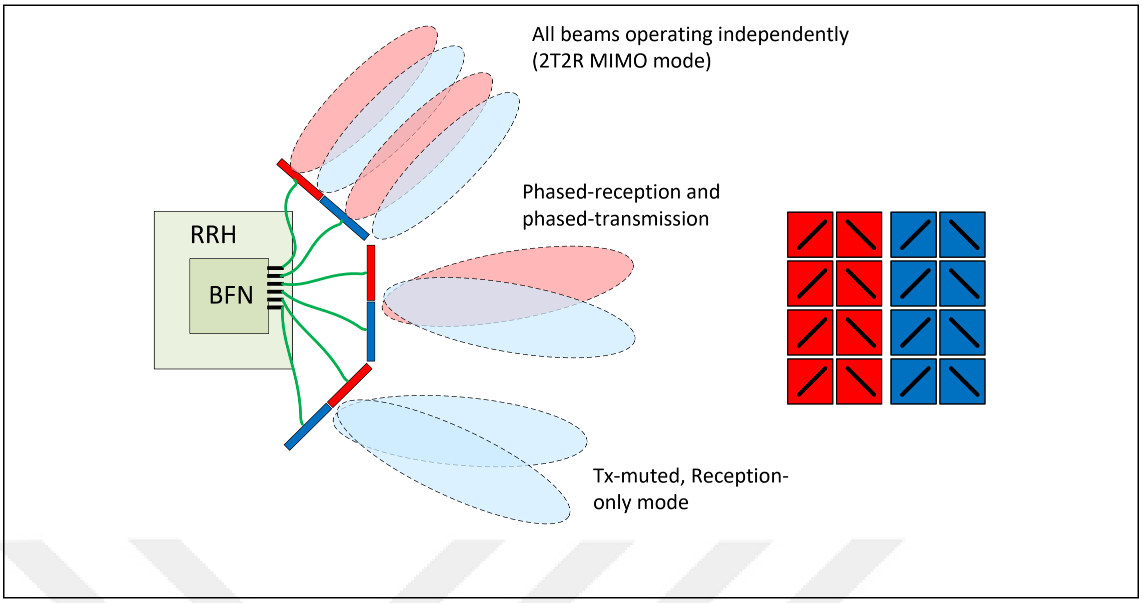

Figure 4.1. General description of array and MIMO concept for 5G mmWave BSA applications where BFN is integrated into Remote Radio Head (RRH).

Table 4.1. Target UE specifications

Frequency	24.25 – 29.5 GHz
Gain	$\geq$ 14 dBi
Gain Flatness	+/- 0.5 dB
VSWR	$\leq$ 1.5 (RL < -14 dB)
Polarization	+/- 45^o
Azimuth HPBW	32.5^o
HPBW Variation	+/- 2^o
Cross Polarization	< -15 dBc
Impedance	50 Ω

Figure 4.2 shows the proposed antenna's geometrical configuration with parameters. Figure 4.2 (a) illustrates the overall structure of the proposed antenna. The proposed antenna is fed by a slot on the adapter's short end, and it is connected to the WR34 flange by a transition waveguide. As illustrated in Figure 4.2 (a), the antenna's main construction comprises of a waveguide, coupling slot, cavity, four slot pairs, and a polarization conversion layer. The

coupling slot is positioned in the cavity's center to provide equal amplitude and phase to each slot of the radiation element. The spacing between adjacent polarizing layer elements is set to less than $0.85\lambda_0$ (λ_0 = 11.1mm @27GHz), $0.75\lambda_0$ in the x-direction and $0.82\lambda_0$ in the y-direction.Figure 4.2 (b) shows a top view of the first four levels, as well as additional factors that define the slots.

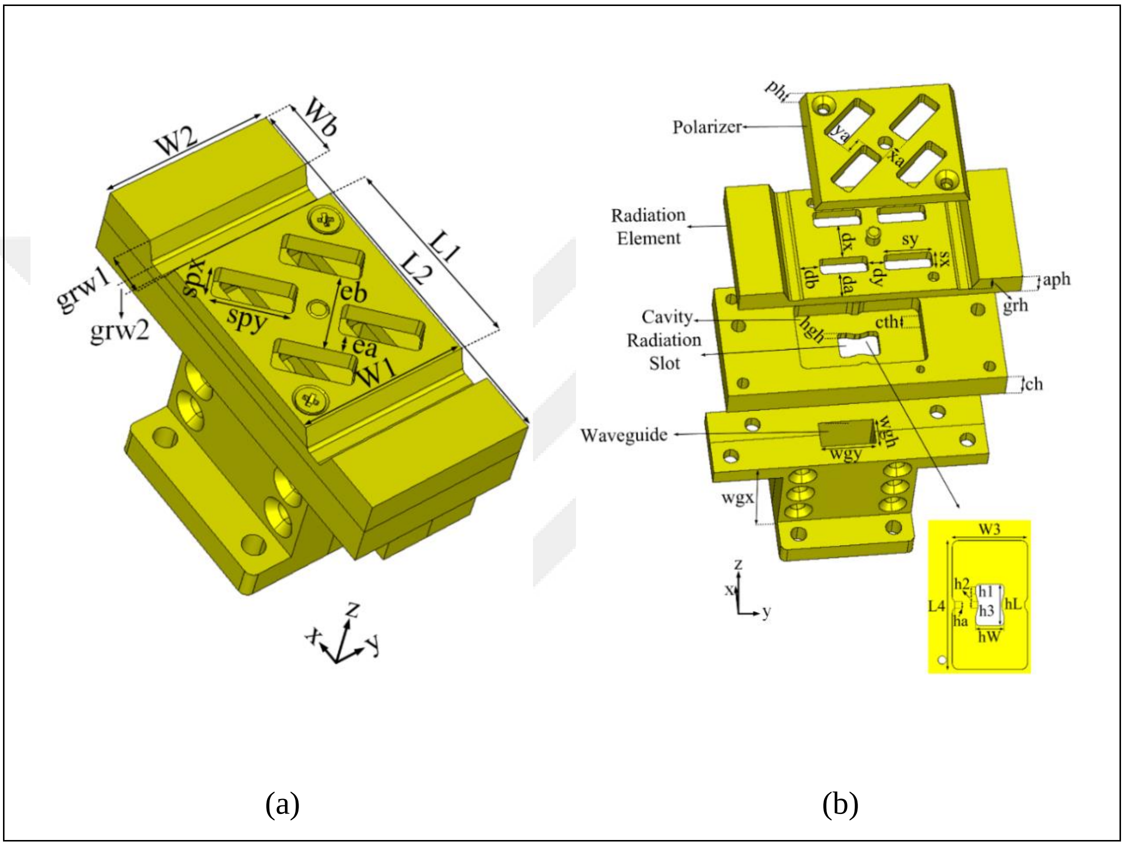

Figure 4.2. Proposed UE antenna structure, (a) overall view, (b) expanded view.

Table 4.2 shows the final dimensions of the 5G antenna modelled using a commercial full-wave electromagnetic solver CST [16].Figure 4.3(a) and Figure 4.3(b) depict the electric field distribution of the radiating slots and the polarization conversion (polarizer) layer of the 2×2 proposed antenna. The existence of a fundamental mode on radiating slots and the polarization conversion layer is confirmed by the distribution. Each slot's field distributions are quite uniform, showing that there is no phase shift. The direction of the electric field in the polarizer layer also shifts 45° in line with the intended slant polarization.

Table 4.2. Dimensions of cavity-backed slot antenna (all values in mm)

L1	*W1*	*spx*	*spy*	*xa*	*ya*	*ea*	*eb*	*L2*	*W2*	*Wb*	*grw1*
21.58	19.32	3.7	8.28	1.01	1.34	2.23	9.17	43.08	19.32	6.65	4.1
sy	***dx***	***dy***	***da***	***db***	***L4***	***W3***	***h1***	***h2***	***h3***	***ha***	***hL***
7.32	5.66	2.5	4.1	3.145	19.63	11.48	0.745	1.174	0.67	0.996	6.299
wgy	***ph***	***grh***	***aph***	***hgh***	***wgh***	***cth***	***ch***	***grw2***	***hW***	***sx***	***wgx***
8.636	2.25	2.56	4.146	1.37	2.159	3.4	4.77	1.33	4.318	2.73	20

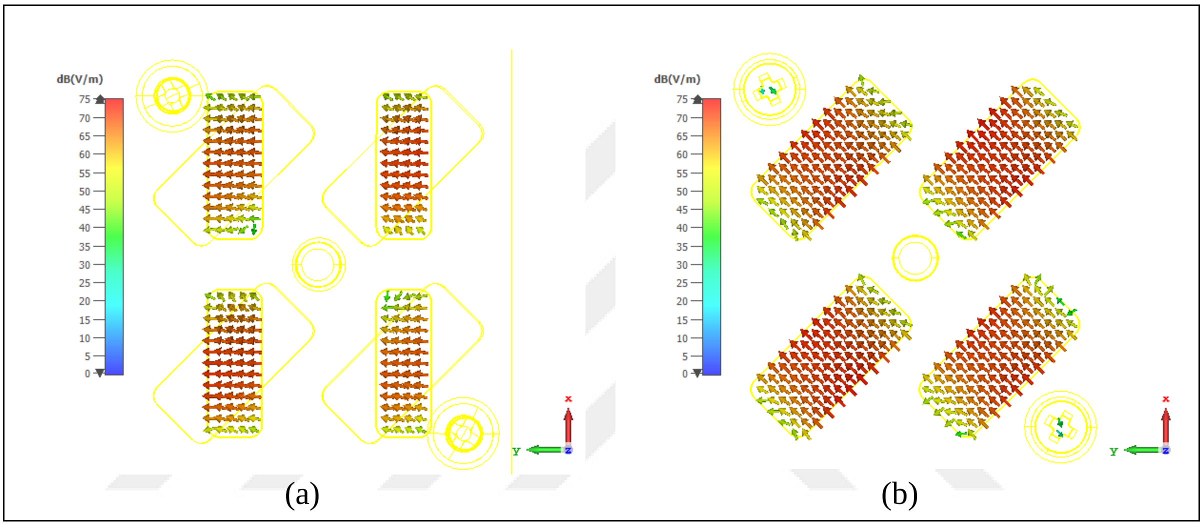

Figure 4.3. The electric field distribution at 26.5 GHz of, (a) the radiating slots (b) the polarization conversion layer

The antenna is manufactured with a CNC machine. Figure 4.4 (a), (b) and (c) show the prototypes in action. In simulations, all screw-hole locations and lateral cuts required for CNC milling have been taken into account. The Aluminum block's properties were also used in antenna simulations.

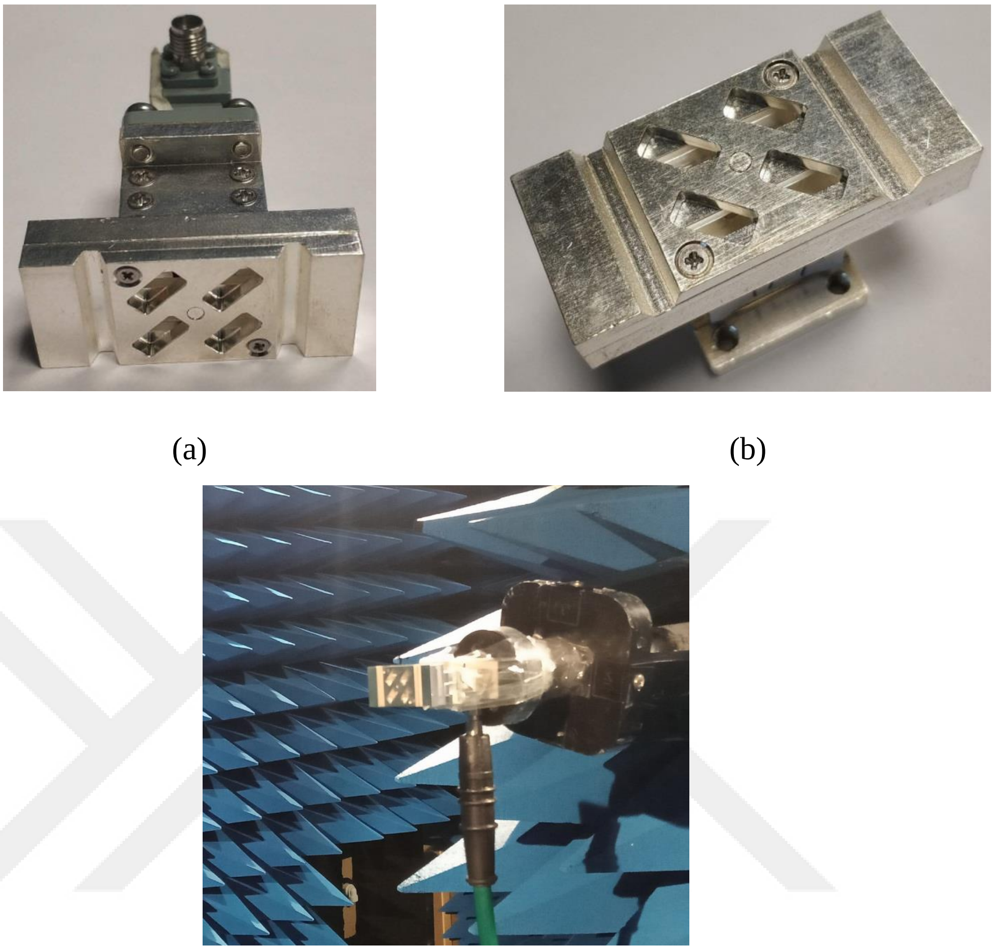

(a) (b)

(c)

Figure 4.4. Prototype antenna, (a) side view with WR34 waveguide to K-connector adapter, (b) top view, (c) Antenna in the measurement system

4.1.1. Simulation and Measurement Results

The reflection coefficient measurements of the proposed antenna were performed using a network analyzer (R&S ZVA-40). Measured and simulated results are shown in Figure 4.5. The simulations and measurements appear to match fairly well. The antenna has 33.5% fractional bandwidth (FBW) from 22.4 GHz to 31.4 GHz if $|S_{11}|$ <-10 dB (VSWR 1.5), and 31.2% FBW between 22.6 GHz and 31 GHz if $|S_{11}|$<-14 dB (VSWR 1.5), according to measured antenna performance.

Antenna pattern measurements were carried out at a full anechoic chamber using a spherical near-field system. The difference between measured and simulated boresight gains is less than 0.9 dB within the target band of 24.25 to 29.5 GHz, as shown in Figure 4.6 (a). More discrepancy is observed between 31 GHz and 32 GHz. Within the intended band, measured gain ranges from 13.9 dBi to 15 dBi. In Figure 4.6 (b), the Azimuth (yoz) and Elevation (xoz) planes are presented in a simulated 3D antenna layout. The Azimuth HPBW is larger than the Elevation HPBW with this orientation of the UE, which is the intended scenario for a typical array setup.

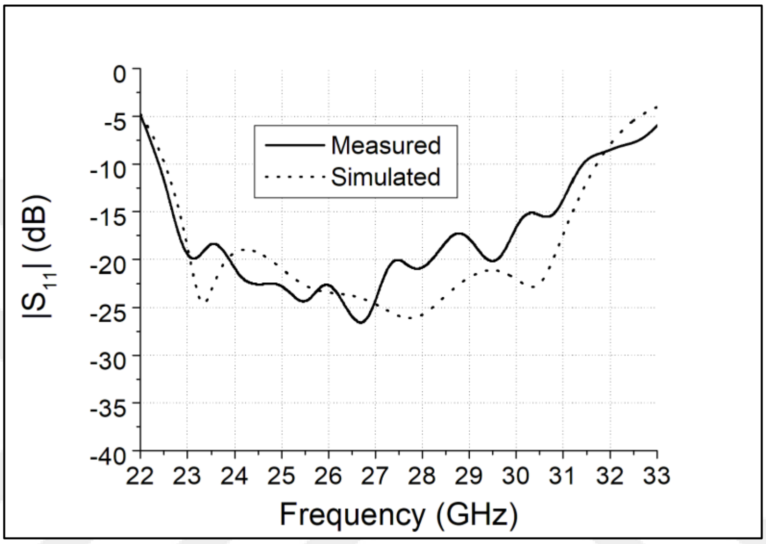

Figure 4.5. Simulated and measured reflection coefficient (S_{11}).

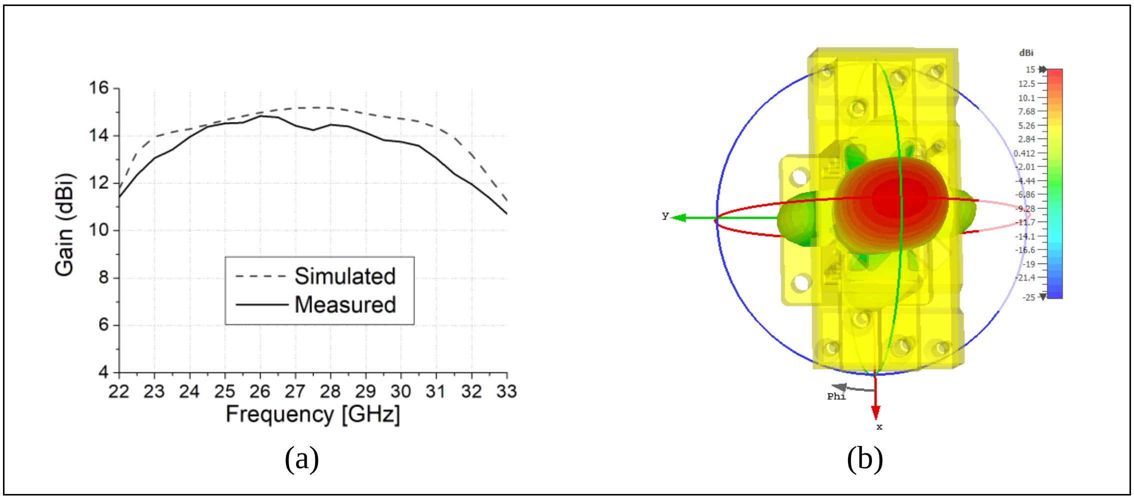

Figure 4.6. (a) Boresight gain of the antenna, (b) 3D simulated pattern.

Figure 4.7 shows the HPBWs for Azimuth and Elevation. The measured and modelled results are fairly similar. For the Azimuth and Elevation planes, HPBW variation throughout the target bandwidth is +/-2.5° and +/-2.0°, respectively.

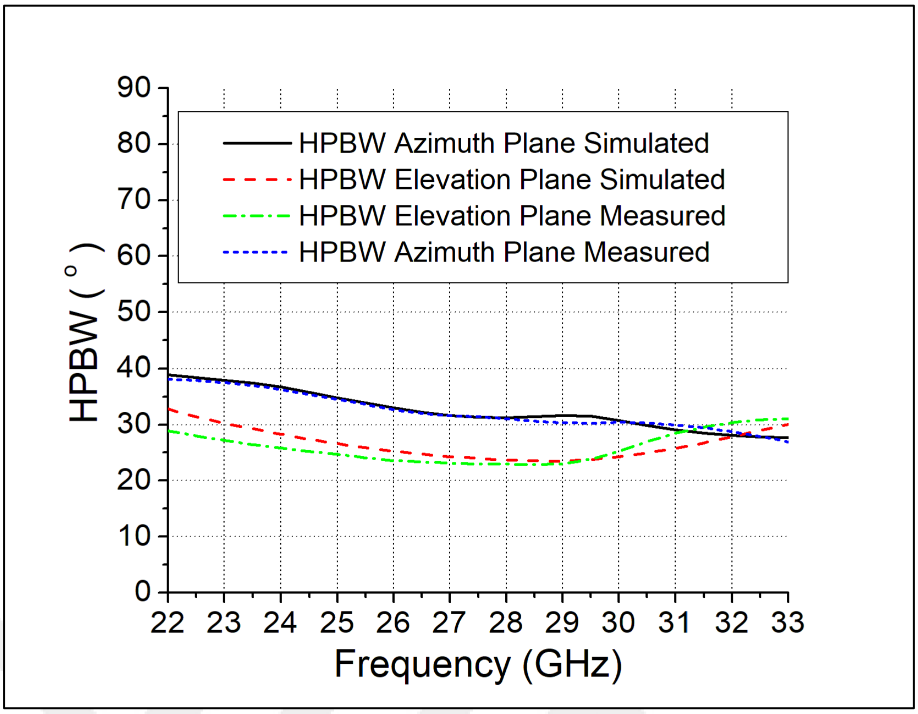

Figure 4.7. HPBW of UE antenna on azimuth and elevation plane

Figure 4.8-Figure 4.26 illustrate the antenna's radiation patterns at three distinct frequencies. At and around boresight directions, measured and simulated patterns are reasonably close to each other, with minor disagreement towards the back of the antenna where cross-polarization and co-polarization levels are close to each other. Because of the feed waveguide's direction, cross-polarization levels are better in azimuth planes than in elevation planes. Due to the small size of the antenna, the measurement system's own cabling has an impact on cross-polarization readings. Isolation between polarization pairs, on the other hand, is more important than individual cross-polarization levels. The prototype's side lobe levels (SLLs) are also around -13.5 dB, which is consistent with the antenna's uniformly-fed slot array on the radiating aperture. In an array setting, these SLLs can be lowered much more.

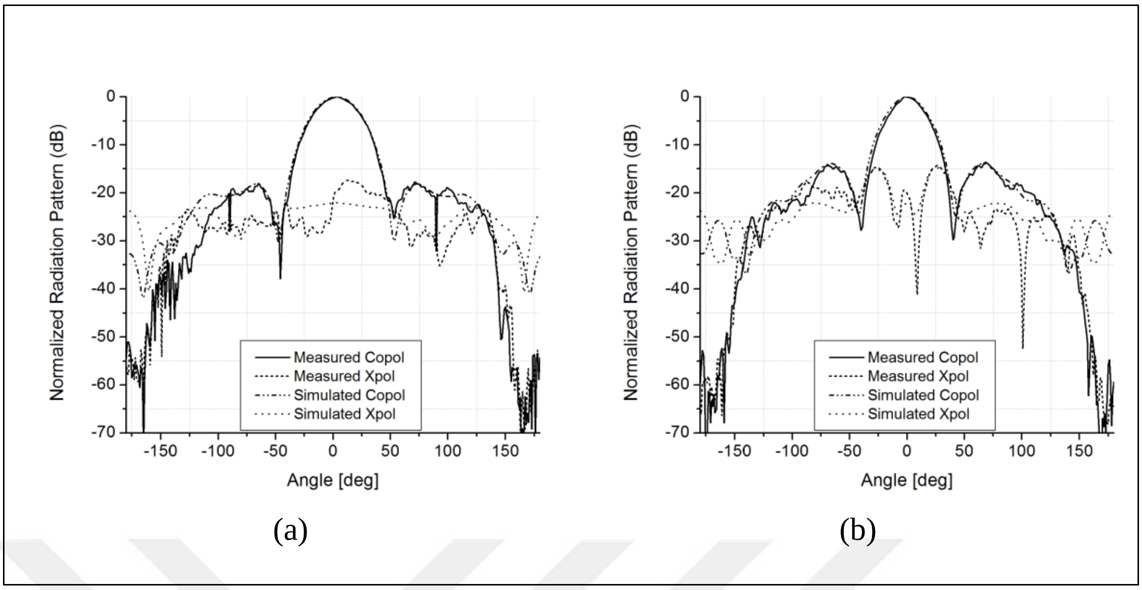

Figure 4.8. Normalized pattern of UE at 22 GHz, (a) Elevation, (b) Azimuthal

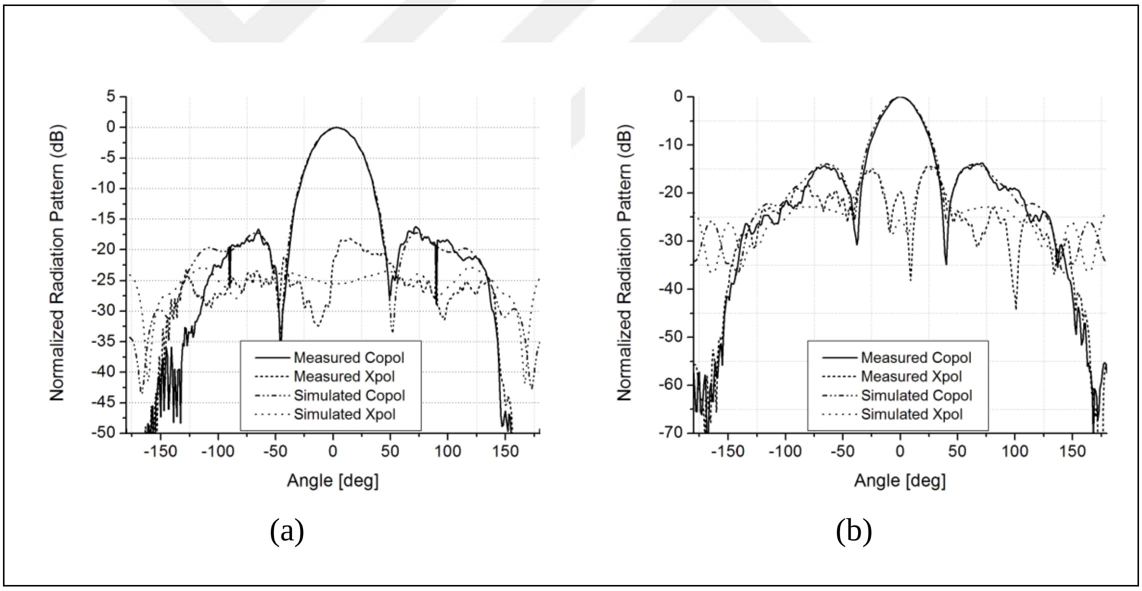

Figure 4.9. Normalized pattern of UE at 22.5 GHz, (a) Elevation, (b) Azimuthal

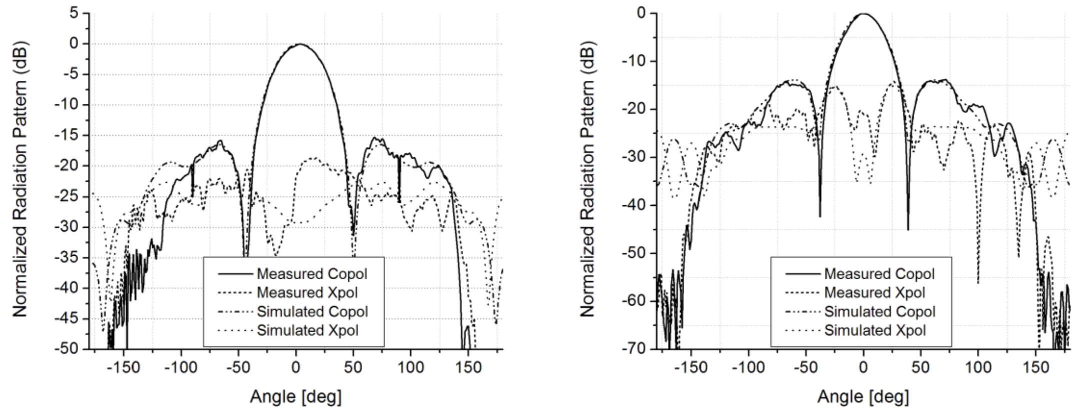

(a) (b)

Figure 4.10. Normalized pattern of UE at 23 GHz, (a) Elevation, (b) Azimuthal

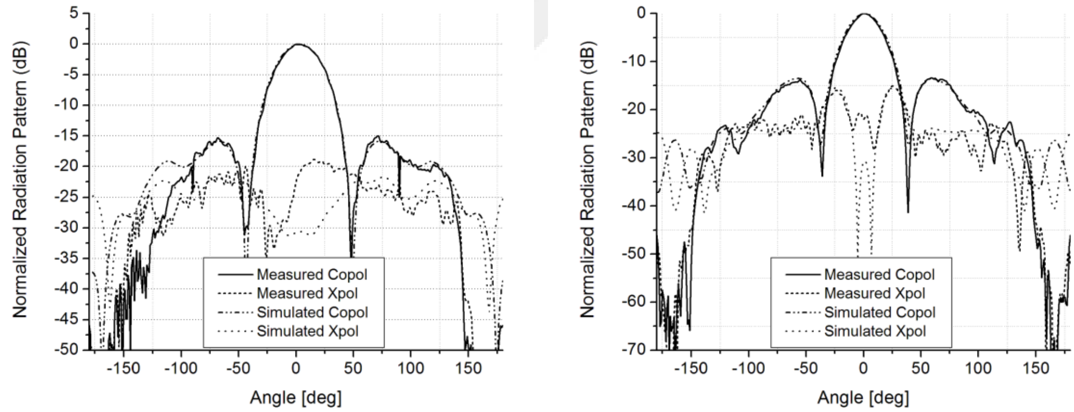

(a) (b)

Figure 4.11. Normalized pattern of UE at 23.5 GHz, (a) Elevation , (b) Azimuthal

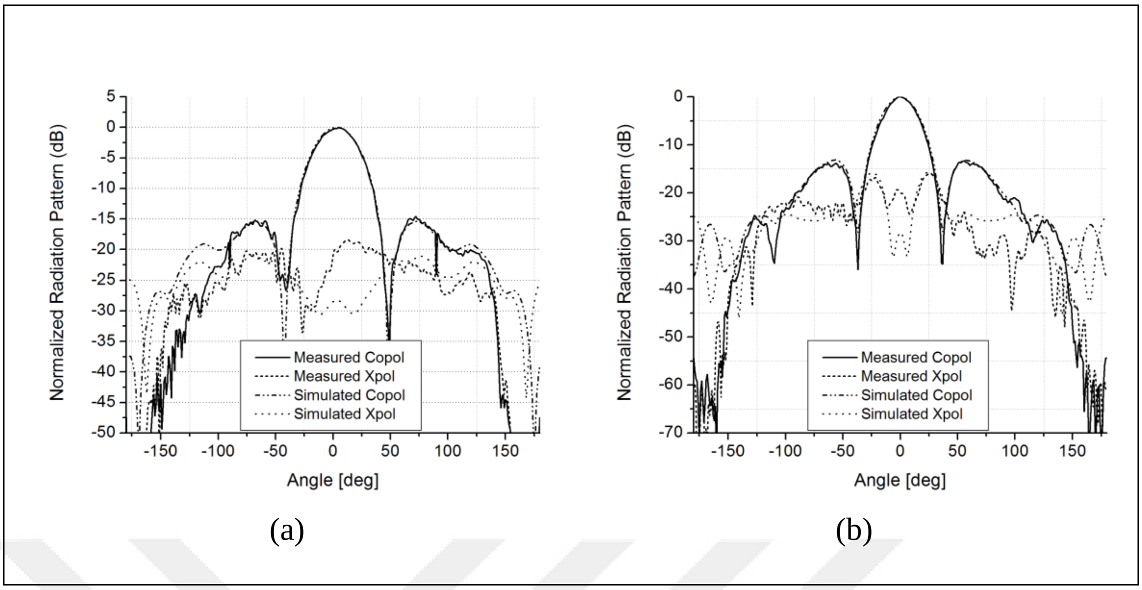

Figure 4.12. Normalized pattern of UE at 24 GHz, (a) Elevation , (b) Azimuthal

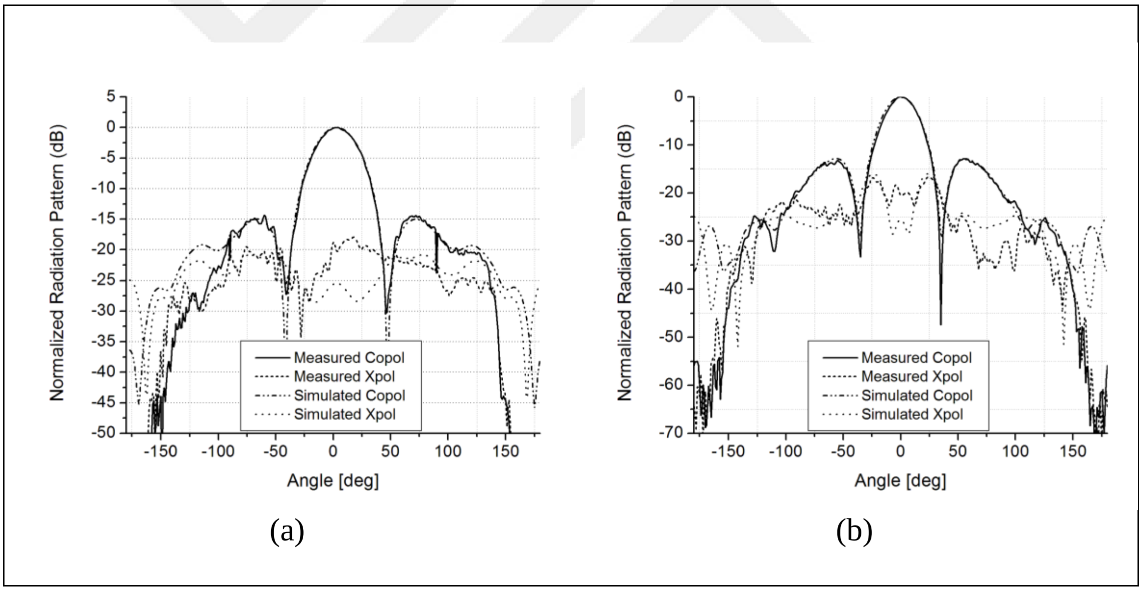

Figure 4.13. Normalized pattern of UE at 24.5 GHz, (a) Elevation , (b) Azimuthal

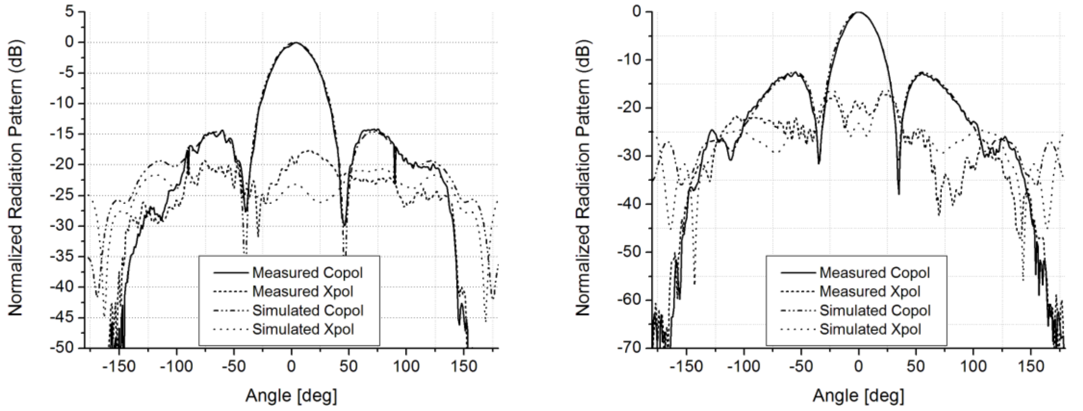

(a) (b)

Figure 4.14. Normalized pattern of UE at 25 GHz, (a) Elevation , (b) Azimuthal

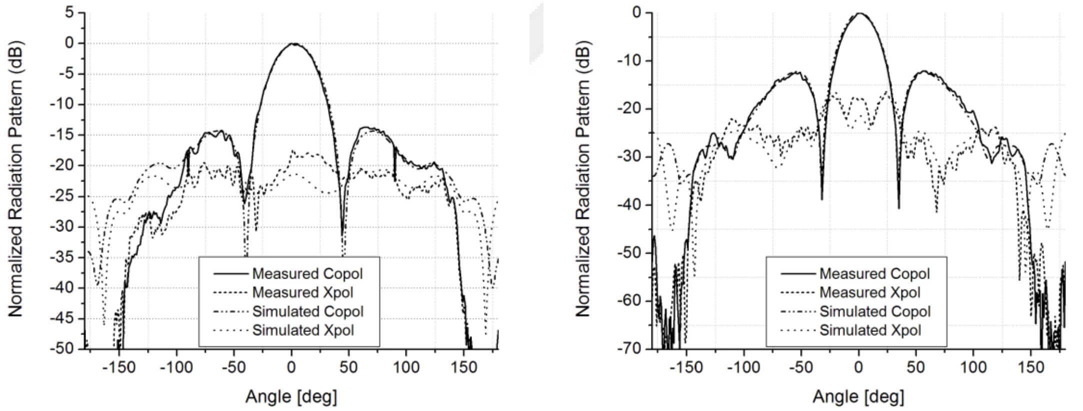

(a) (b)

Figure 4.15. Normalized pattern of UE at 25.5 GHz, (a) Elevation , (b) Azimuthal

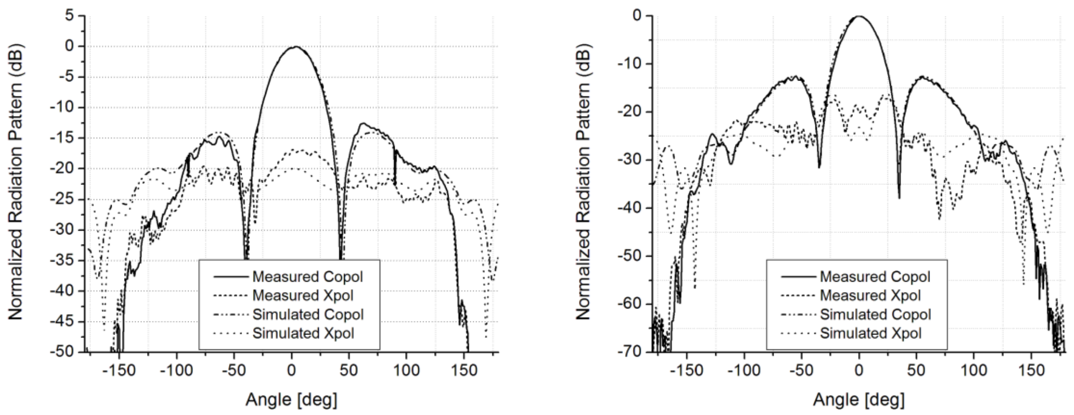

(a) (b)

Figure 4.16. Normalized pattern of UE at 26 GHz, (a) Elevation , (b) Azimuthal

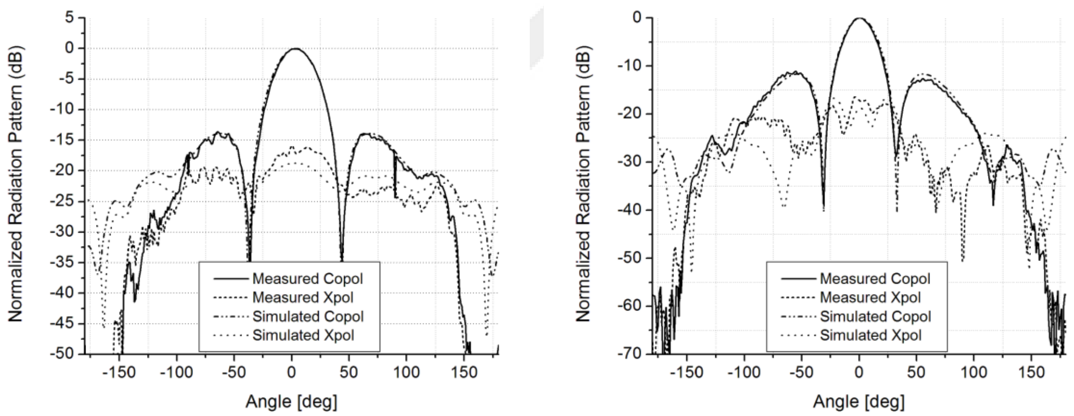

(a) (b)

Figure 4.17. Normalized pattern of UE at 26.5 GHz, (a) Elevation , (b) Azimuthal

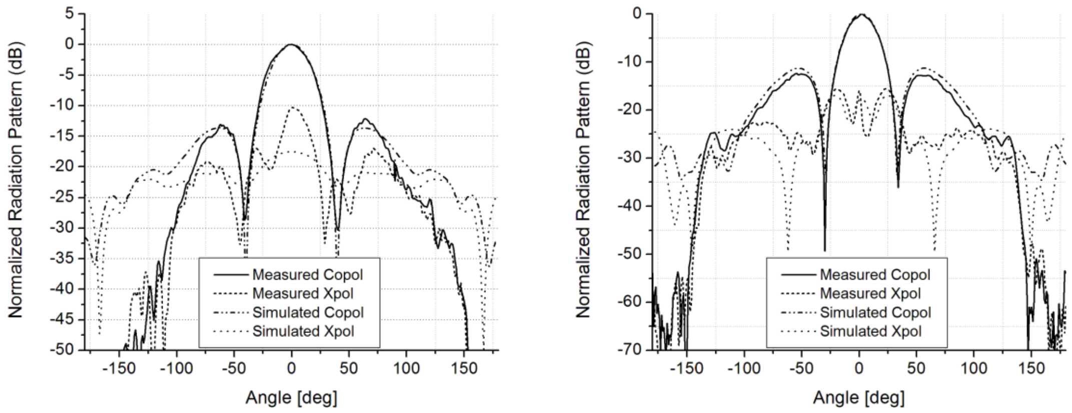

(a) (b)

Figure 4.18. Normalized pattern of UE at 27 GHz, (a) Elevation , (b) Azimuthal

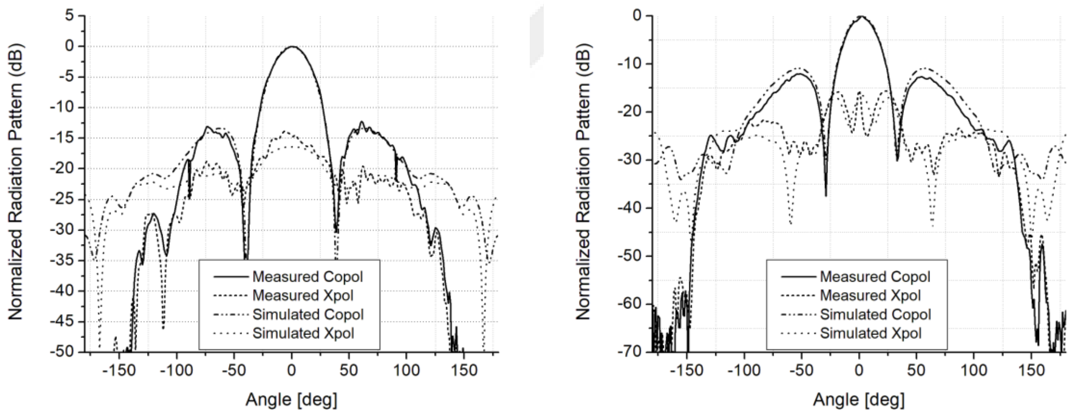

(a) (b)

Figure 4.19. Normalized pattern of UE at 27.5 GHz, (a) Elevation , (b) Azimuthal

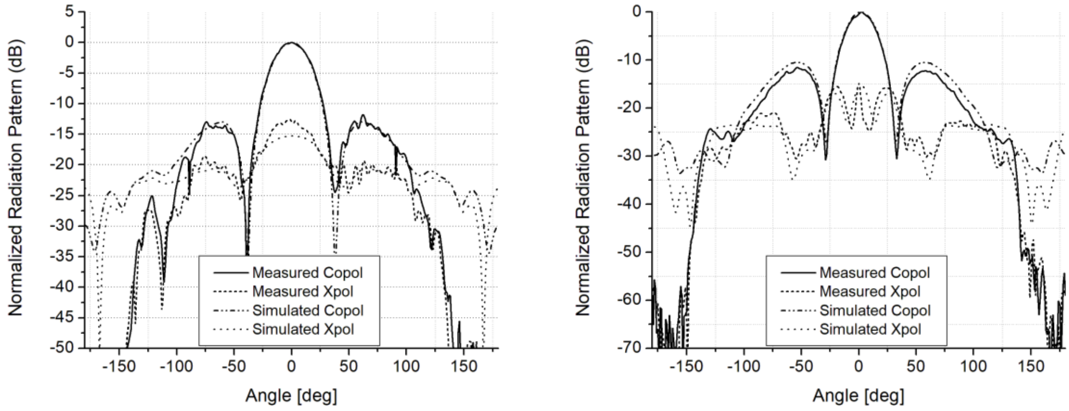

(a) (b)

Figure 4.20. Normalized pattern of UE at 28 GHz, (a) Elevation , (b) Azimuthal

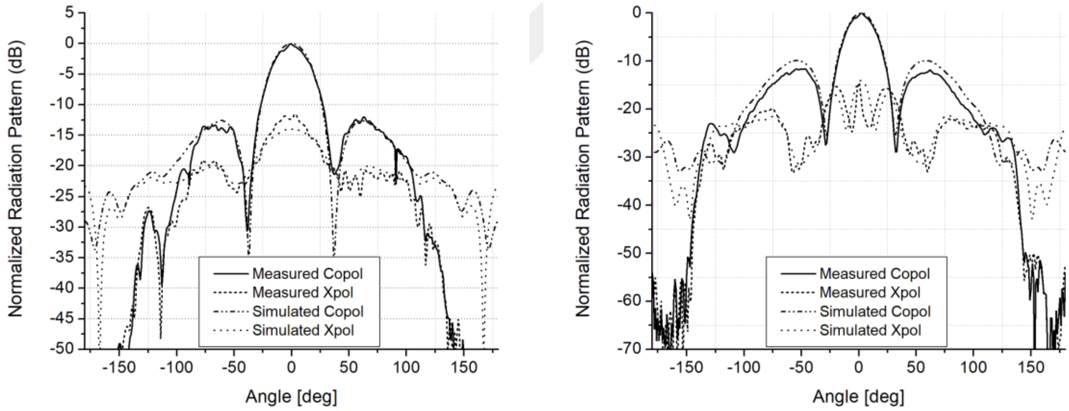

(a) (b)

Figure 4.21. Normalized pattern of UE at 28.5 GHz, (a) Elevation , (b) Azimuthal

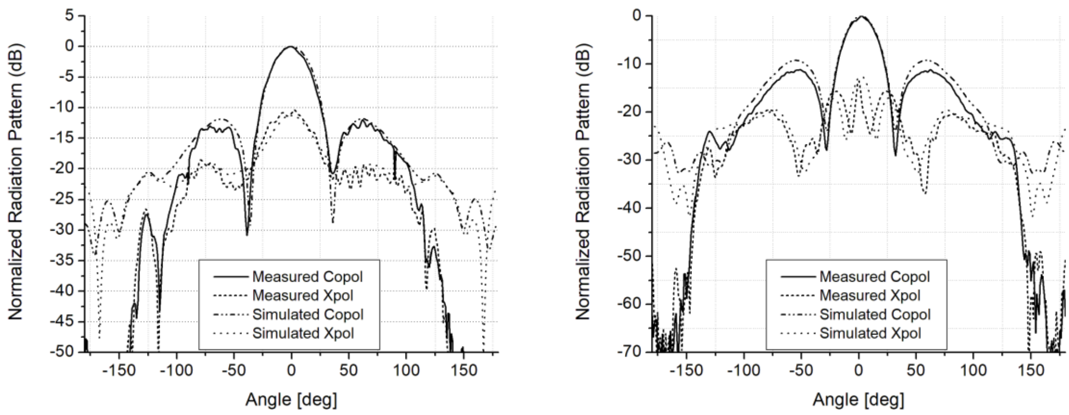

(a) (b)

Figure 4.22. Normalized pattern of UE at 29 GHz, (a) Elevation , (b) Azimuthal

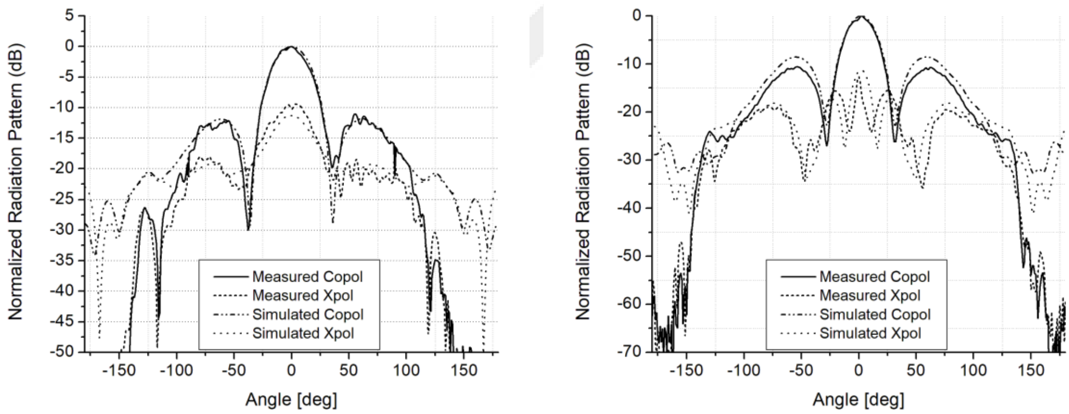

(a) (b)

Figure 4.23. Normalized pattern of UE at 29.5 GHz, (a) Elevation , (b) Azimuthal

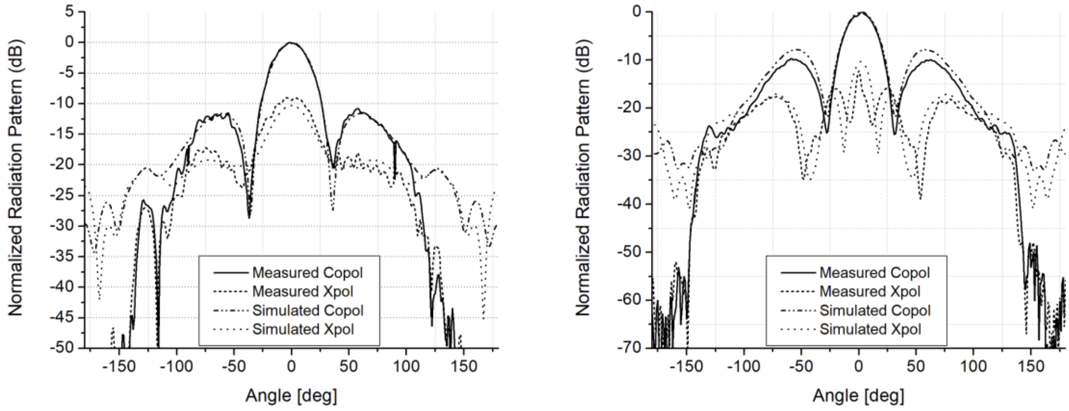

(a) (b)

Figure 4.24. Normalized pattern of UE at 30 GHz, (a) Elevation , (b) Azimuthal

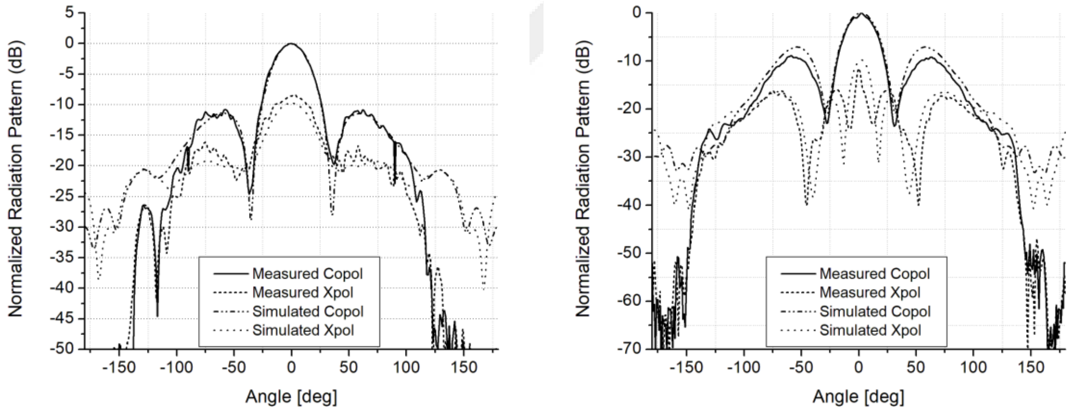

(a) (b)

Figure 4.25. Normalized pattern of UE at 30.5 GHz, (a) Elevation , (b) Azimuthal

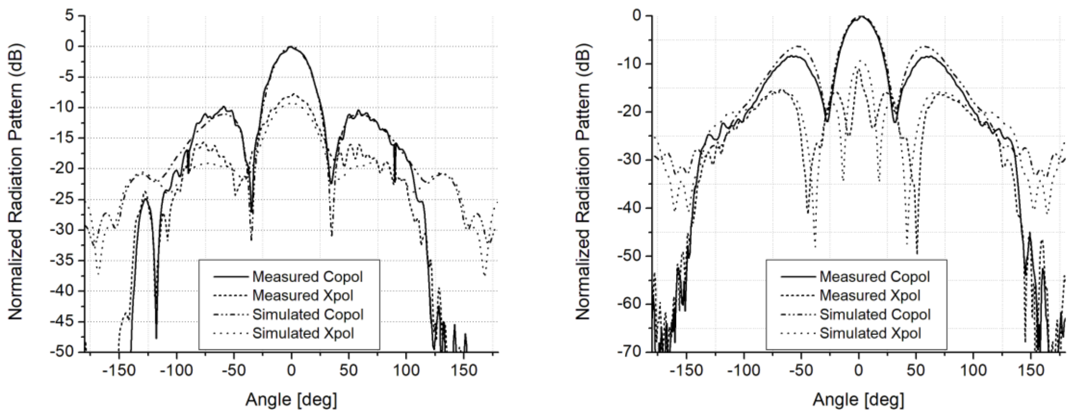

Figure 4.26. Normalized pattern of UE at 31 GHz, (a) Elevation , (b) Azimuthal

Table 4.3 compares the antenna's performance to that of previous studies. For comparison with other works, FBW is set to -10 dB. The antenna in [40] has similar properties to the present suggested design, but has a significantly lower FBW. Furthermore, gap-ridge waveguide technique was adopted, which required sophisticated manufacturing techniques. Over the whole 5G mm-wave band, the proposed antenna offers a greater than 71% antenna efficiency.

Table 4.3. A comparison of the performance of existing high-gain antennas for 5G applications

Ref	**Freq (GHZ) FBW**	**No of Elements**	**Planar Size (λ_oxλ_o)**	**Gain (dBi)**	**Gain Flatness (dB)**	**Az HPBW (deg)**	**XPD (dB)**	**Efficiency (%)**
This work	22.5 - 31.5 33.5%	2×2	3.88 ×1.74	15	±0.5	32 ±2.5°	>15	>71 (Measured)
[38]	27.2 - 28.8 6%	2×8	11.5 ×2.24	16.7	±1	-	>25	75 (Simulated)
[39]	34 - 36 6.2%	1×8	8.37 ×6.3	14	±0.5	-	-	84 (Simulated)
[40]	28.8 - 34 16.5%	4×4	3.5 ×3.4	19	±0.5	14.4	>35	70 (Measured)
[41]	3.45 - 3.55 < 5%	1×2	3.55 ×3.55	10	-	60	>30	-

[42]	27.5-28.35 4.2 %	2×2	13.5 ×6.8	7.9	±2	-	-	98 (Measured)
[43]	29.5 - 37 22%	1×4	4×4.2	15.5	±1	-	>20	87 (Simulated)
[44]	23 – 30.5 28%	8×8	7.6 ×7.6	26.4	±1.5	25.2	>40	60 (Measured)

For mmWave 5G base stations, an unique and low-profile wideband, high gain cavity supported 2×2 element slot antenna fed by waveguide has been designed and constructed. To obtain the appropriate slant polarization, the E-field is rotated with a 45° polarizer layer. The wideband performance of the fabricated antenna is 31.2% ($|S_{11}| < -14$), reaching beyond the 5G mmWave band. Extended bandwidth allows a target band to be maintained in a multi-antenna array or in a MIMO scenario with multiple antennas. The proposed antenna also offers a high gain and steady HPBW in the 24–29 GHz range, according to measurements. The proposed antenna is an ideal candidate for 5G base station applications because of these features.

4.2. +45° AND -45° SLANT POLARIZED 2X4 SLOT ARRAY CAVITY BACK WAVEGUIDE ANTENNA

After the 2x2 slot unit antenna is designed, the feeder network must be designed in order to array this unit element. Corporate feeding is chosen in this feeding network arrangement. The reason for choosing this waveguide structure is its wideband and low loss. The antenna structure consists of a power divider structure in addition to the polarizer, radiating layer and coupling layer as in the unit antenna. The polarizer part can be changed as +45° and -45° structure like a head, and this antenna structure is shown in the Figure 4.27 below.

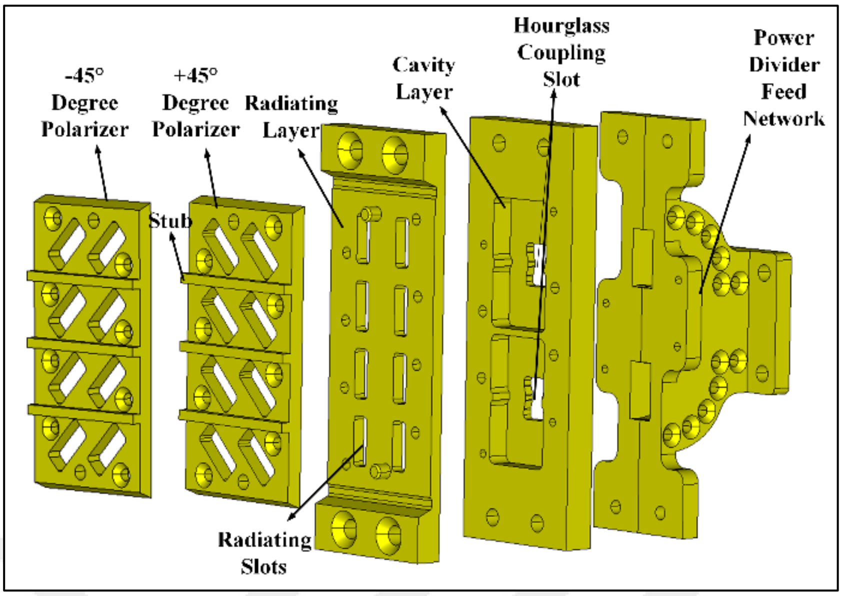

Figure 4.27. +45° and -45° slant polarized dual antenna

A dual structure is formed by deriving the unit antenna in the y-axis direction. Since the reflection coefficient of the power divider structure designed behind the cavity structure is less than -20 dB, it works in perfect compatible. Stubs are used to increase gain at higher operating frequencies and control mutual coupling between radiating elements. Antenna structure and parameters are shown in the Figure 4.28 below for +45° slant polarization.

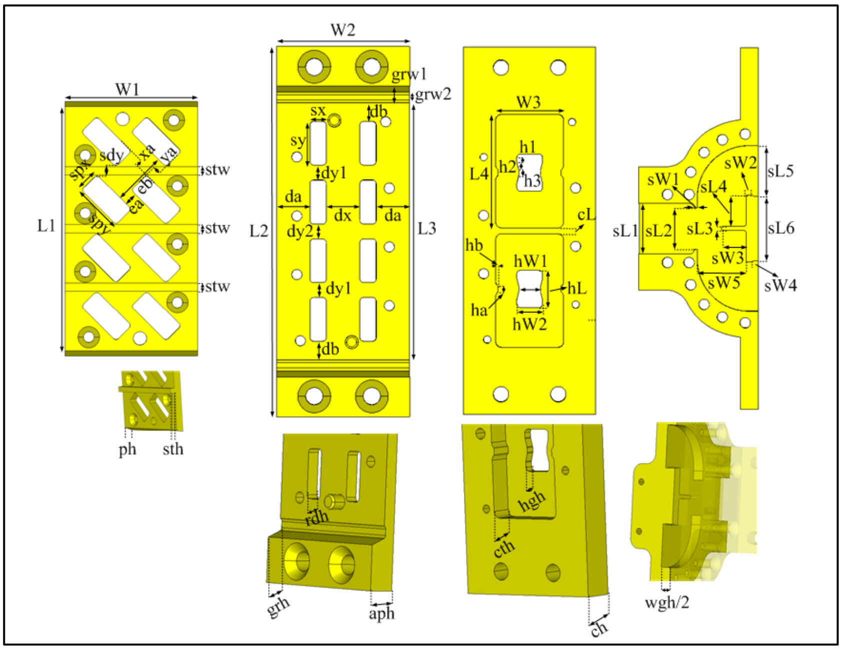

Figure 4.28. +45° Slant polarized dual antenna with variables

Except for the screws, all antenna components are silver plated to improve solderability. This ensures that even the tiniest gaps are filled with solder paste and baked to prevent leakage. The usage of thin metal at the layer where the radiation occurs might cause problems during the manufacturing and assembly processes, as well as affecting the antenna's effectiveness by increasing the antenna's reflection. Groove structures can be employed to solve these assembly challenges and prevent the creation of grating lobes. To avoid these issues in this study, a stub structure is constructed on the horizontal axis between the radiation slots. In order to avoid grating lobes, the elemental spacing must also be properly set. The cavity dimensions are adjusted to increase bandwidth and excite radiating parts with equal amplitude and phase. At both the x ($0.5\lambda_0$) and y ($0.23\lambda_0$) axes, slot spacing is less than one wavelength. Table 4.4 shows the final optimized values for the 2×4 dual array. CST microwave studio's parametric optimization tool is used to optimize the sub array.

Table 4.4. +45° Slant polarized dual antenna dimensions (mm)

L1	**W1**	**spx**	**spy**	**sdy**	**xa**	**ya**	**ea**	**eb**	**stw**
41.193	22.32	3.7	8.28	1.86	1.01	1.34	2.23	9.17	1.4
sth	**ph**	**L2**	**W2**	**L3**	**grw1**	**grw2**	**sx**	**sy**	**dx**
1.42	2.25	61.82	22.32	43.04	25.266	0.89	2.73	7.32	5.6
dy1	**dy2**	**da**	**db**	**rdh**	**grh**	**aph**	**W3**	**L4**	**h1**
2.5	2.5	4.1	3.13	1.89	2.56	4.146	11.48	19.14	0.745
h2	**h3**	**hb**	**ha**	**hL**	**hW1**	**hW2**	**cL**	**hgh**	**cth**
1.174	0.67	0.8	1	6.3	3.65	4.318	1	1.37	3.4
ch	**SL1**	**SL2**	**SL3**	**SL4**	**SL5**	**SL6**	**sW1**	**sW2**	**sW3**
4.77	8.636	7.036	0.7	5.352	8.626	11.024	0.6	1	4.3
sW4	**sW5**	**wgh**							
1	8.4	2.159							

Figure 4.29 shows the simulated electric field distributions on the coupling and radiating slots at 22 GHz, 25 GHz, 28 GHz and 31 GHz.

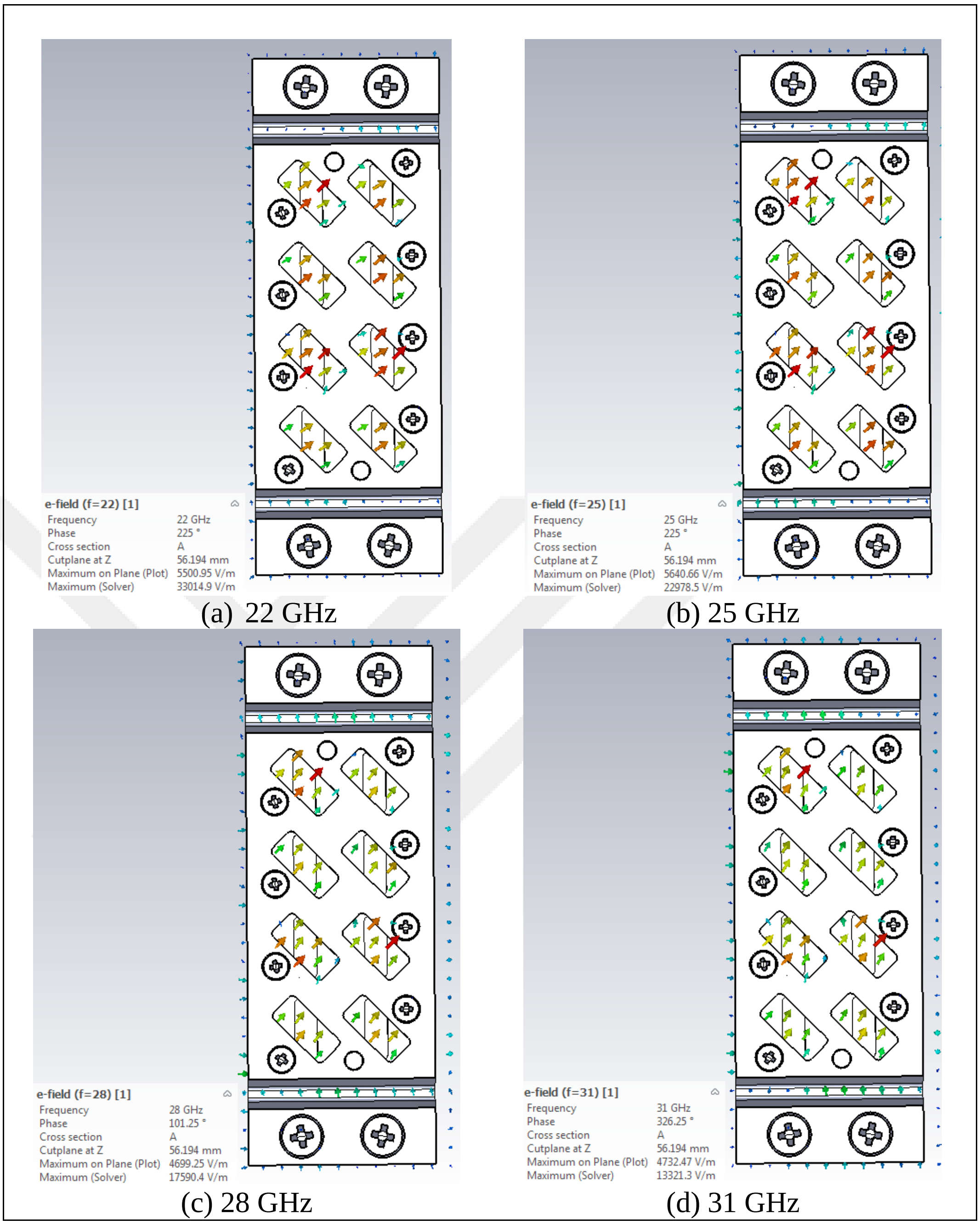

Figure 4.29. Electric field distribution on slots (a) at 22 GHz (b) at 25 GHz (c) at 28 GHz (d) at 31 GHz

After successful design and iterative simulations, the CST model was split into manufacturable parts in Solidworks and sent to production after hundreds of iterations. In the Figure 4.30 below, the horizontal and vertical image of the antenna and its image on the measurement system are given.

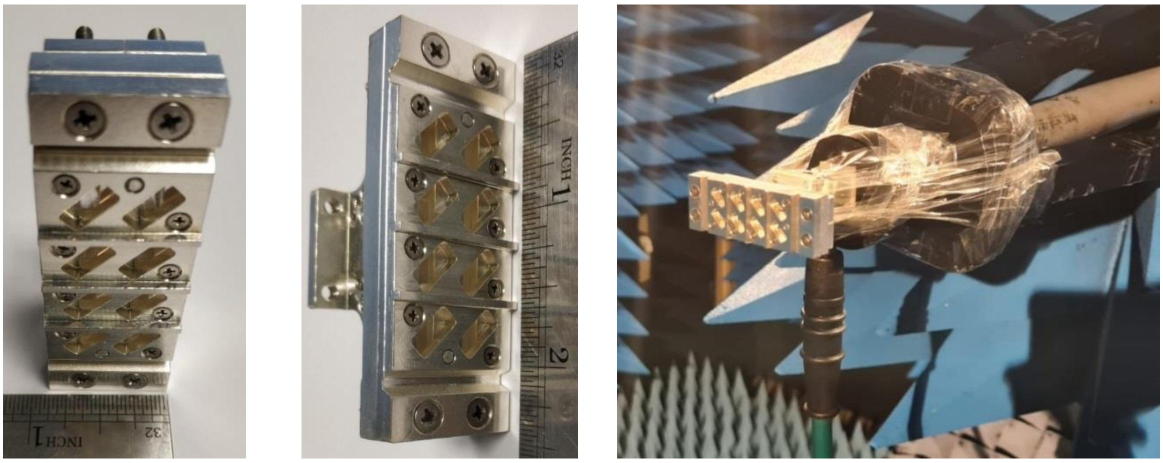

(a) (b) (c)

Figure 4.30. +45° Polarized (a) vertical dimension (b) horizontal dimension (c) On the measurement system in chamber

4.2.1. Simulation and Measurement Results

A network analyzer (R&S ZVA-40) was used to measure the reflection coefficient of the proposed antenna. Compared to the UE antenna, it was observed that the band became slightly wider and the reflection coefficient slightly worsened, but the $|S_{11}|$ value still remained below -15 dB. Measured antenna performance reveal that the antenna has 35.25% fractional bandwidth (FBW) from 22.3 GHz to 32.15 GHz, if $|S_{11}| < -10\,\text{dB}$, and 31.26% FBW between 22.2 GHz and 31.7 GHz, if $|S_{11}| < -14\,\text{dB}$ (VSWR < 1.5). A comparison of measurement and simulation results is given in the Figure 4.11 below.

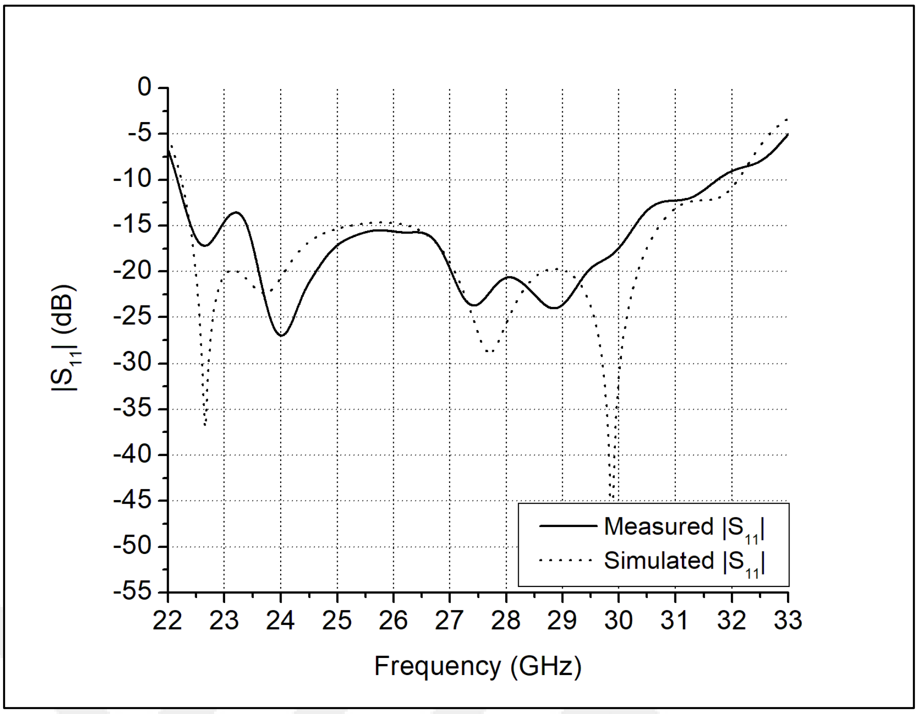

Figure 4.31. +45° Polarized dual antenna simulated vs measured reflection coefficient

The photograph of the antenna in the laboratory environment when the measurement is performed against the network analyzer is given in the Figure 4.32.

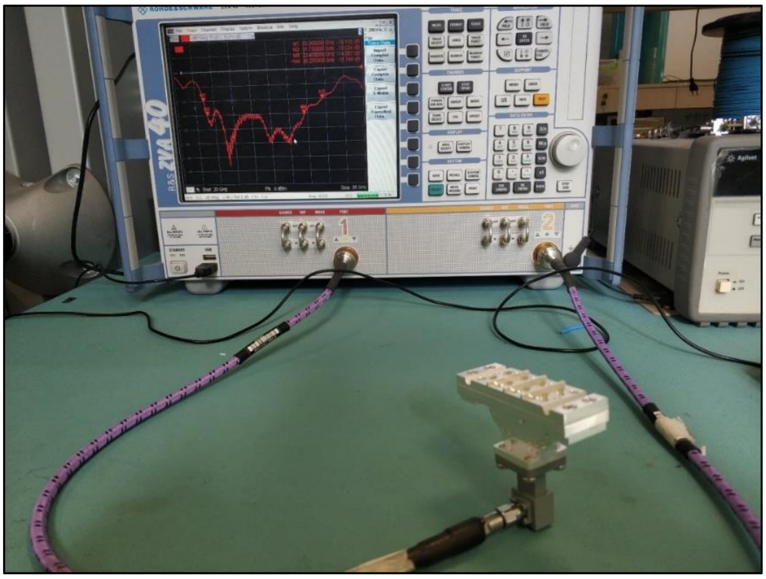

Figure 4.32. +45° Polarized dual antenna measured reflection coefficient with ZVA40 vector network analyzer

The gain measurement of the antenna was performed in the full anechoic chamber using the spherical measurement system. The difference between measured and simulated boresight improvements is less than 1.1 dB within the target band of 23 to 30.7 GHz, as shown in Figure 4.33. Within the intended band, measured gain ranged from 17 to 18.1 dBi.

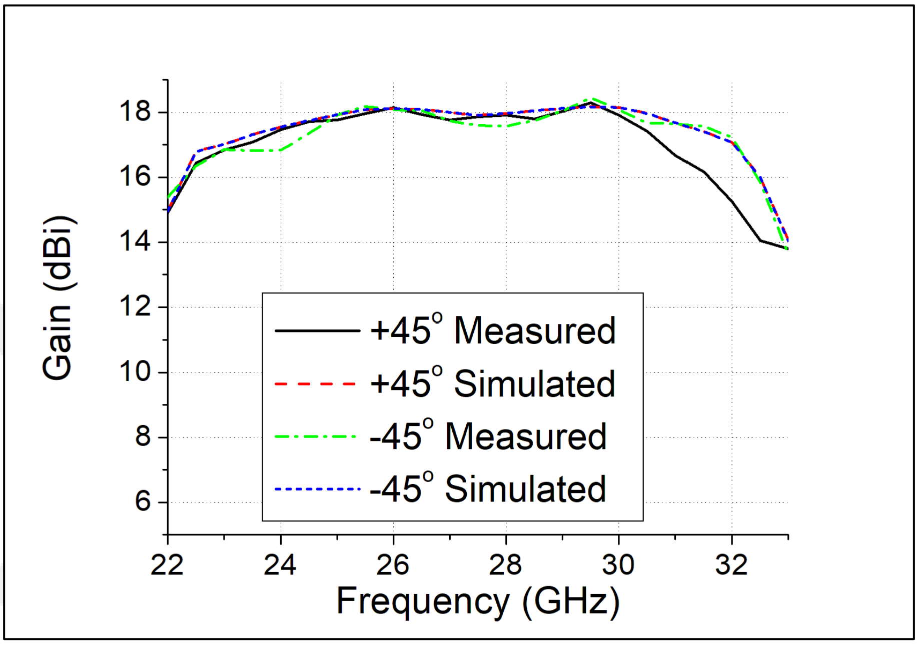

Figure 4.33. Boresight gain of the dual antenna

Figure 4.34 shows the HPBWs for Azimuth and Elevation for +45° and -45° slant polarized dual antenna. The measured and simulated results are fairly similar. For the Azimuth and Elevation planes, HPBW variation throughout the target bandwidth is +/-2.5° and +/-2.15°, respectively between 24.25 GHz and 29.5 GHz.

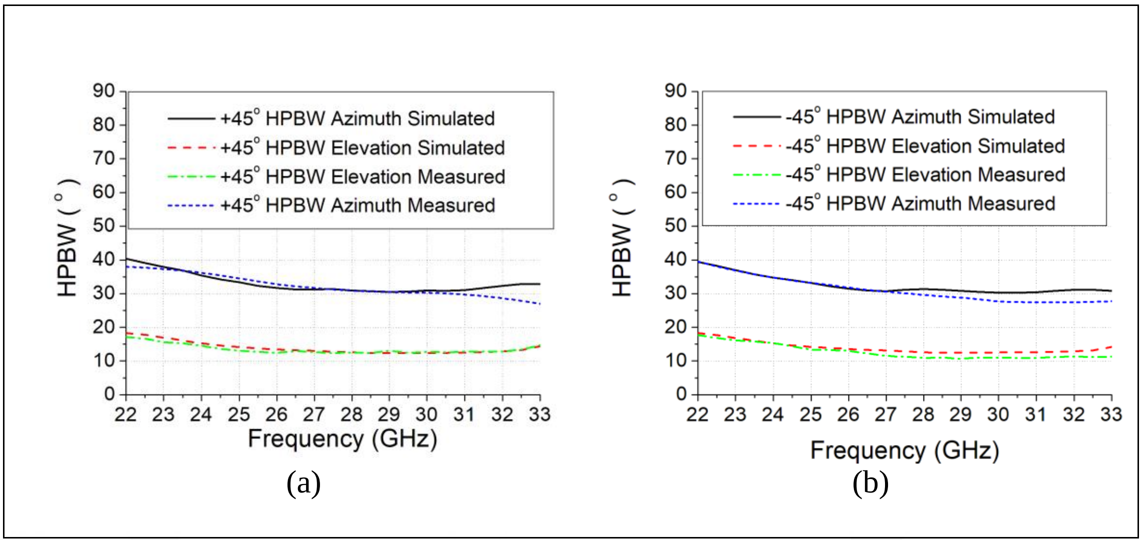

Figure 4.34. HPBW of a) +45° b) -45° Slant Polarized Dual Antenna

For the frequency points 22 to 31 GHz with 0.5 GHz steps, radiation pattern measurements of the constructed antennas are done in an anechoic chamber using a commercially available spherical near field measurement device. Figure 4.35-Figure 4.53 illustrates the results for +45 slant polarized dual antenna on elevation and azimuth planes.

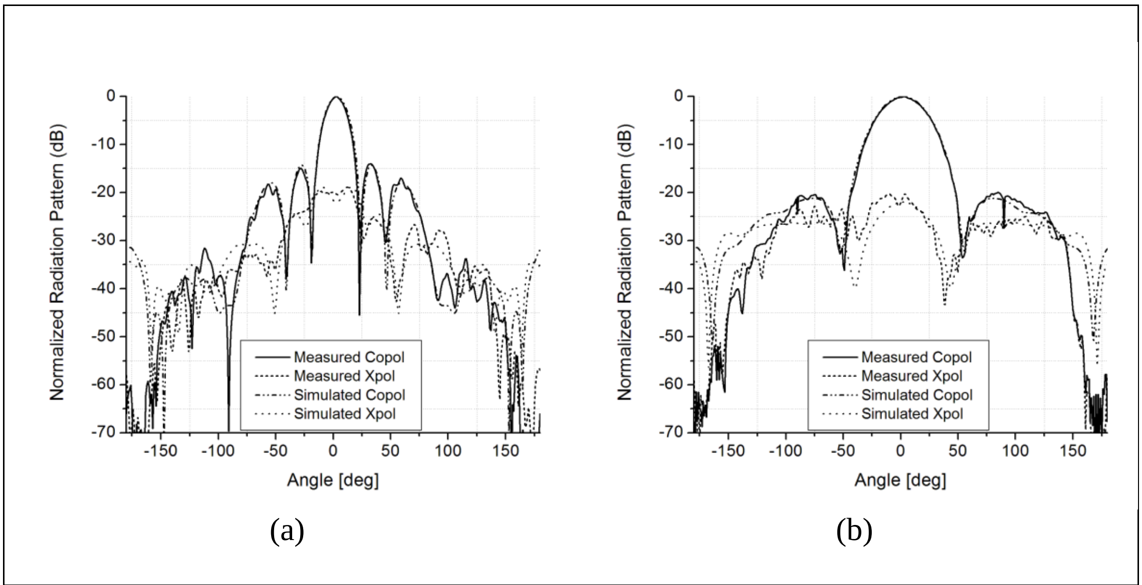

Figure 4.35. Normalize pattern at 22 GHz, (a) Elevation, (b) Azimuthal

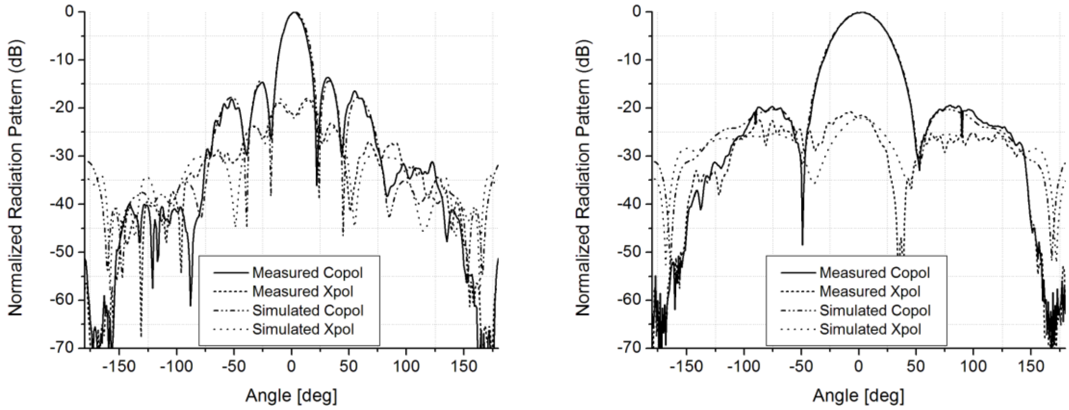

(a) (b)

Figure 4.36. Normalize pattern at 22.5 GHz, (a) Elevation, (b) Azimuthal

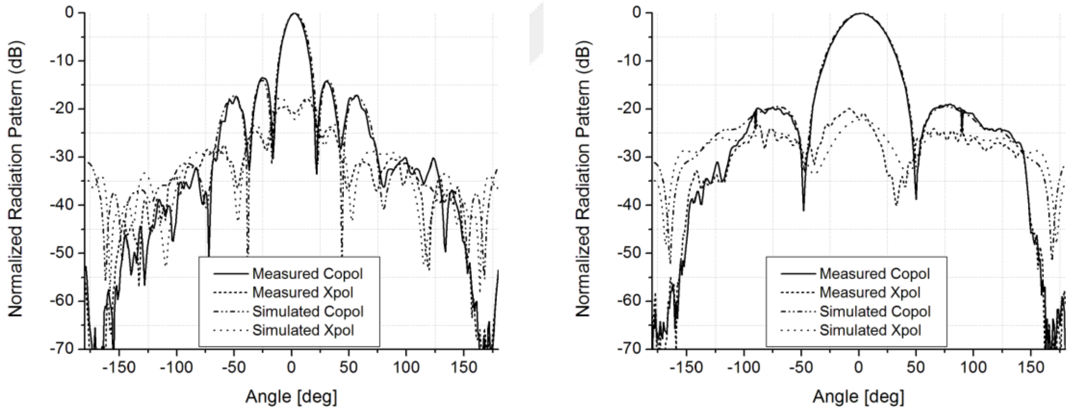

(a) (b)

Figure 4.37. Normalize pattern at 23 GHz, (a) Elevation, (b) Azimuthal

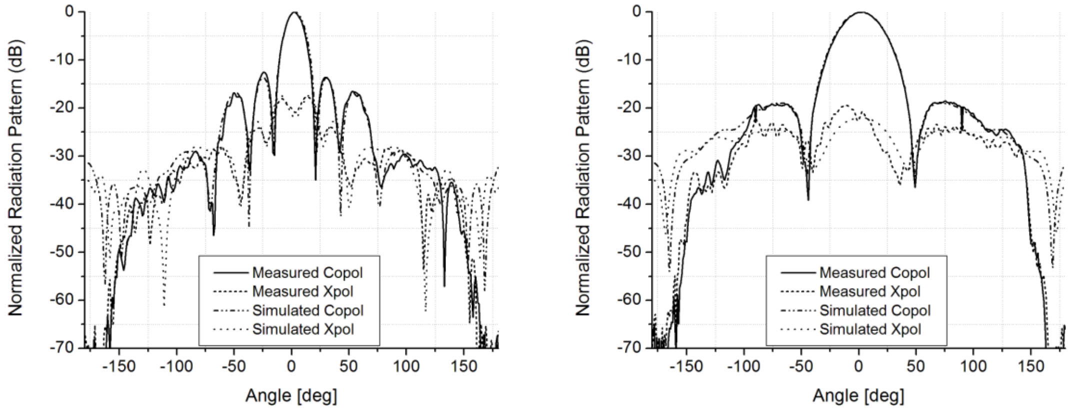

(a) (b)

Figure 4.38. Normalize pattern at 23.5 GHz, (a) Elevation, (b) Azimuthal

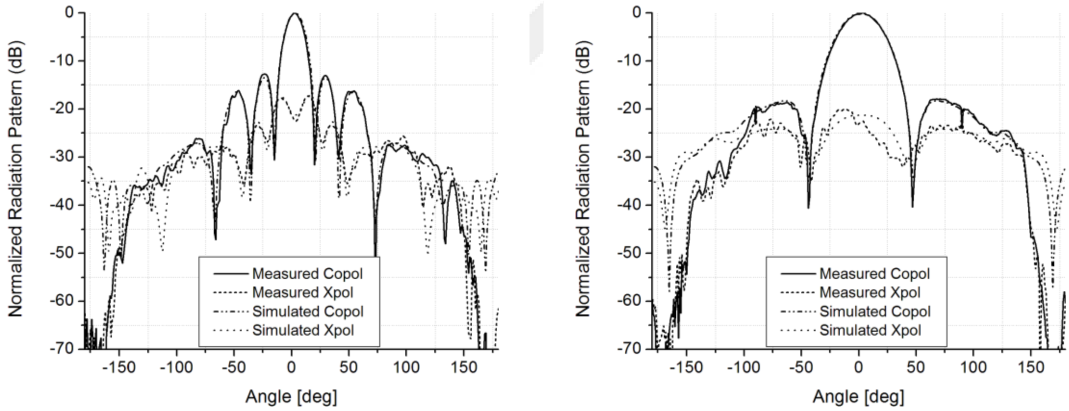

(a) (b)

Figure 4.39. Normalize pattern at 24 GHz, (a) Elevation, (b) Azimuthal

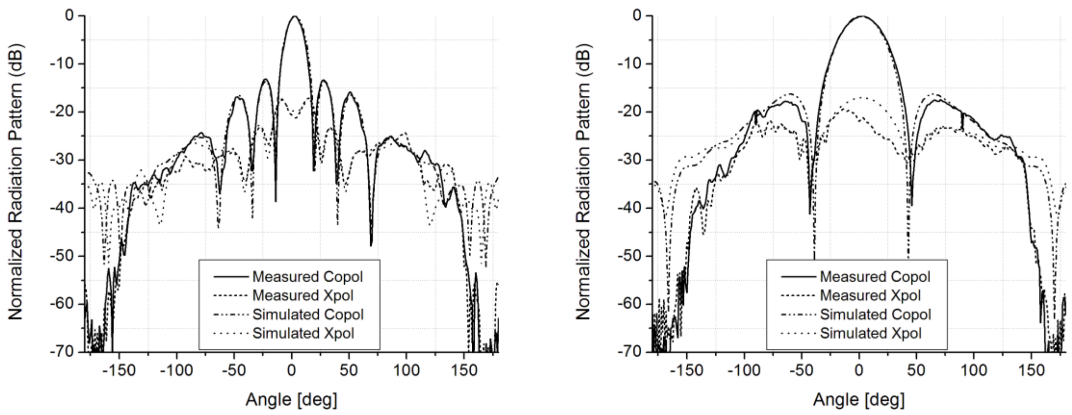

(a) (b)

Figure 4.40. Normalize pattern at 24.5 GHz, (a) Elevation, (b) Azimuthal

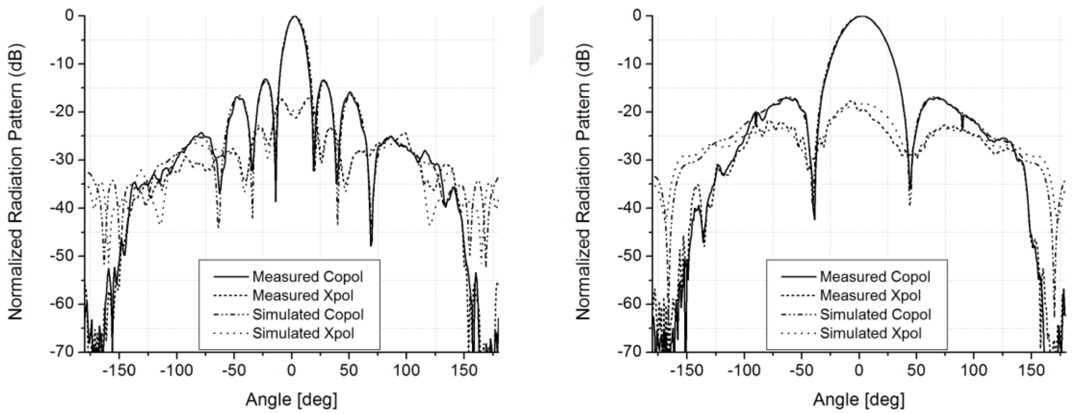

(a) (b)

Figure 4.41. Normalize pattern at 25 GHz, (a) Elevation, (b) Azimuthal

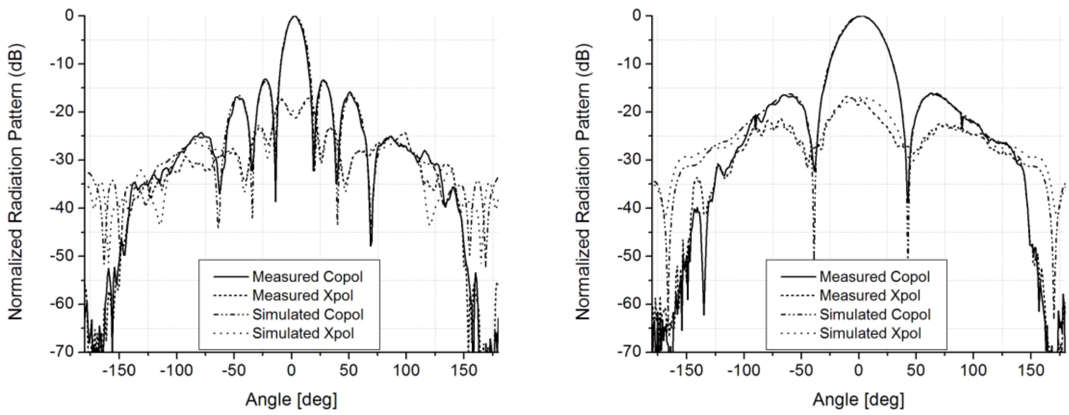

(a) (b)

Figure 4.42. Normalize pattern at 25.5 GHz, (a) Elevation, (b) Azimuthal

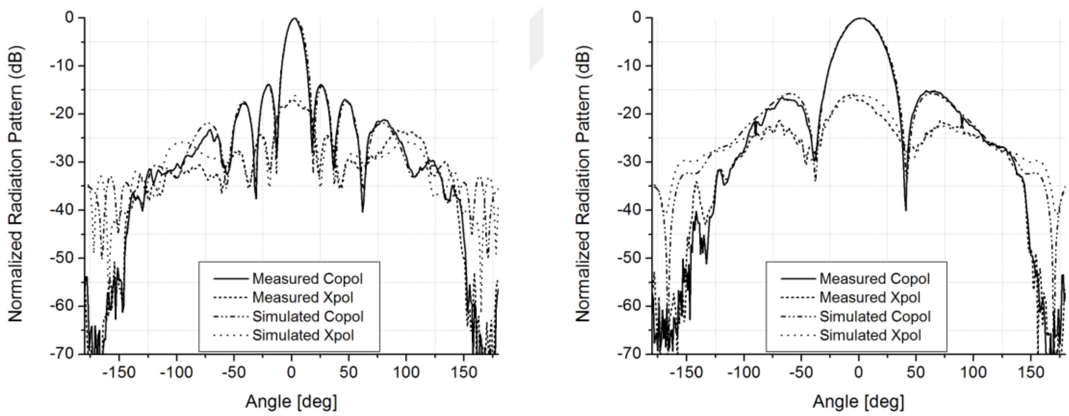

(a) (b)

Figure 4.43. Normalize pattern at 26 GHz, (a) Elevation, (b) Azimuthal

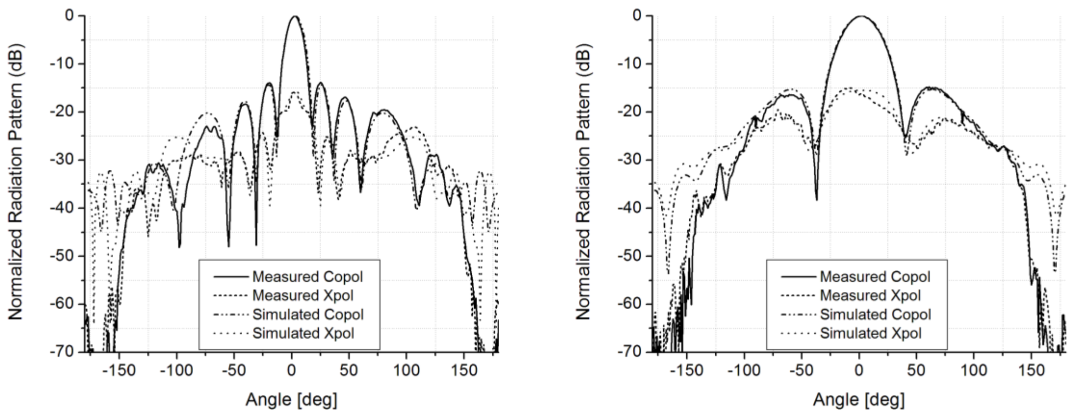

(a) (b)

Figure 4.44. Normalize pattern at 26.5 GHz, (a) Elevation, (b) Azimuthal

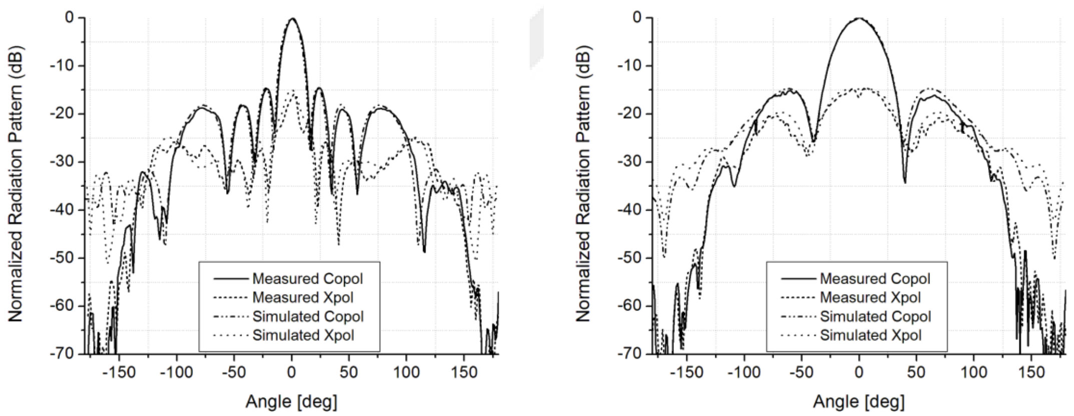

(a) (b)

Figure 4.45. Normalize pattern at 27 GHz, (a) Elevation, (b) Azimuthal

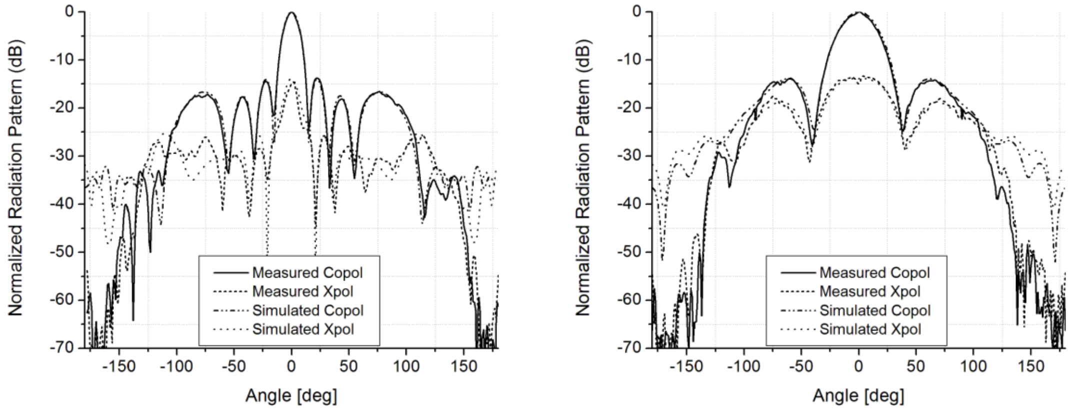

(a) (b)

Figure 4.46. Normalize pattern at 27.5 GHz, (a) Elevation, (b) Azimuthal

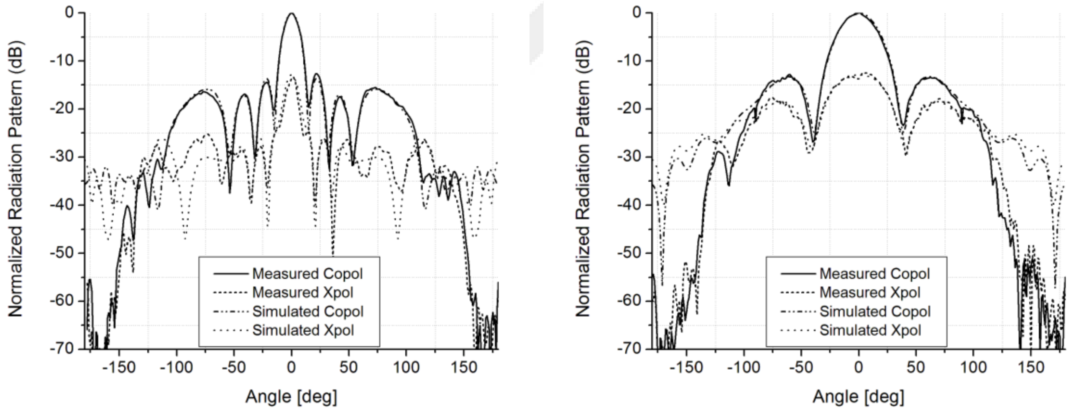

(a) (b)

Figure 4.47. Normalize pattern at 28 GHz, (a) Elevation, (b) Azimuthal

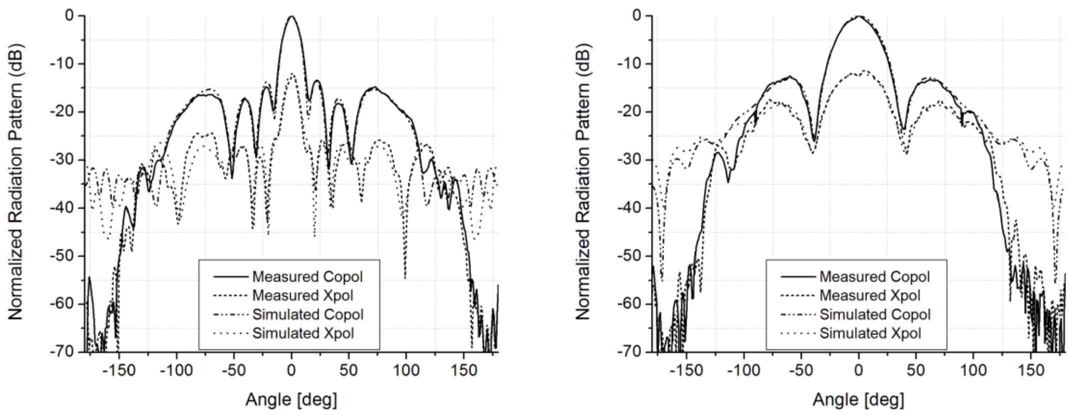

(a) (b)

Figure 4.48. Normalize pattern at 28.5 GHz, (a) Elevation, (b) Azimuthal

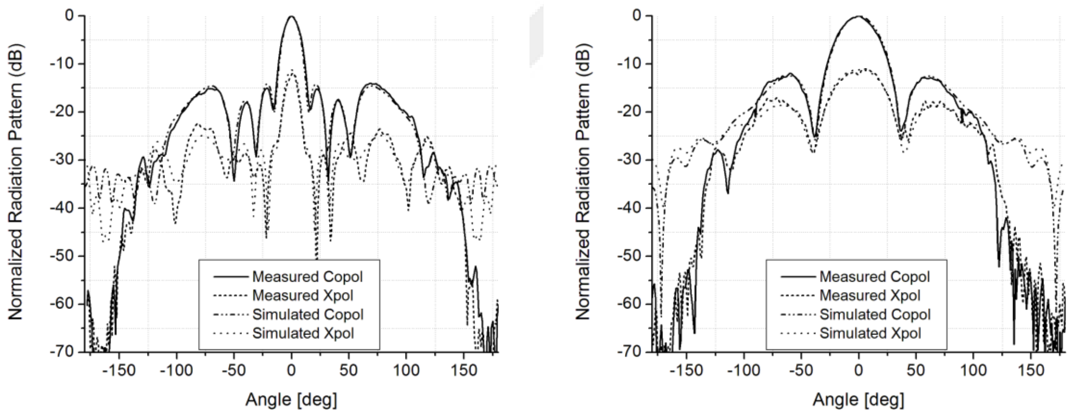

a) b)

Figure 4.49. Normalize pattern at 29 GHz, (a) Elevation, (b) Azimuthal

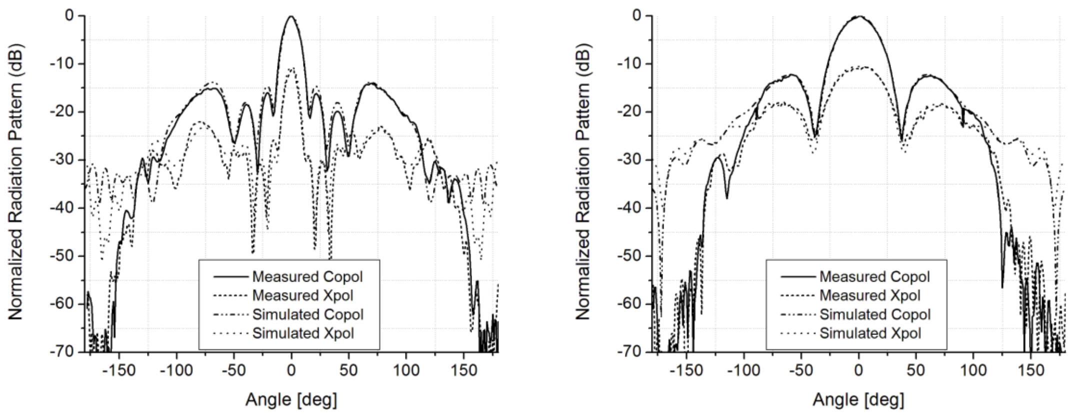

(a) (b)

Figure 4.50. Normalize pattern at 29.5 GHz, (a) Elevation, (b) Azimuthal

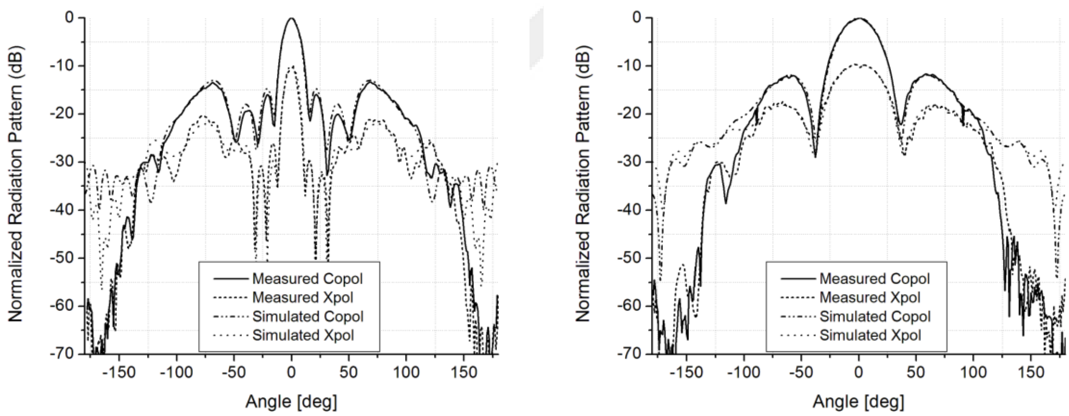

(a) (b)

Figure 4.51. Normalize pattern at 30 GHz, (a) Elevation, (b) Azimuthal

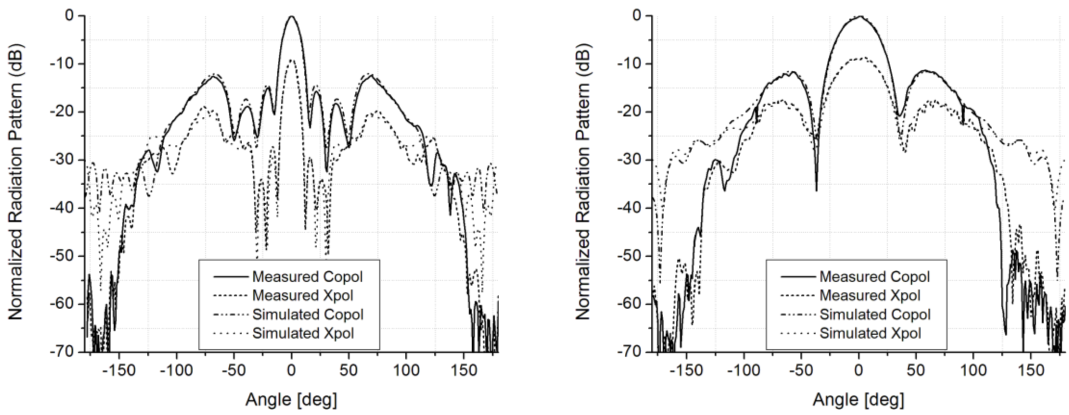

(a) (b)

Figure 4.52. Normalize pattern at 30.5 GHz, (a) Elevation, (b) Azimuthal

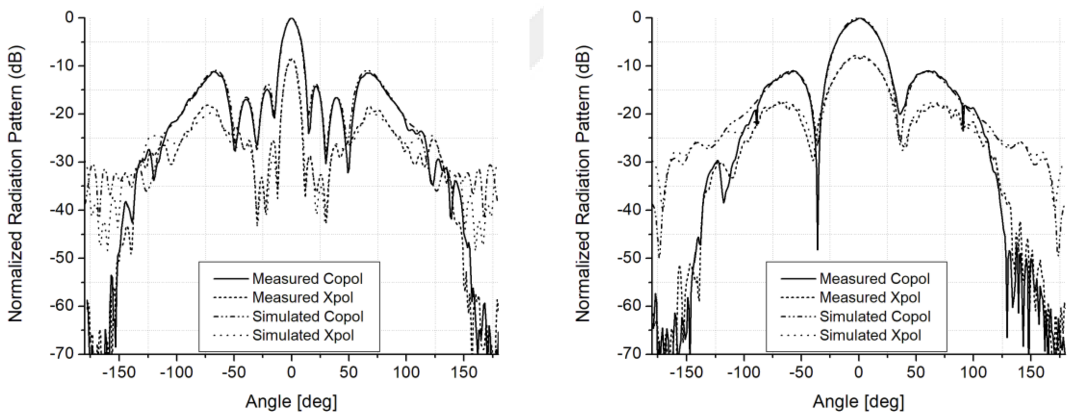

(a) (b)

Figure 4.53. Normalize pattern at 31 GHz, (a) Elevation, (b) Azimuthal

At and around boresight directions, measured and simulated patterns are quite similar, although there is considerable disagreement towards the back of the antenna where cross-polarization and co-polarization levels are close to each other. Despite the fact that the measured and simulated radiation patterns are absolutely consistent, especially for the mainlobe, there is a discrepancy after 45°. While the variation is minimal between 45° and 130° due to the antenna under test being mounted on the measurement system, it increases significantly after 130° due to the azimuth axis rotator and positioner system being blocked. The first SLL levels for both the Azimuth and Elevation Planes are below -13dB, while the XPol values for both the Azimuth and Elevation Planes are better than -10dB.

4.3. ±45° SLANT POLARIZED 2X4 SLOT ARRAY CAVITY BACK DUAL WAVEGUIDE ANTENNA

Space diversity is much less practical at the base station than it is at the mobile because the small angle of incidence fields necessitates huge antenna spacings. For broadside propagation, base station antennas must be distanced by 25λ , and for in-line propagation, they must be spaced by well over 100λ. Due to the high costs of spatial diversity at the base station, orthogonal polarizations are being considered. Space diversity [45], [46] and polarization diversity [47] have been the main focus of research into base station diversity reception systems. Effective diversity can be obtained with a correlation coefficient of less than 0.7 in general [48], [49]. Space diversity for a base station requires antenna spacing of up to around 20 wavelengths for the broadside case, and more for the in-line case, to keep correlation below 0.7. Mounting a diversity antenna on a tower with a 20λ antenna spacing can be difficult at times. Polarization diversity at a base station, on the other hand, does not necessitate antenna space [50]. Between the mobile units and the base station, there was no direct line of sight. Therefore, the transceiver antenna pair, designed as ±45° slant polarized, is combined on a single body in order to work in harmony with the beamforming network structure at the base station. This structure is formed by combining two antennas with +45° and -45° slant polarity above and is shown in the Figure 4.54 below.

Antenna dimensions are the same as in dual antenna construction, where the critical parameters are the distances between slots with different polarization. These values are given in Table 4.5.

Table 4.5. ±45° Slant polarized dual antenna unknown dimensions (mm)

aW1	aW2	aW3
5.95	11.2	10.84

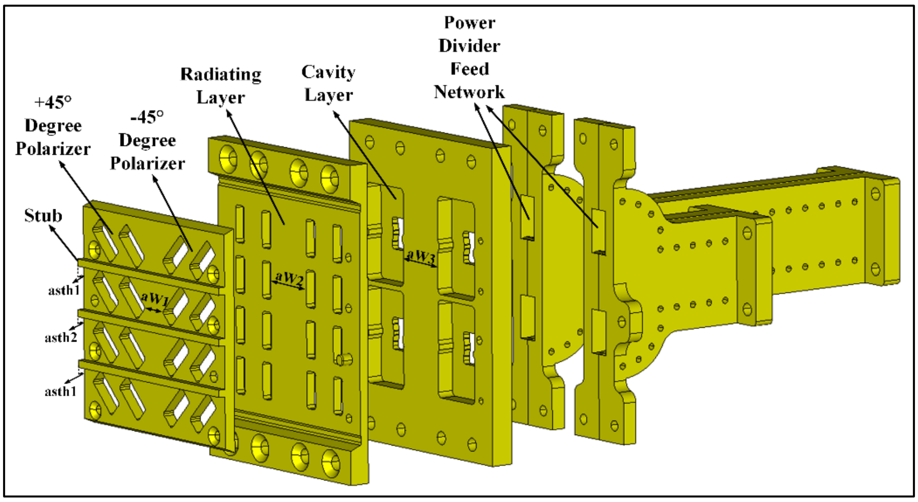

Figure 4.54. ±45° Slant Polarized Dual Antenna with variables

Because the antenna is fed from two different ports, the electric field distributions on the antenna surface are illustrated separately. When the field distributions are analyzed, it can be seen that the TE10 mode is spread out and that the two antennas have minor effect on each other, the field distributions are shown in two different representations.

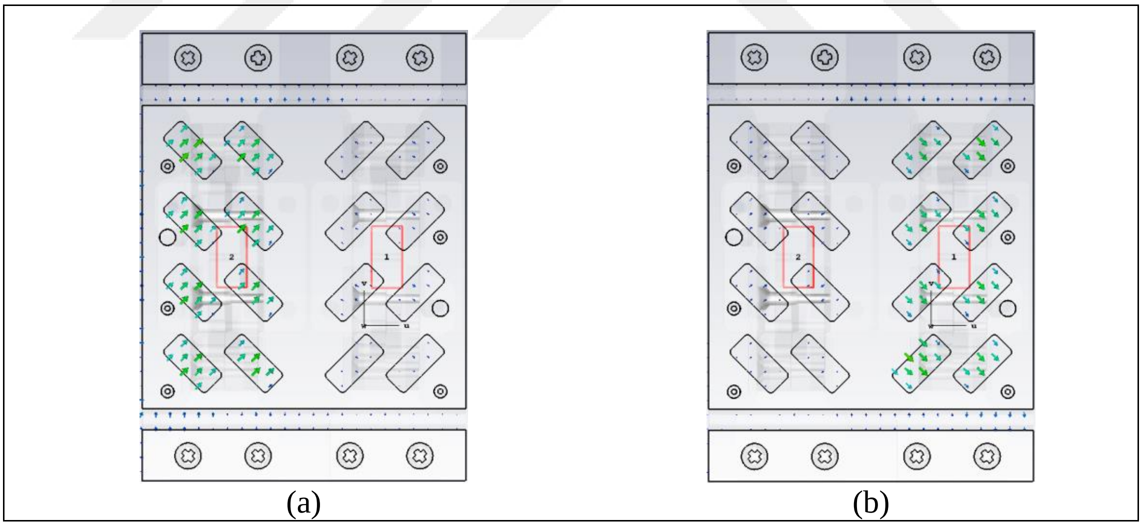

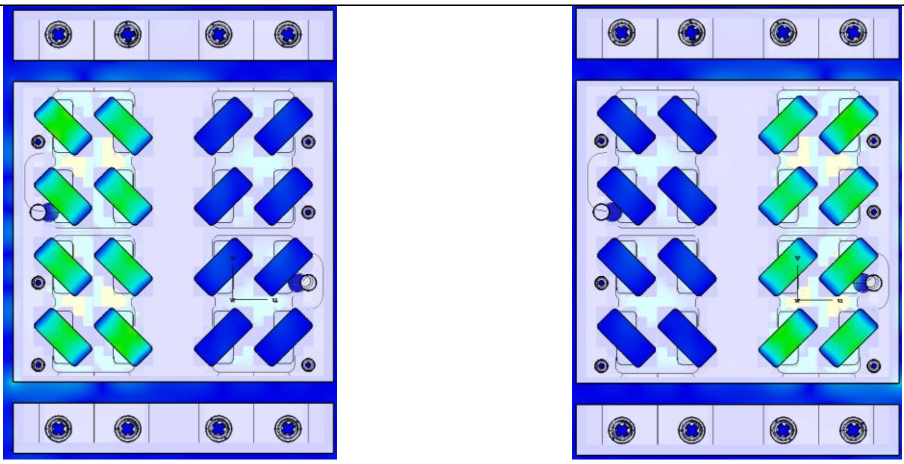

(c) (d)

Figure 4.55. ±45° Slant polarized dual antenna E-fields Z-cutplane

The power splitter structure, which distributes equal amplitude and phase in the antenna structure, is of critical importance. When the field distributions on two separate ports are observed, it is seen that the amplitude phase values are shared equally. The propagation of the electric field along the waveguide ports is shown in the Figure 4.56 below, on the X-axis section.

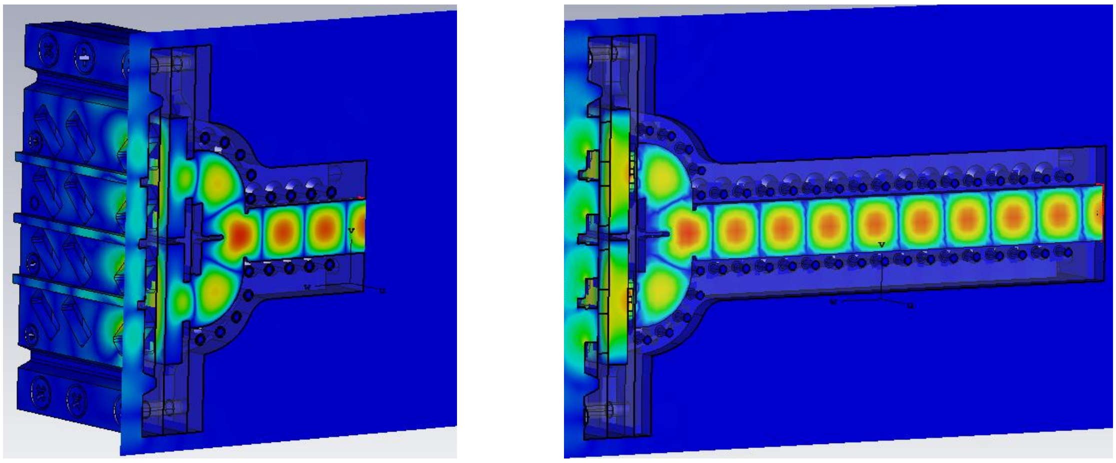

(a) (b)

Figure 4.56. ±45° Slant polarized dual antenna E-fields X-cutplane

The antenna structure was manufactured piecemeal in CNC, with dimensions of $4.06\lambda_0$ on the x-axis and $5.62\lambda_0$ on the y-axis when combined, and the outer surfaces of the parts were coated with silver. The photo of the antenna produced and assembled is given in the Figure 4.57 below.

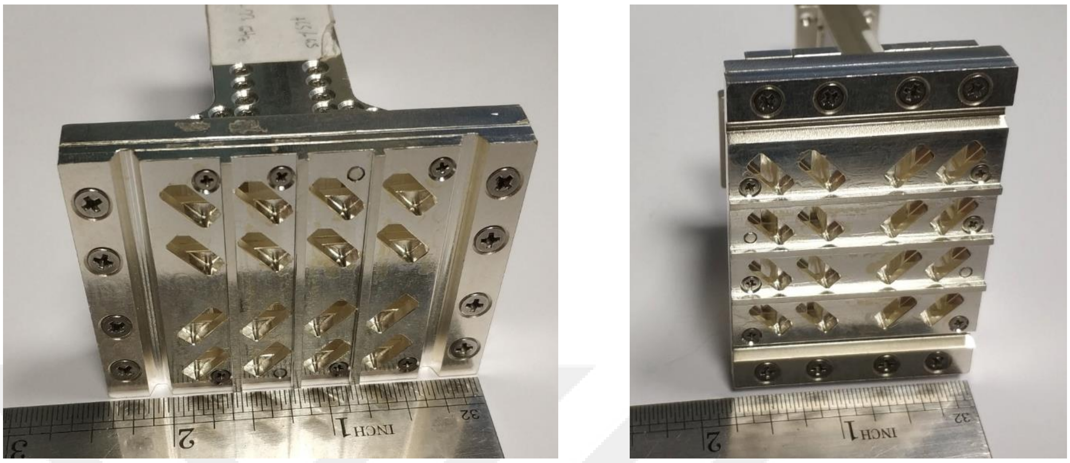

(a) (b)

Figure 4.57. ±45° slant polarized dual antenna (a) vertical dimension (b) horizontal dimension

4.3.1. Simulation and Measurement Results

The reflection coefficient measurements of the antenna were performed using a network analyzer (R&S ZVA-40). The following figure shows the measurement performed in the laboratory environment and the device attached to the spherical antenna measurement system.

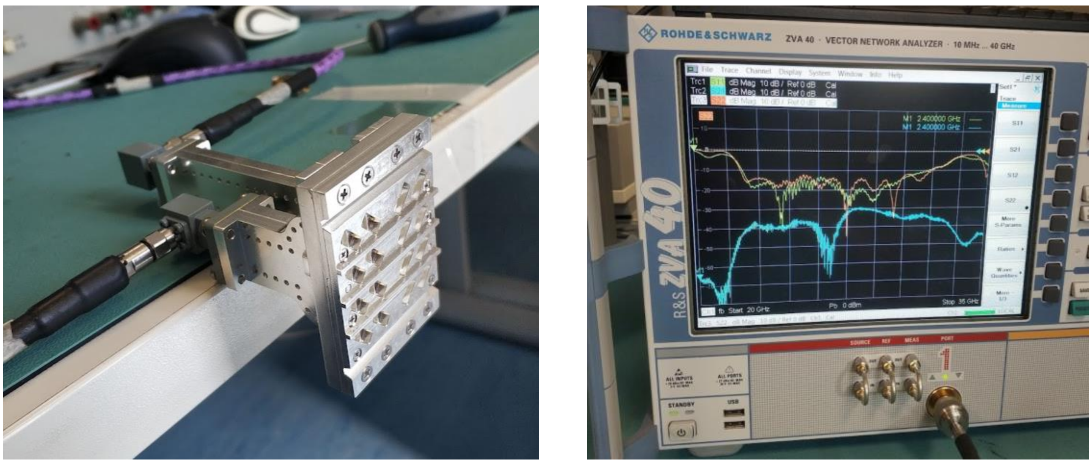

(a) (b)

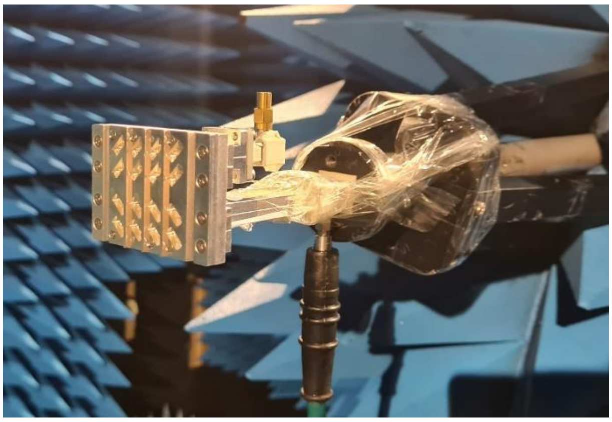

(c)

Figure 4.58. ±45° polarized dual antenna measured reflection coefficient with ZVA40 vector network analyzer (a) Antenna under test (b) Measurement results (c) Antenna in the chamber

The simulations and measurements are pretty accurate and the results are consistent with the dual antennas results. The antennas have 33.7% fractional bandwidth (FBW) from 22.2 GHz to 31.2 GHz if $|S_{11}| < -10\,\text{dB}$ (VSWR 1.5), and for +45° slant polarized side 30.2% FBW between 22.7 GHz and 30.2 GHz, for -45° slant polarized side 27% FBW between 22.7 GHz and 39.2 GHz, if $|S_{11}| < -14\,\text{dB}$ (VSWR 1.5), according to measured antenna performance. The antenna gain was measured using the spherical measurement system in a fully anechoic environment. Within the target band of 24.25 to 29.5 GHz, the difference between measured and simulated boresight improvements is less than 1.1 dB.

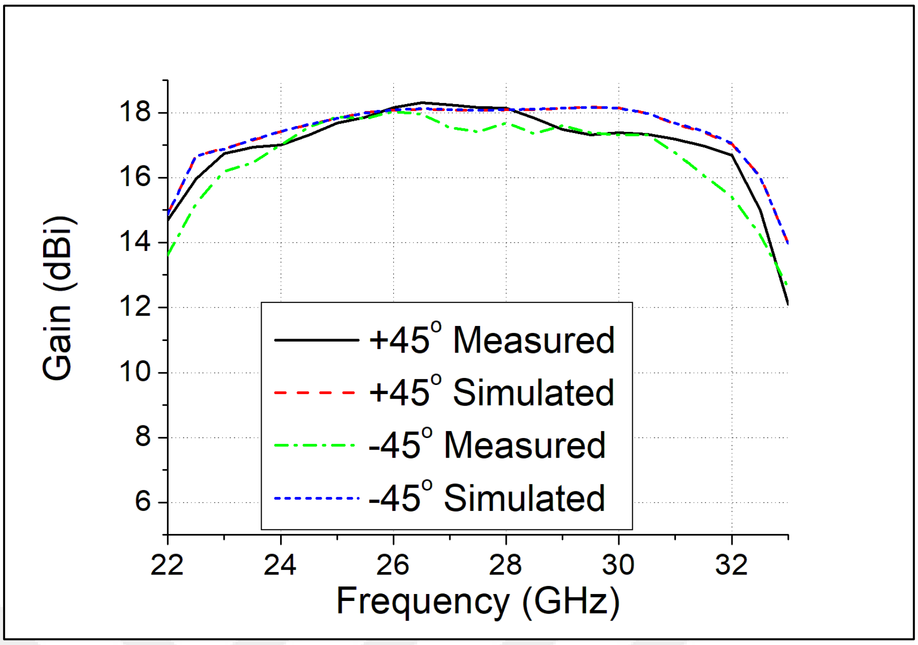

Figure 4.59. Boresight gain of the ±45° slant polarized dual antenna

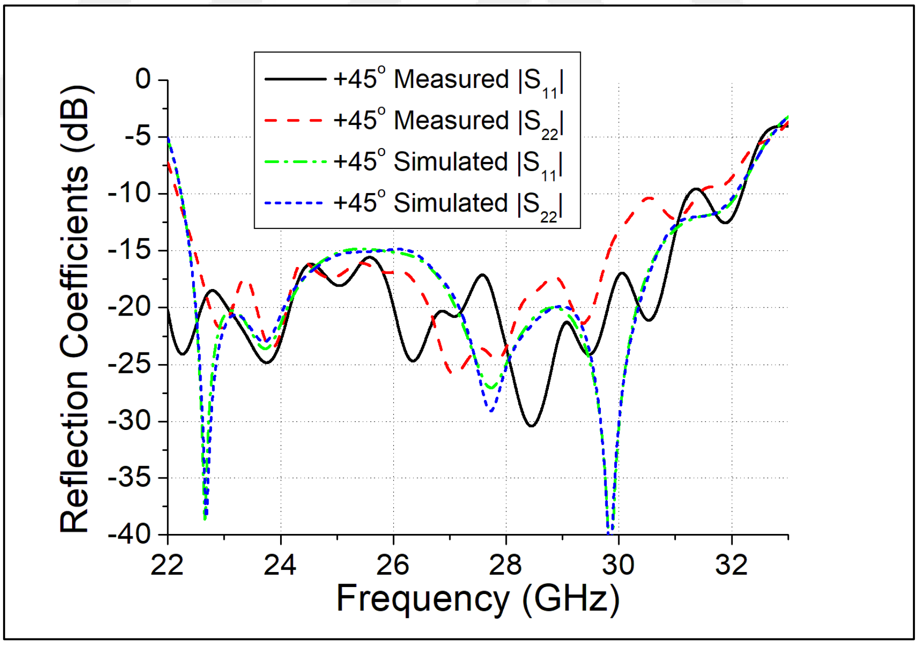

Figure 4.60. ±45° Slant polarized dual antenna simulated vs measured reflection coefficient

The S21 value, which is one of the most critical values in this antenna, in other words the coupling between the transceiver antenna, is below -30 dB throughout the band. Given that a value of less than -25 dB is considered excellent, the performance obtained is absolutely remarkable. This value is also the isolation value between two antennas, and the measurement and simulation results are given in the figure below.

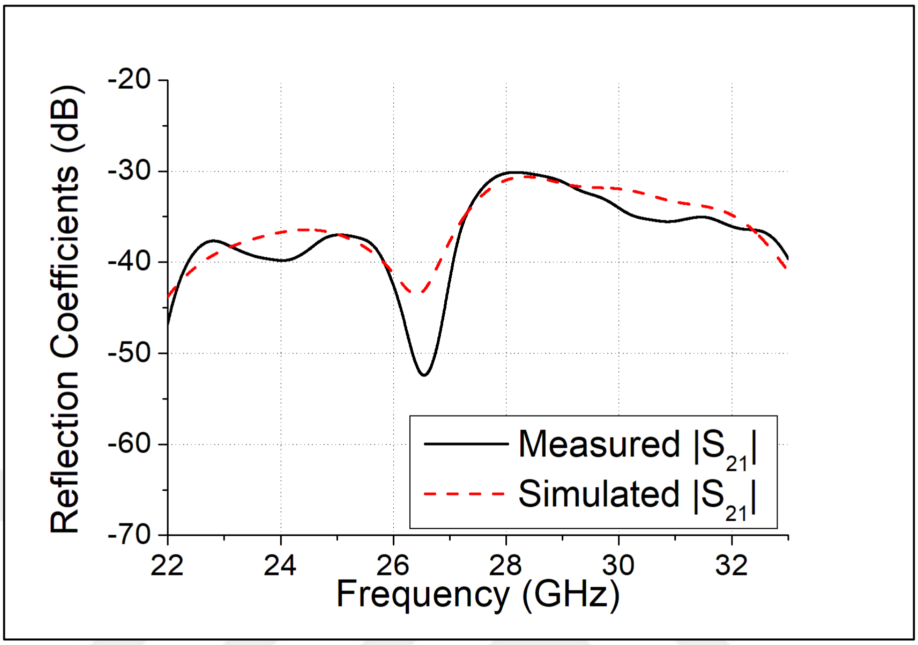

Figure 4.61. ±45° Slant polarized dual antenna simulated vs measured isolation level $|S_{21}|$

The radiation pattern of this antenna was measured in the near-field spherical measurement system, as in the antennas above. Since there are two antennas with +45° and -45° slant polarization in this antenna structure, the radiation patterns for both antennas are extracted separately. Figure 4.62-Figure 4.80 shows the radiation patterns in the azimuth and elevation plane of the antenna with +45° slant polarization. Figure 4.81-Figure 4.98 shows the radiation patterns in the azimuth and elevation plane of the antenna with -45° slant polarization.

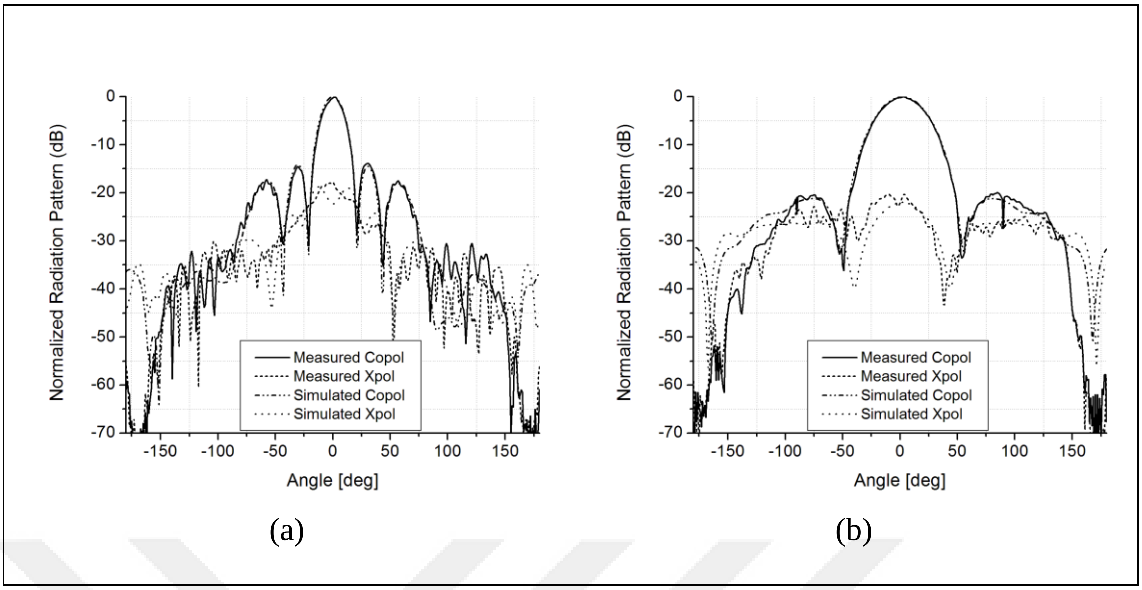

Figure 4.62. Normalize pattern of +45º slant polarized antenna at 22 GHz, (a) Elevation, (b) Azimuthal

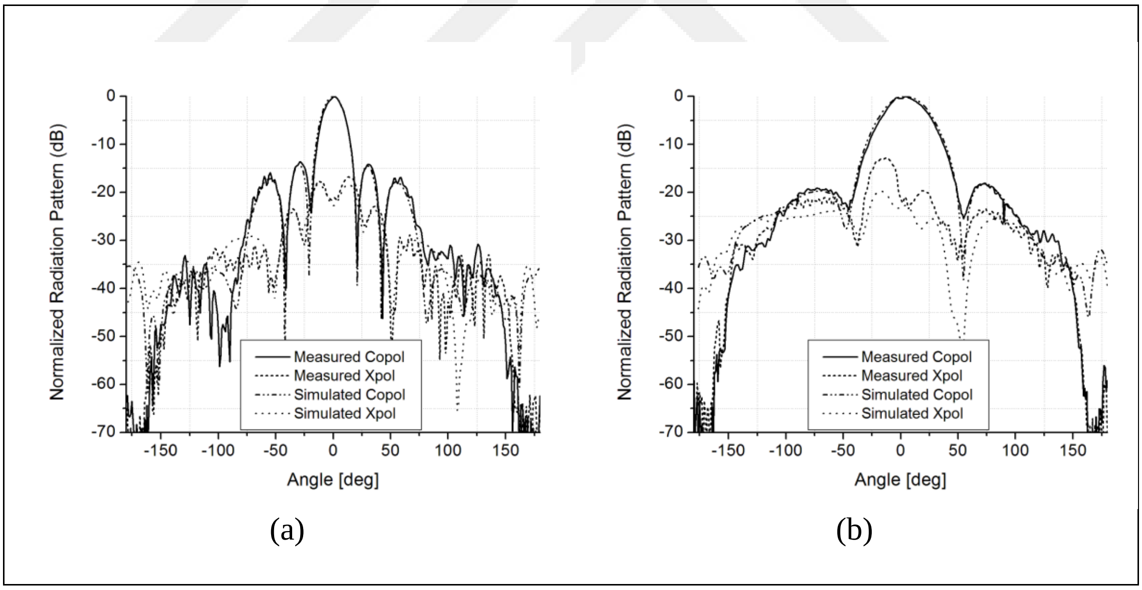

Figure 4.63. Normalize pattern of +45º slant polarized antenna at 22.5 GHz, (a) Elevation, (b) Azimuthal

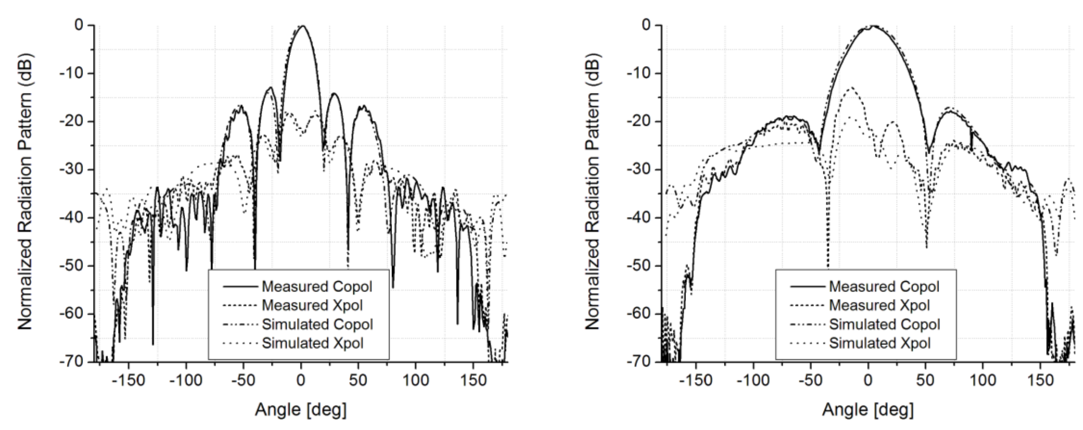

(a) (b)

Figure 4.64. Normalize pattern of +45º slant polarized antenna at 23 GHz, (a) Elevation, (b) Azimuthal

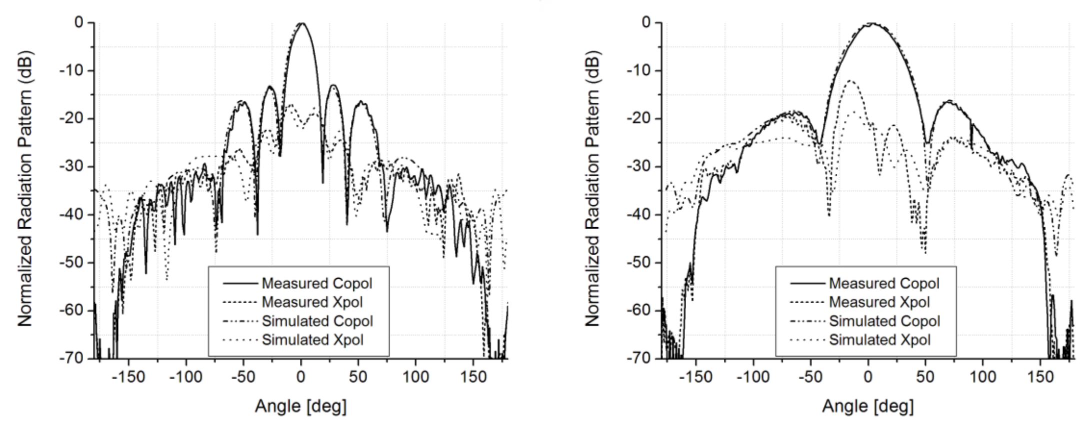

a) b)

Figure 4.65. Normalize pattern of +45º slant polarized antenna at 23.5 GHz, (a) Elevation, (b) Azimuthal

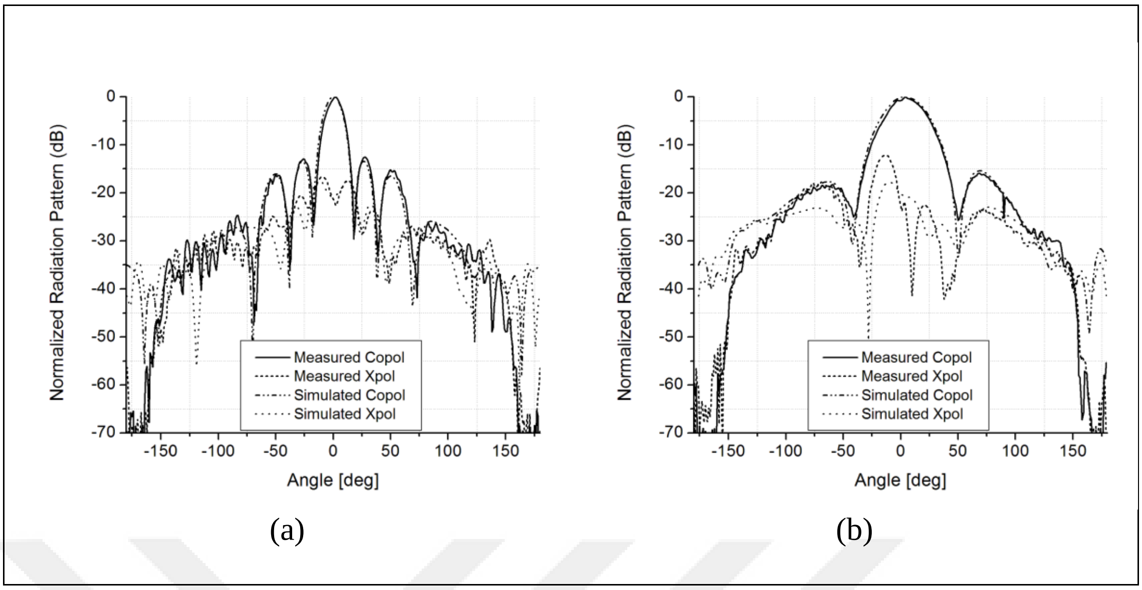

Figure 4.66. Normalize pattern of +45º slant polarized antenna at 24 GHz, (a) Elevation, (b) Azimuthal

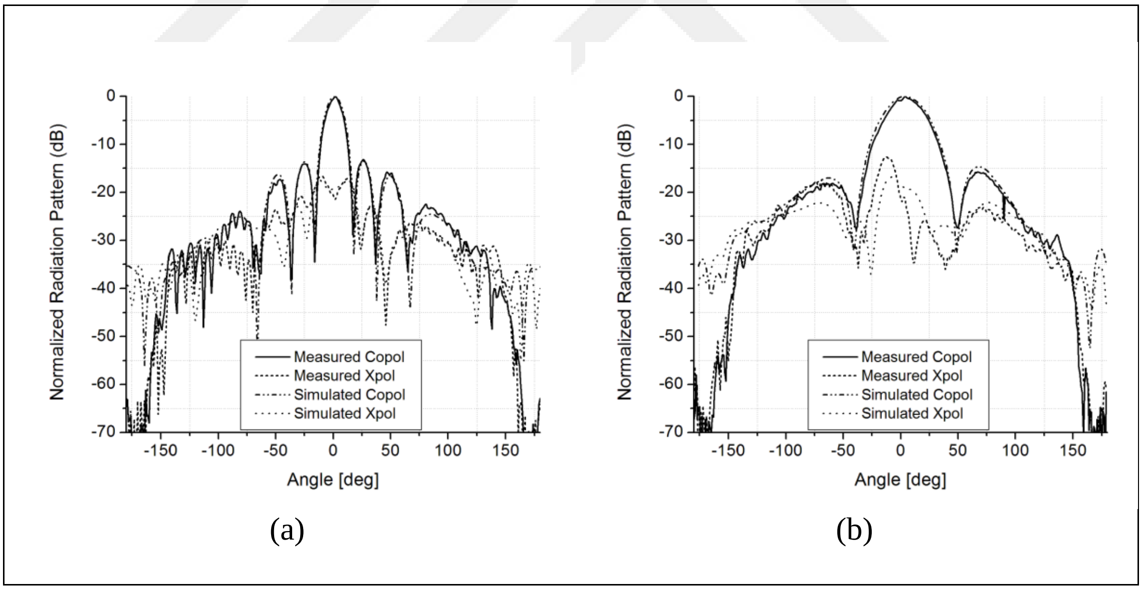

Figure 4.67. Normalize pattern of +45º slant polarized antenna at 24.5 GHz, (a) Elevation, (b) Azimuthal

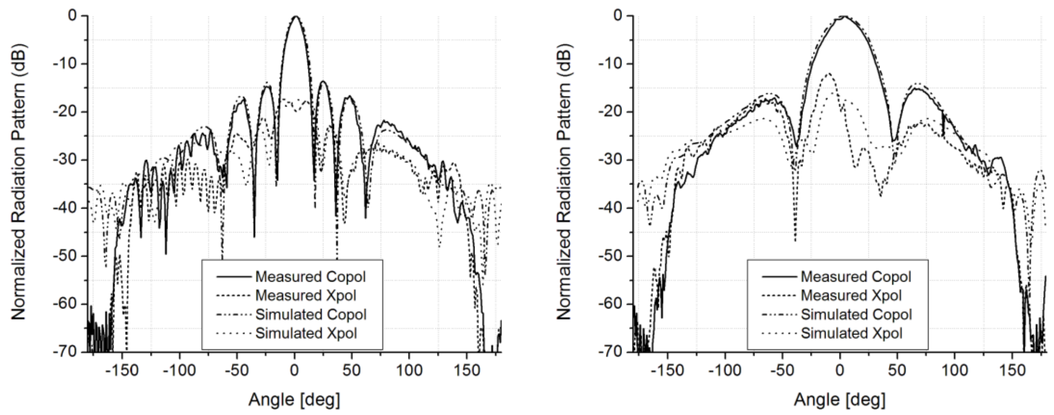

(a) (b)

Figure 4.68. Normalize pattern of +45º slant polarized antenna at 25 GHz, (a) Elevation, (b) Azimuthal

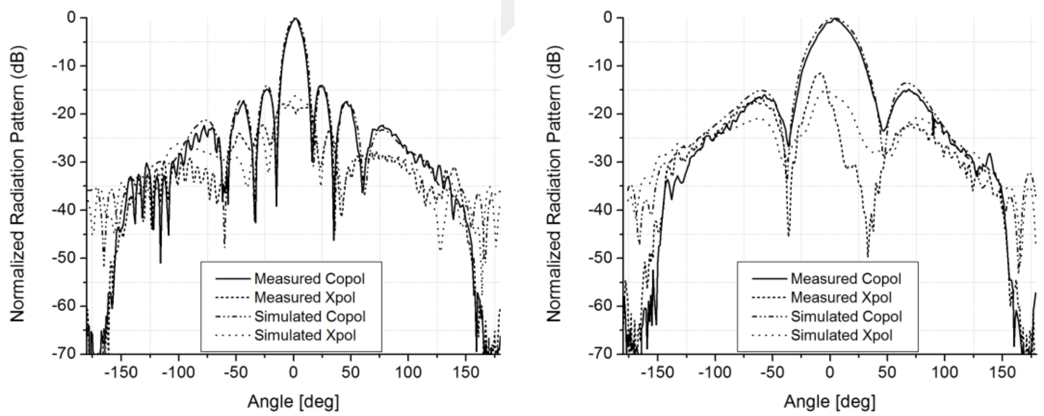

(a) (b)

Figure 4.69. Normalize pattern of +45º slant polarized antenna at 25.5 GHz, (a) Elevation, (b) Azimuthal

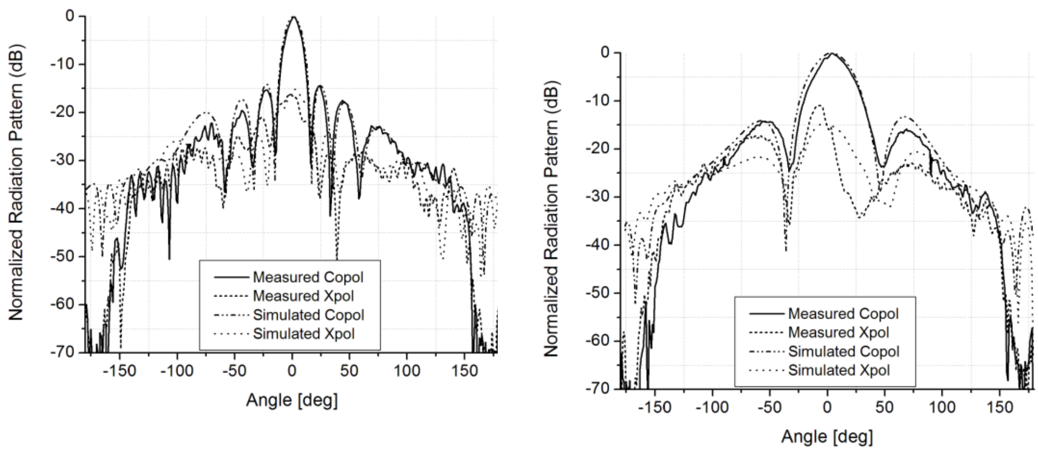

(a) (b)

Figure 4.70. Normalize pattern of +45º slant polarized antenna at 26 GHz, (a) Elevation, (b) Azimuthal

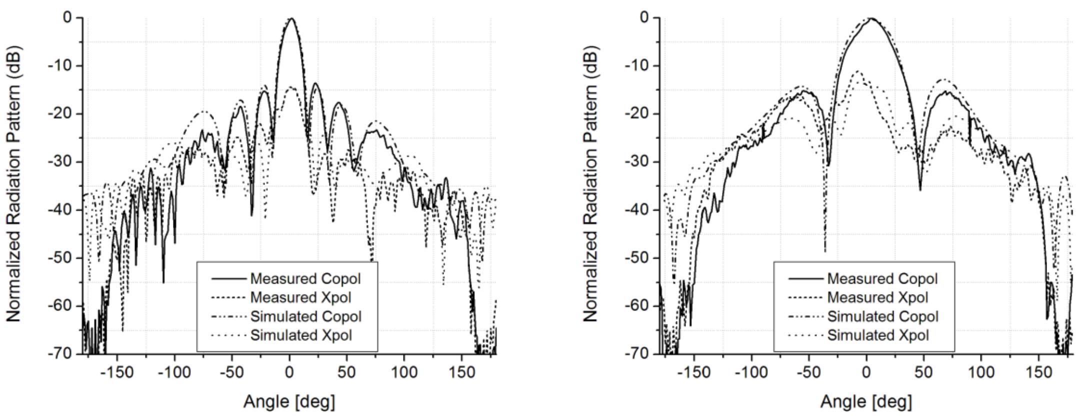

(a) (b)

Figure 4.71. Normalize pattern of +45º slant polarized antenna at 26.5 GHz, (a) Elevation, (b) Azimuthal

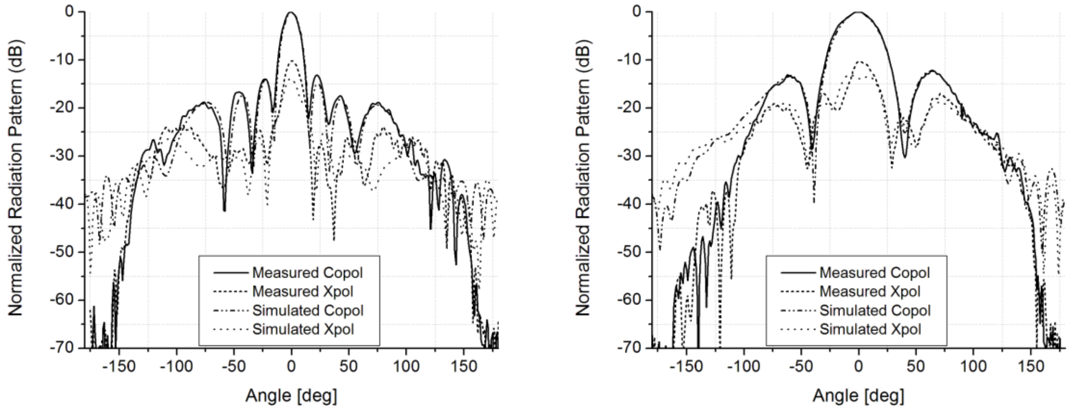

(a) (b)

Figure 4.72. Normalize pattern of +45º slant polarized antenna at 27 GHz, (a) Elevation, (b) Azimuthal

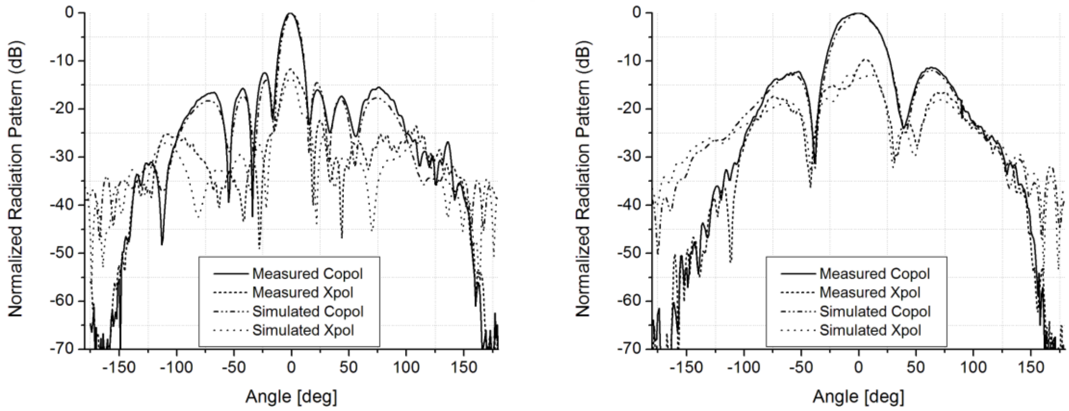

(a) (b)

Figure 4.73. Normalize pattern of +45º slant polarized antenna at 27.5 GHz, (a) Elevation, (b) Azimuthal

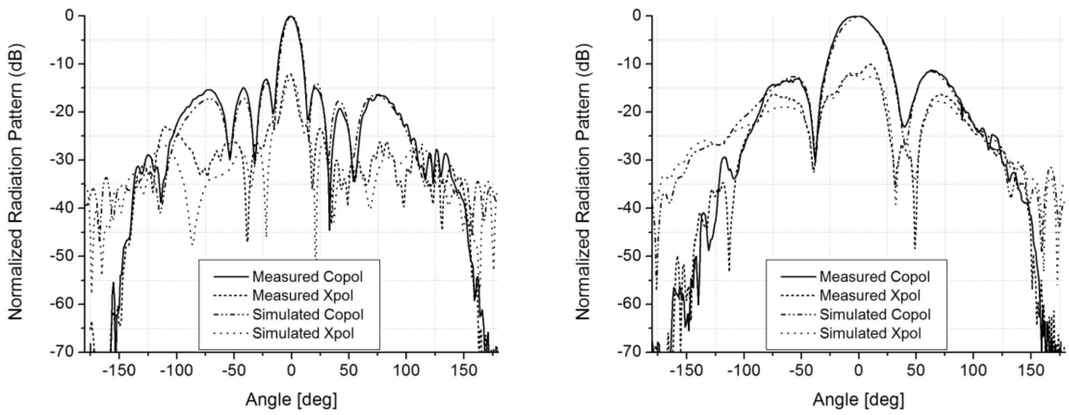

(a) (b)

Figure 4.74. Normalize pattern of +45º slant polarized antenna at 28 GHz, (a) Elevation, (b) Azimuthal

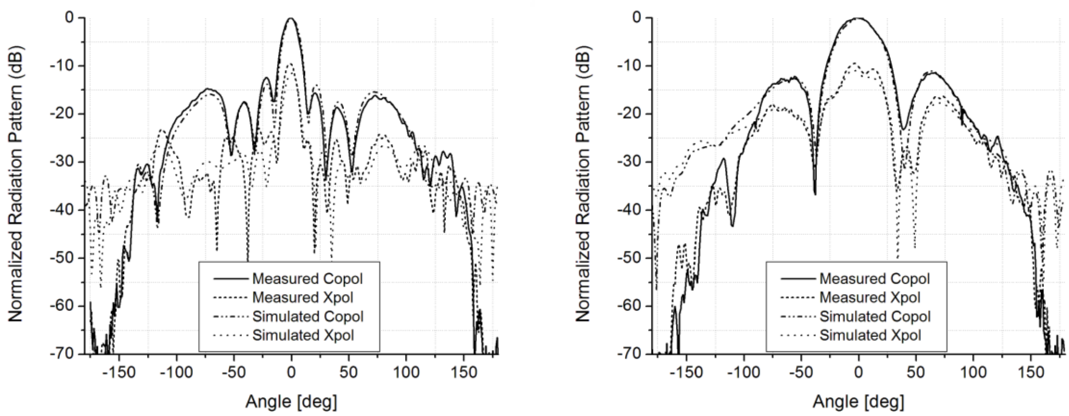

(a) (b)

Figure 4.75. Normalize pattern of +45º slant polarized antenna at 28.5 GHz, (a) Elevation, (b) Azimuthal

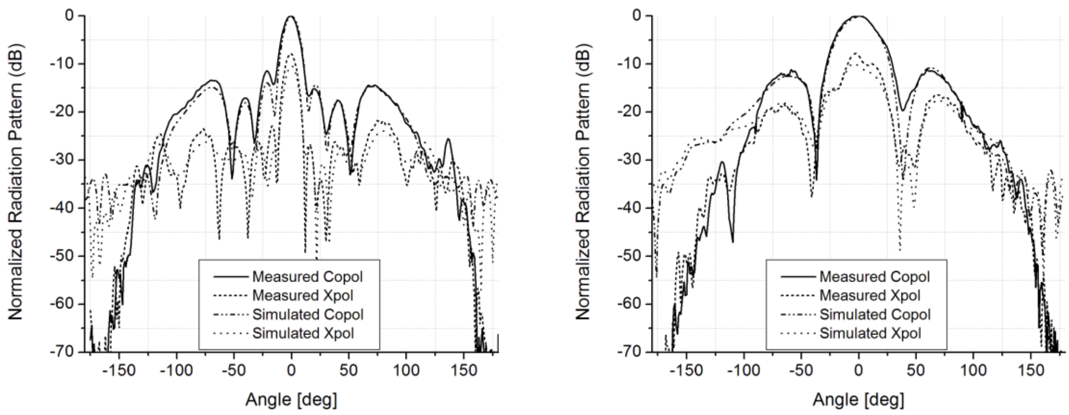

(a) (b)

Figure 4.76. Normalize pattern of +45º slant polarized antenna at 29 GHz, (a) Elevation, (b) Azimuthal

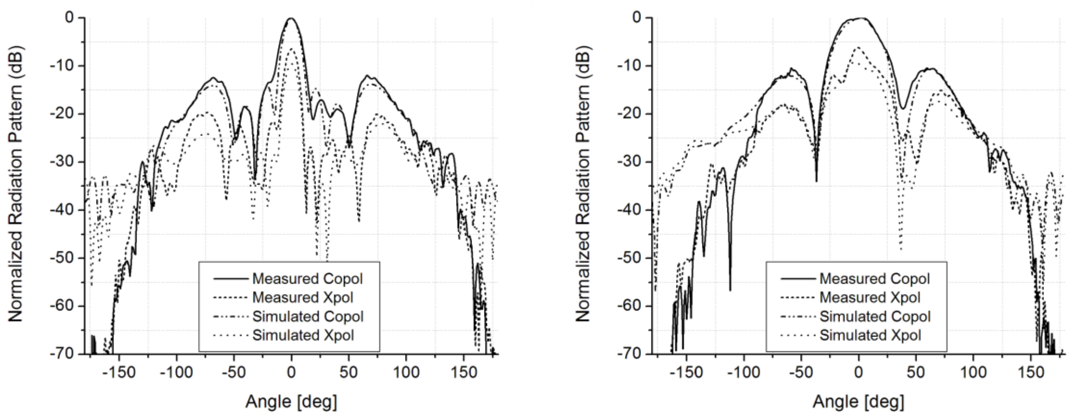

(a) (b)

Figure 4.77. Normalize pattern of +45º slant polarized antenna at 29.5 GHz, (a) Elevation, (b) Azimuthal

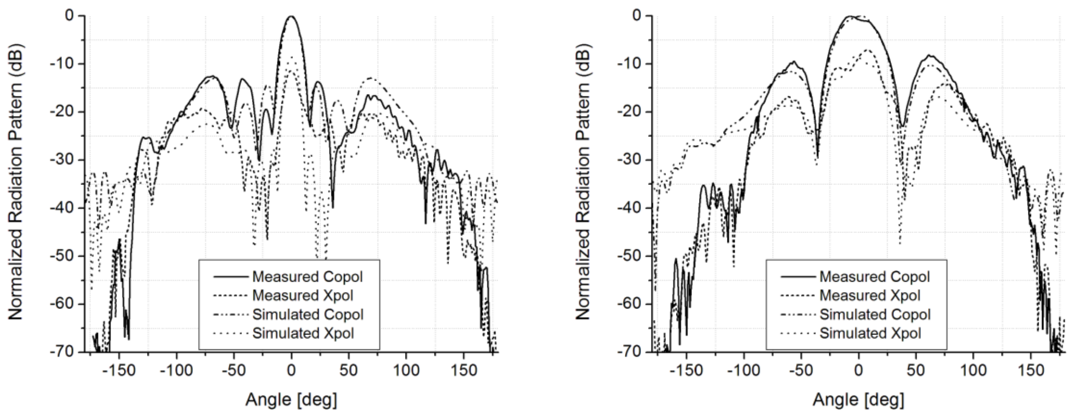

(a) (b)

Figure 4.78. Normalize pattern of +45º slant polarized antenna at 30 GHz, (a) Elevation, (b) Azimuthal

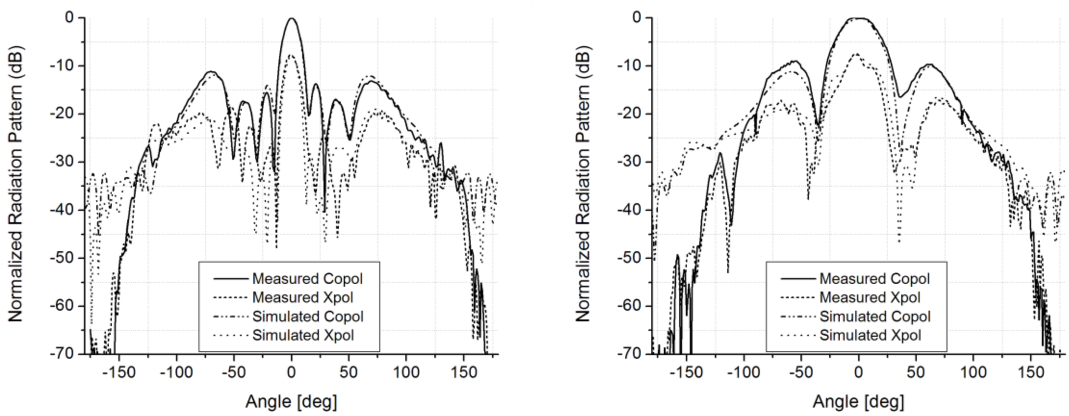

(a) (b)

Figure 4.79. Normalize pattern of +45º slant polarized antenna at 30.5 GHz, (a) Elevation, (b) Azimuthal

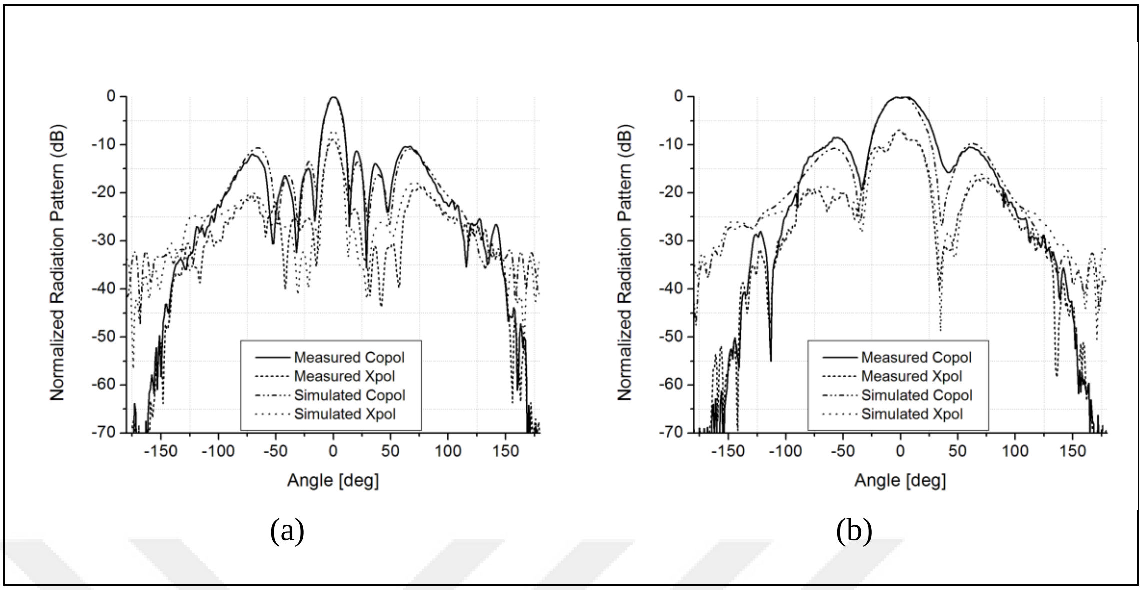

Figure 4.80. Normalize pattern of +45º slant polarized antenna at 31 GHz, (a) Elevation, (b) Azimuthal

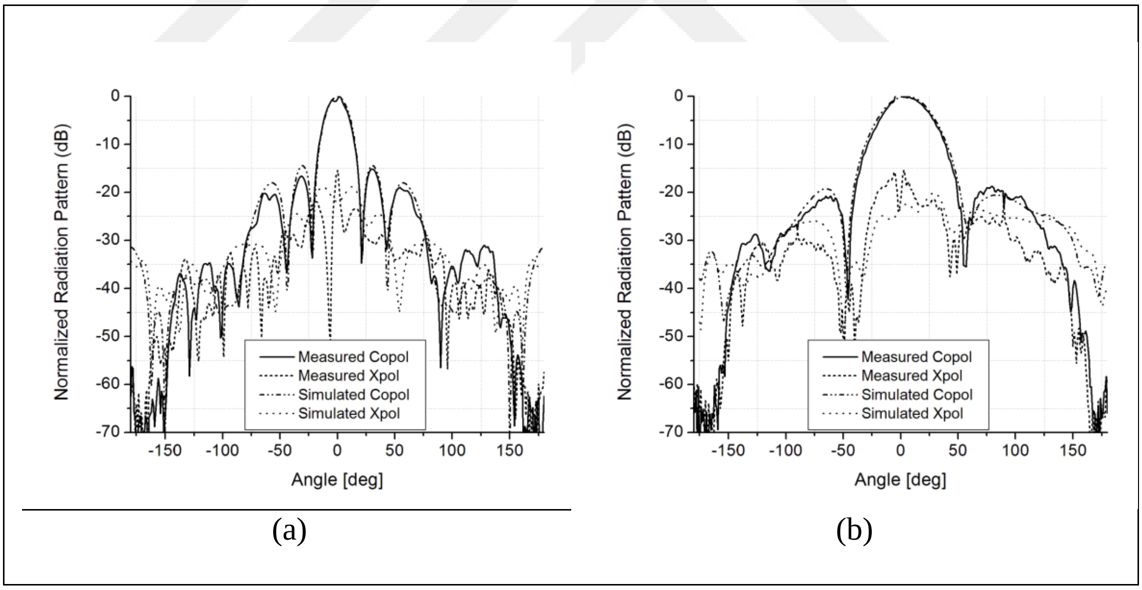

Figure 4.81. Normalize pattern of -45º slant polarized antenna at 22 GHz, (a) Elevation, (b) Azimuthal

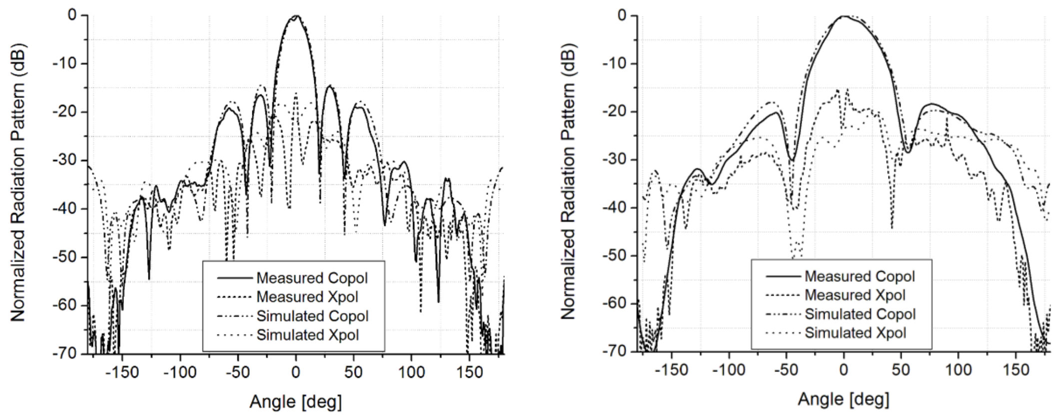

(a) (b)

Figure 4.82. Normalize pattern of -45º slant polarized antenna at 22.5 GHz, (a) Elevation, (b) Azimuthal

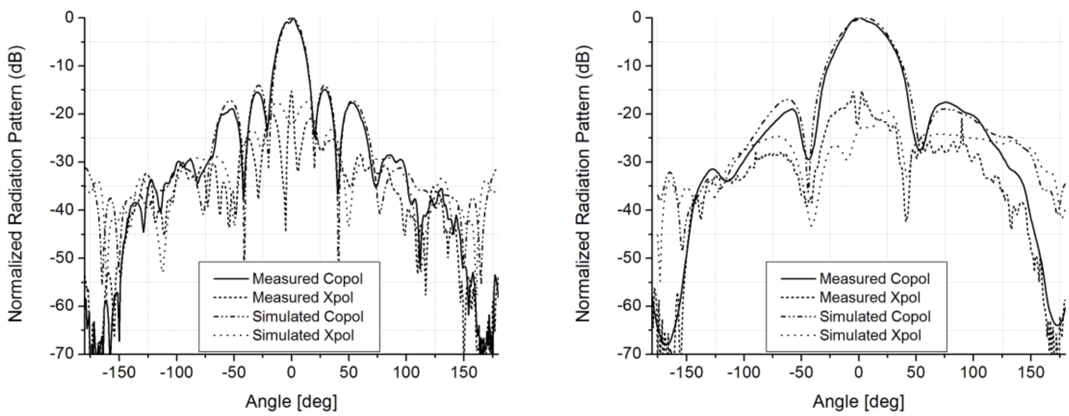

(a) (b)

Figure 4.83. Normalize pattern of -45º slant polarized antenna at 23 GHz, (a) Elevation, (b) Azimuthal

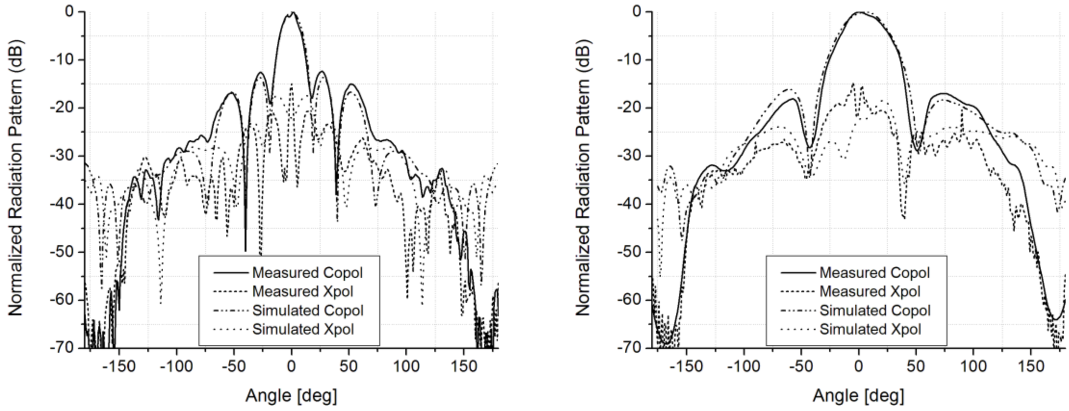

(a) (b)

Figure 4.84. Normalize pattern of -45º slant polarized antenna at 23.5 GHz, (a) Elevation, (b) Azimuthal

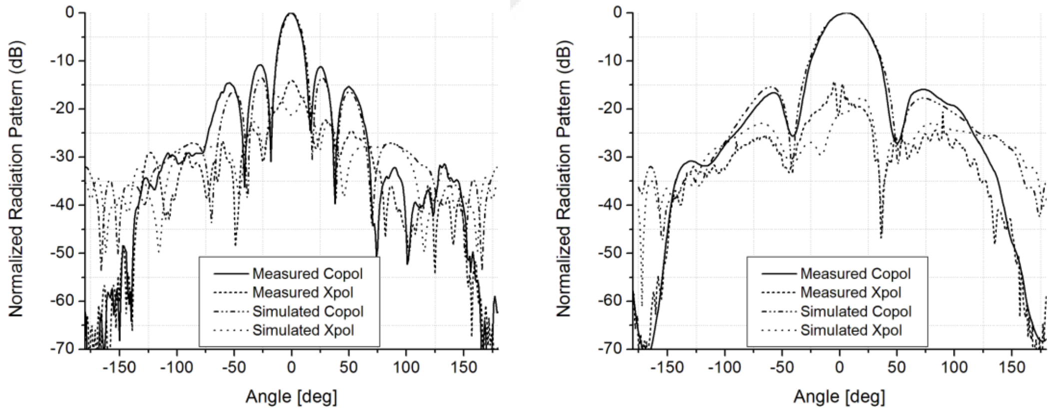

(a) (b)

Figure 4.85. Normalize pattern of -45º slant polarized antenna at 24 GHz, (a) Elevation, (b) Azimuthal

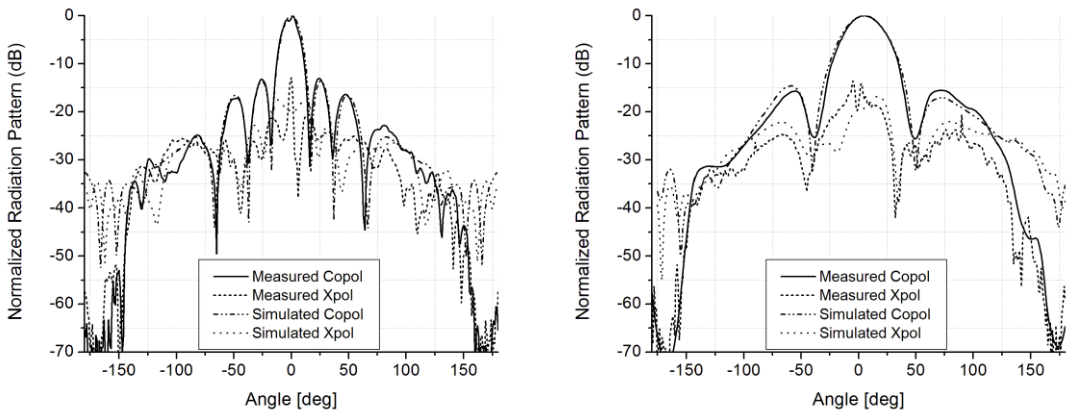

(a) (b)

Figure 4.86. Normalize pattern of -45º slant polarized antenna at 24.5 GHz, (a) Elevation, (b) Azimuthal

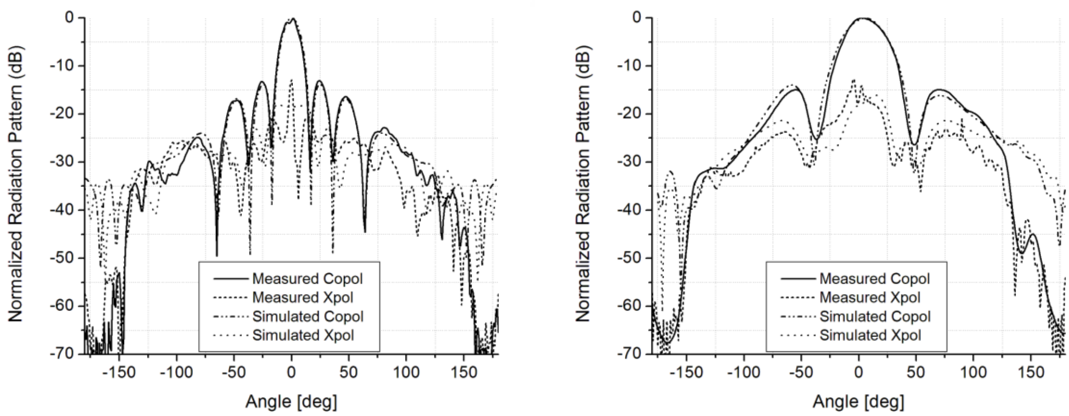

(a) (b)

Figure 4.87. Normalize pattern of -45º slant polarized antenna at 25 GHz, (a) Elevation, (b) Azimuthal

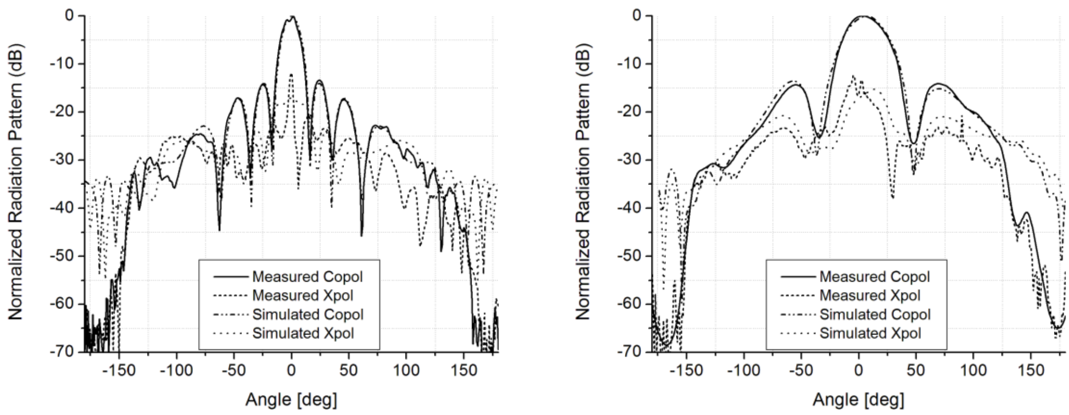

(a) (b)

Figure 4.88. Normalize pattern of -45º slant polarized antenna at 25.5 GHz, (a) Elevation, (b) Azimuthal

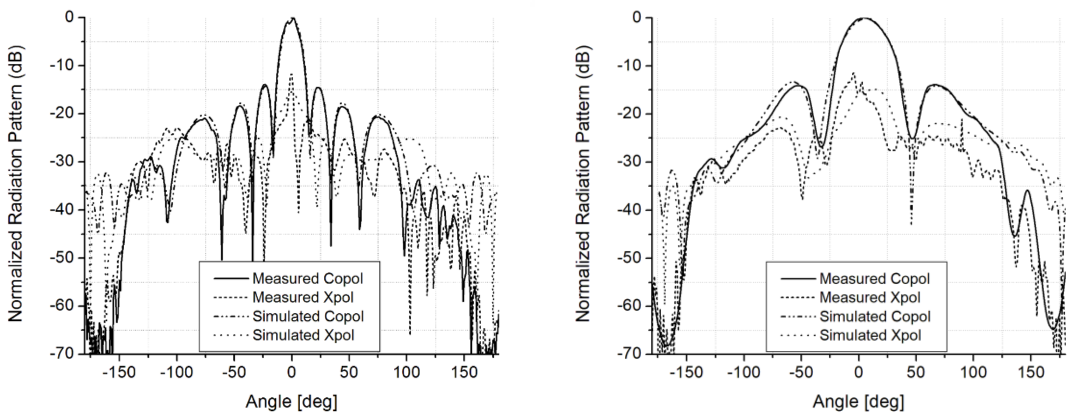

(a) (b)

Figure 4.89. Normalize pattern of -45º slant polarized antenna at 26 GHz, (a) Elevation, (b) Azimuthal

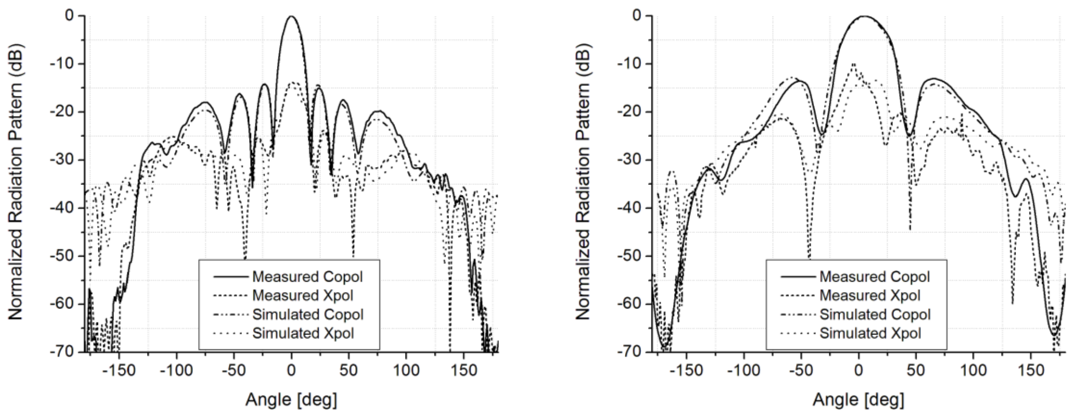

(a) (b)

Figure 4.90. Normalize pattern of -45º slant polarized antenna at 26.5 GHz, (a) Elevation, (b) Azimuthal

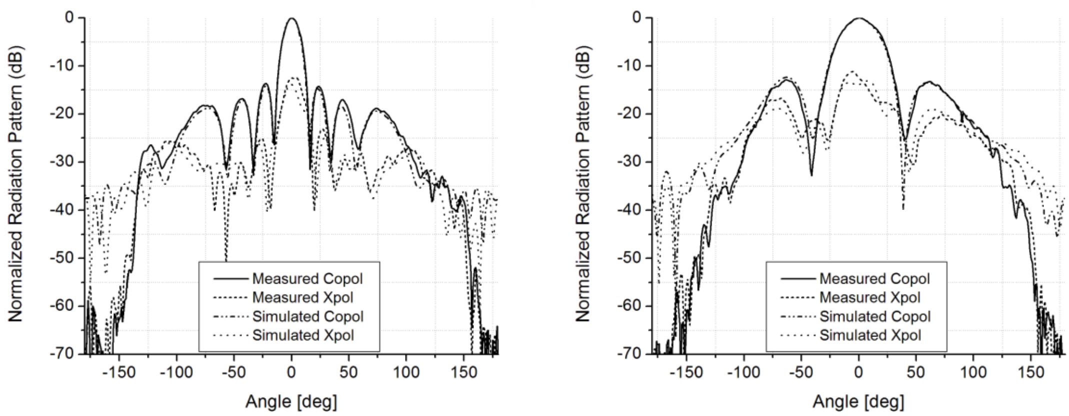

(a) (b)

Figure 4.91. Normalize pattern of -45º slant polarized antenna at 27 GHz, (a) Elevation, (b) Azimuthal

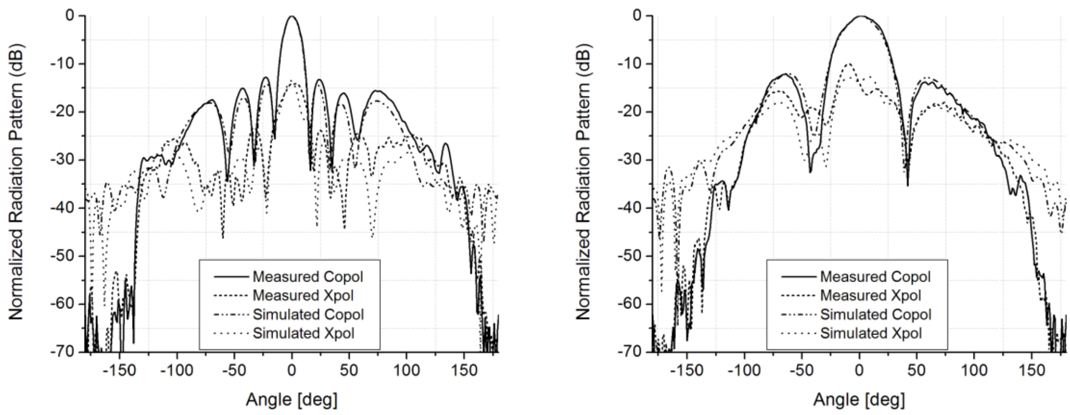

(a) (b)

Figure 4.92. Normalize pattern of -45º slant polarized antenna at 27.5 GHz, (a) Elevation, (b) Azimuthal

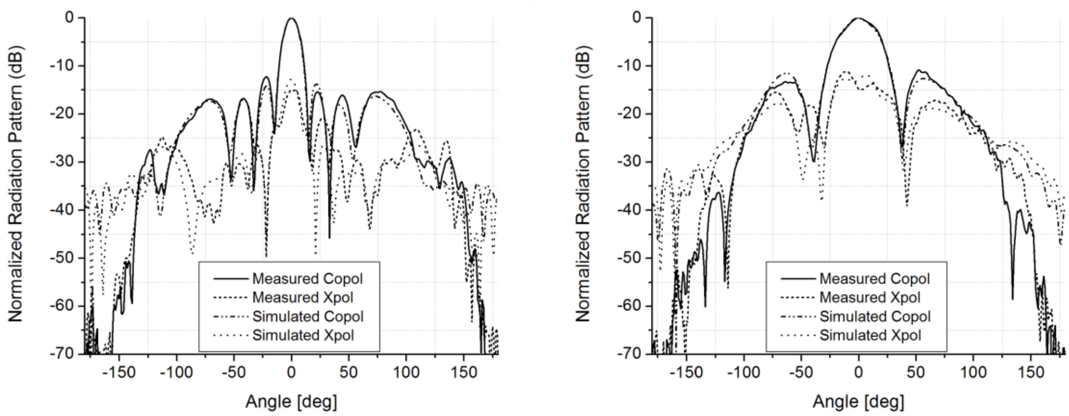

(a) (b)

Figure 4.93. Normalize pattern of -45º slant polarized antenna at 28 GHz, (a) Elevation, (b) Azimuthal

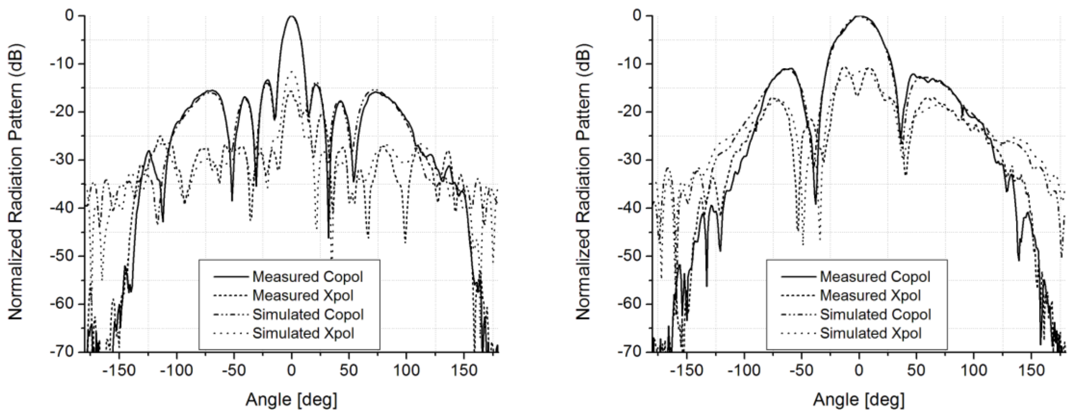

(a) (b)

Figure 4.94. Normalize pattern of -45º slant polarized antenna at 28.5 GHz, (a) Elevation, (b) Azimuthal

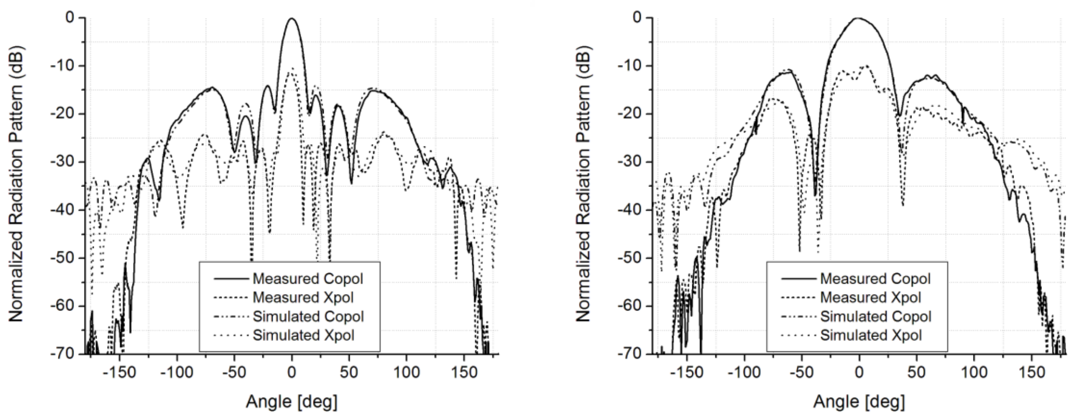

(a) (b)

Figure 4.95. Normalize pattern of -45º slant polarized antenna at 29.5 GHz, (a) Elevation, (b) Azimuthal

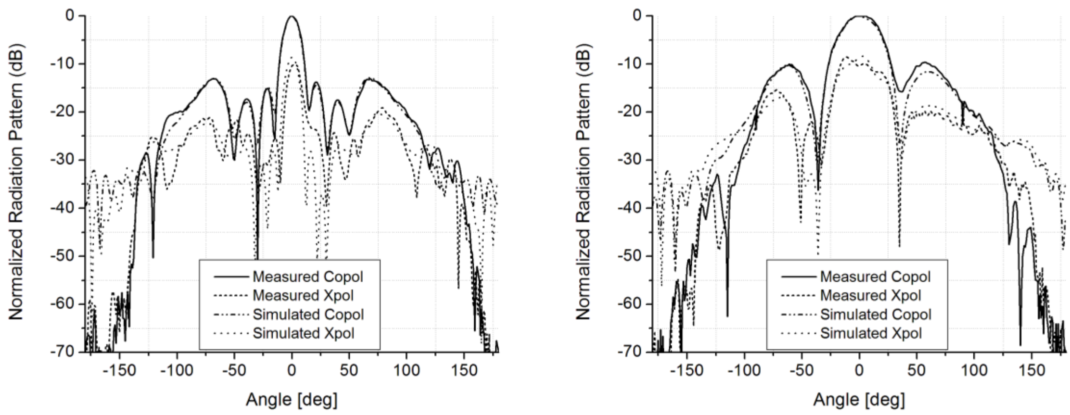

(a) (b)

Figure 4.96. Normalize pattern of -45º slant polarized antenna at 30 GHz, (a) Elevation, (b) Azimuthal

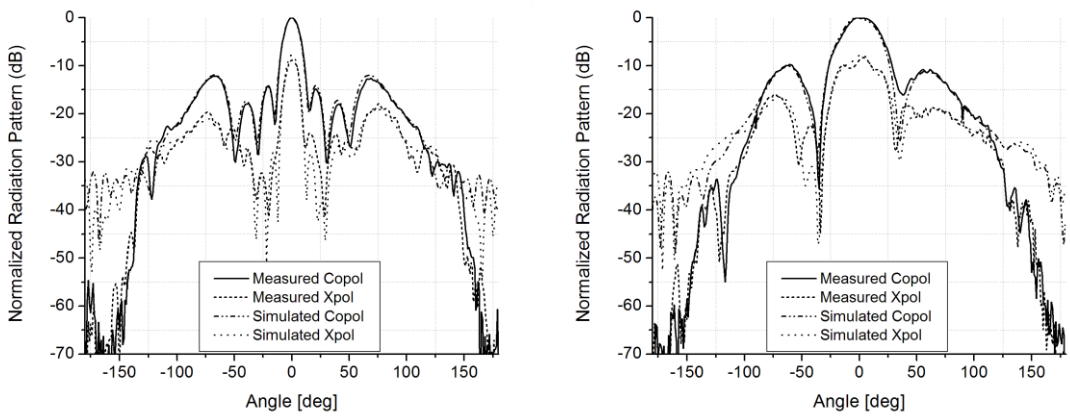

(a) (b)

Figure 4.97. Normalize pattern of -45º slant polarized antenna at 30.5 GHz, (a) Elevation, (b) Azimuthal

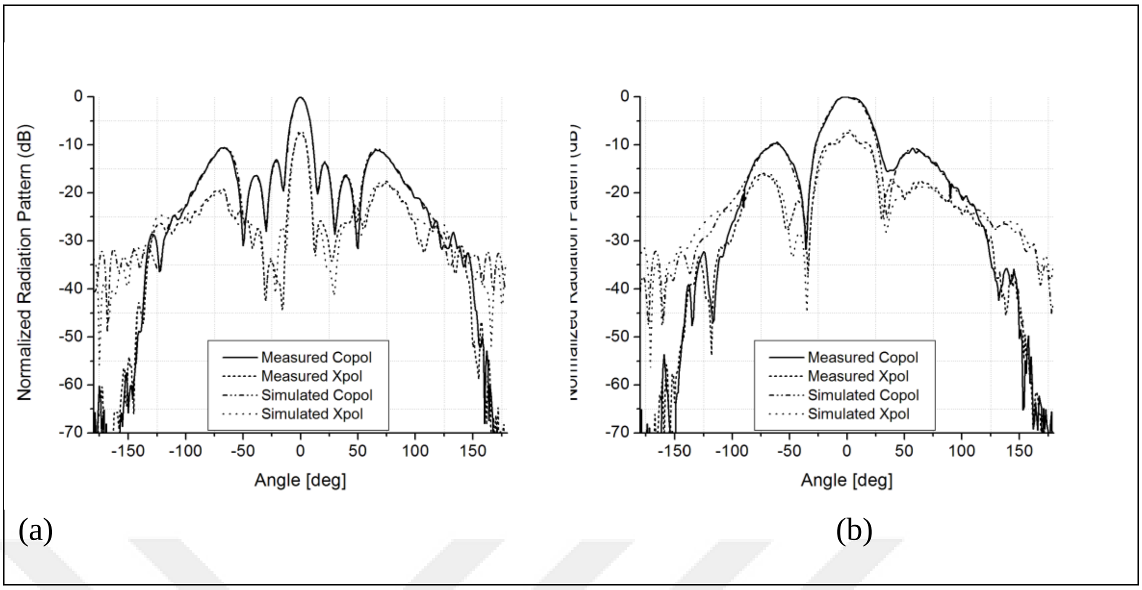

Figure 4.98. Normalize pattern of -45º slant polarized antenna at 31 GHz, (a) Elevation, (b) Azimuthal

5. CONCLUSION

In this study, low profile, wideband, low reflection coefficient, high gain +45° slant polarized 2 × 2 element slotted cavity back unit antenna fed by waveguide has been designed for 5G base stations in mmWave band. The antenna offers good directivity and flat gain because of the groove structure on its surface. Measured results of the fabricated unit antenna has 31.2% fractional impedance bandwidth ($|S_{11}|$<-14 dB, 22.6-31 GHz) and 14.5 dBi average boresight gain. The $|S_{11}|$ has been significantly decreased as a result of the hourglass structure utilized in the cavity transition from the waveguide. It also exhibits +/-0.5 dB gain flatness and +/- 2.5° azimuth beam width variation over the entire 5G mmWave band. Being made of metal, the antenna can handle high power and is simple to mount on any platform.

After unit element antenna, 2 × 4 element slotted array with +45° and -45° slant polarizations has been designed by using two unit antennas placed in the vertical plane and with center fed power network connected to them. Signal splitter consists of a T-junction that divides amplitude and phase equally over broadband. The simulated and measured gain, reflection coefficient and normalized radiation diagram results of both antennas were very close to each other. The gain was around 18 dBi and the $|S_{11}|$ value was below -15 dB between 23.5-30.3 GHz. While the azimuth HPBW value was close to that of the unit antenna (32°), the HPBW in elevation has been reduced to 17 degrees.

The purpose of producing two antennas with different polarizations was actually to combine them side by side and use them as a dual-polarized unit antenna. Although the transceiver antenna structure is very close to each other, an isolation of 30 dB has been achieved. This antenna structure can be used individually or as a part of the massive MIMO structure. With the BFN structure, it can be provided to radiate in the desired direction as a part of the MIMO system.

5.1. FUTURE WORK

The antenna structure with ±45° polarization can be multiplexed and placed around a circle to cover the whole azimuthal plane. The following figure shows the configuration created for eight transceiver antenna structures. However, it requires 110 GB RAM to solve this in CST simulation. These antennas can be connected to a BFN for practical applications.

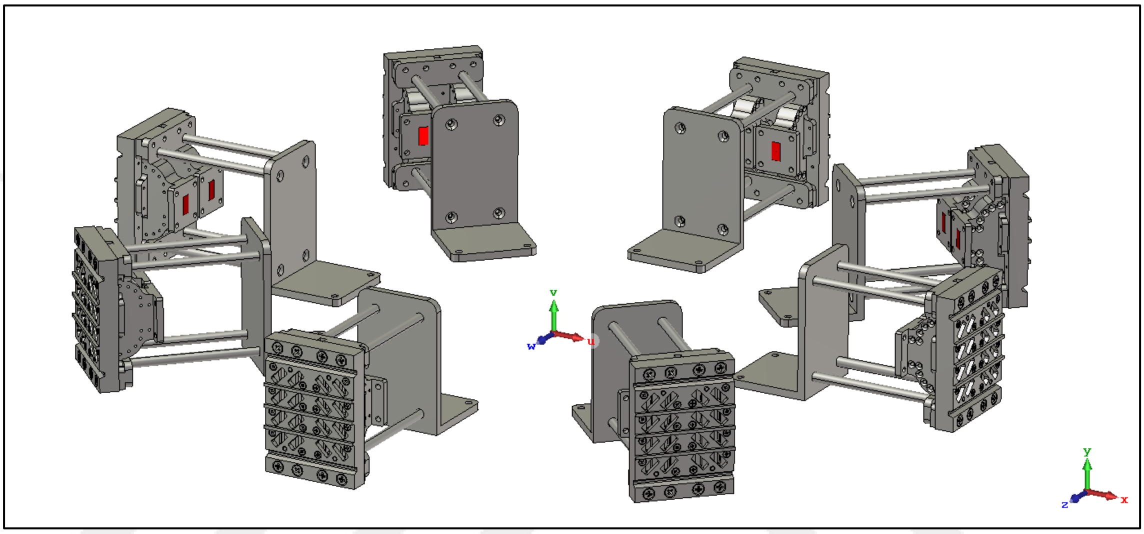

Figure 5.1. Transceiver antenna structures placed in the azimuth plane

REFERENCES

1. Forouzan BA. *Data Communication and Networking. 3rd/4th Edition*, Tata McGraw; 2008.

2. Deutsche Telekom, https://www.telekom.com

3. Kodnoeih MRD. Development of Next-Generation 5G Directive Antennas at Millimeter Waves. Ph.D Thesis, Universite De Nantes, 2018

4. Rappaport TS. Millimeter Wave Mobile Communications for 5G Cellular: It Will Work! *IEEE Access*. 2013; 1: 335-349.

5. Holma H, Toskala A, Nakamura T. *5G Technology: 3GPP New Radio. 1st Edition.* West Sussex UK: John Wiley & Sons; 2020.

6. Quan X, Li R, Fan Y and Anagnostou DE. Analysis and Design of a 450 Slant-Polarized Omnidirectional Antenna. *IEEE Trans. Antennas Propagat.* Jan. 2014; 62(1): 86-93.

7. You Y, Lu Y, Skaik T, Wang Y, Huang J. Millimeter-Wave 45° Linearly Polarized Corporate-Fed Slot Array Antenna With Low Profile and Reduced Complexity. *IEEE Trans. Antennas Propagat.* 2021.

8. Liu X, Zhang W, Hao D, and Liu Y. Broadband Surface-Mount Dipole Antenna Array Using Highly Isolated via Fence for 5G Millimeter-Wave Applications. *Progress In Electromagnetics Research Letters*. 2021; 100: 27-34.

9. Yang Q. Cavity-Backed Slot-Coupled Patch Antenna Array With Dual Slant Polarization for Millimeter-Wave Base Station Applications. *IEEE Trans. Antennas Propagat.* March 2021; 69(3): 1404-1413.

10. Li Y and Luk K. 60-GHz Substrate Integrated Waveguide Fed Cavity-Backed Aperture-Coupled Microstrip Patch Antenna Arrays. *IEEE Trans. Antennas Propagat.* March 2015; 63(3): 1075-1085.

11. Asci Y and Yegin K. Additively Manufactured High Gain Cavity Backed Ku-Band Slot Antenna. *AEU International Journal of Electronics and Communications,* April 2021.

12. Zhang L. Wideband 45° Linearly Polarized Slot Array Antenna Based on Gap Waveguide Technology for 5G Millimeter-Wave Applications. *IEEE Antennas and Wireless Propagat. Letters,* July 2021; 20(7): 1259-1263.

13. Bilgiç M and Yeğin K. Design of L-plate proximity fed base station antenna element," *International Journal of Microwave and Wireless Technologies*, 2015; 7(2): 205-208.

14. Balanis AB. *Antenna Theory*. John Wiley & Sons, 2005

15. Chen ZN and Luk KM. Antennas for Base Stations in Wireless Communications. *McGraw-Hill Professional*, 2009.

16. www.cst.com, CST Microwave Studio, 2017 (Last Accessed 25/05/2022)

17. Levine E, Malamud G, Shtrikman S, and Treves D. A study of microstrip array antennas with the feed network. *IEEE Trans. Antennas Propag.* Apr. 1989; 37(4): 426-434.

18. Gueye MB. Définition, Conception et Réalisation d'une Antenne Compacte en Ondes Millimétriques (71GHz -86 GHz) pour des Liaisons Haut Débit Numérique. Ph.D Thesis, Université Paris Ouest Nanterre La Defense, 2014

19. Kimura Y, Takahashi M and Haneishi M. 76 GHz alternating-phase fed single-layer slotted waveguide arrays with maximum gain and sidelobe suppression. *Antennas and Propagation Society International Symposium*. Jun. 2005; 3: 1042-1045.

20. Park S, Tsunemitsu Y, Hirokawa J, and Ando M. Center feed single layer slotted waveguide array. *IEEE Trans. Antennas Propag.* May 2006; 54(5): 1474-1480.

21. Miura Y, Hirokawa J, Ando M, Shibuya Y, and Yoshida G. Doublelayer full-corporate-feed hollow-waveguide slot array antenna in the 60- GHz Band. *IEEE Trans. Antennas Propag.* Aug. 2011; 59(8): 2844-2851.

22. Rajo-Iglesias E, Ferrando-Rocher M and Zaman A U. Gap Waveguide Technology for Millimeter-Wave Antenna Systems. *IEEE Communications Magazine,* July 2018; 56(7): 14-20.

23. Fujino T, Hirokawa J, Ando M, Seki T, Sasaki K, Oshima I. Design and Fabrication of a Dual-polarized Corporate-feed Waveguide 32x32-slot Array Antenna with an Orthomode Transducer for 40 GHz Band. *2016 International Symposium on Antennas and Propagation*. Oct. 2016: 24-28

24. Xu X, Zhang M, Hirokawa J and Ando M. E-Band Plate-Laminated Waveguide Filters and Their Integration Into a Corporate-Feed Slot Array Antenna With Diffusion Bonding Technology. *IEEE Transactions on Microwave Theory and Techniques*. Nov. 2016; 64(11): 3592-3603.

25. Vosoogh A, Kildal P, and Vassilev V. A Multi-Layer Gap Waveguide Array Antenna Suitable for Manufactured by Die-Sink EDM. *10th European Conference on Antennas and Propagation (EUCAP)*. 2016.

26. Chen R, Zhu L, Lin J, Wong S, Lin Y, Zhang L, He Y. High Efficiency and Wideband Dual-Resonance Full-Metal Cavity-Backed Slot Antenna Array. *IEEE Antennas and Wireless Propag. Letters.* Aug. 2020; 19(8).

27. Farahbakhsh A, Zarifi D, and Zaman AU. 60-GHz Groove Gap Waveguide Based Wideband H-Plane Power Dividers and Transitions: For Use in High-Gain Slot Array Antenna. *IEEE Trans. Microwave Theory and Techniques*. Nov. 2017; 65(11): 4111–4121.

28. Farahbakhsh A, Zarifi D, and Zaman AU. A mmWave Wideband Slot Array Antenna Based on Ridge Gap Waveguide With 30% Bandwidth. *IEEE Transactions on Antennas and Propagation*. Feb. 2018; 66(2): 1008-1013.

29. Zaman AU, Kildal P. Wide-Band Slot Antenna Arrays With Single-Layer Corporate-Feed Network in Ridge Gap Waveguide Technology. *IEEE Transactions on Antennas and Propagation*. June 2014; 62(6): 2992-3001.

30. Jiménez Sáez A, Valero-Nogueira A, Herranz JI and Bernardo B. Single-Layer Cavity-Backed Slot Array Fed by Groove Gap Waveguide. *IEEE Antennas and Wireless Propagation Letters*. 2016; 15: 1402-1405.

31. Sehm T, Lehto A and Raisanen AV. A large planar 39-GHz antenna array of waveguide-fed horns. *IEEE Trans. Antennas Propag*. 1998; 46(8): 1189–1193.

32. Hirokawa J, Tomura T, Miura Y, Zhang M, and Ando M. Platelaminated-waveguide corporate-feed slot array antennas with a polarization conversion layer. *2011 IEEE MTT-S International Microwave Workshop Series on Millimeter Wave Integration Technologies*, Sitges. 2011: 29-32.

33. Lee B, Jung K, and Yang S. High-efficiency planar slot array antenna with a single waveguide-fed cavity-backed subarray. *Microw. Opt. Technol. Lett.* 2004; 43(3): 228–231.

34. Cheng DK., *Fundamentals of Engineering Electromagnetics (1 st ed.)*, Addison-Wesley, 1993.

35. Sorrentino R and Bianchi G, *Microwave and RF Engineering*, John Wiley & Sons, 2010.

36. Ishimaru A. *Electromagnetic Wave Propagation, Radiation, and Scattering*, Prentice Hall, 1991: 173.

37. Nikolova NK., *Modern Antennas in Wireless Telecommunications*, McMaster University, 2020; 17.

38. Yang Q. Cavity-Backed Slot-Coupled Patch Antenna Array With Dual Slant Polarization for Millimeter-Wave Base Station Applications. *IEEE Transactions on Antennas and Propagation*. March 2021; 69(3): 1404-1413.

39. Abdallah MS, Wang Y, Abdel-Wahab WM and Safavi-Naeini S. Design and Optimization of SIW Center-Fed Series Rectangular Dielectric Resonator Antenna Array With 45° Linear Polarization. *IEEE Transactions on Antennas and Propagation.* Jan. 2018; 66(1): 23-31.

40. Sorkherizi MS, Dadgarpour A, and Kishk AA. Planar High-Efficiency Antenna Array Using New Printed Ridge Gap Waveguide Technology. *IEEE Trans. Antennas Propag.* Jul. 2017; 65(7): 3772–3776.

41. Shaw M, Choukiker YK. Omnidirectional conformal microstrip array antenna with electronically beam switching capabilities for 5G applications. *AEU - International Journal of Electronics and Communications*. 2022; 151

42. Aghoutane B, Das S, Ghzaoui ME, Madhav BTP, Faylali HE. A novel dual band high gain 4-port millimeter wave MIMO antenna array for 28/37 GHz 5G applications. *AEU - International Journal of Electronics and Communications*. 2022; 145.

43. Sifat SM, Ali MMM, Shams SI, and Sebak AR. High Gain Bow-Tie Slot Antenna Array Loaded With Grooves Based On Printed Ridge Gap Waveguide Technology. *IEEE Access.* 2019; 7: 36177–36185.

44. Yong WY, Haddadi A, Emanuelsson T, and Glazunov AA. A Bandwidth-Enhanced Cavity-Backed Slot Array Antenna for mmWave Fixed-Beam Applications. *IEEE Antennas and Wireless Propag. Letters*. Nov. 2020; 19(11): 1924-1928.

45. Lee WCY. Effects on correlation between two mobile radio base station antennas. *IEEE Trans. Commun*. Nov. 1973; 21: 1214-1224.

46. Sang-Bin and Zysman GI. Results of suburban base station spatial diversity measurements in the UHF band. IEEE Trans. Commun. Oct. 1974; 22: 1630-1636.

47. Lee WCY and Yeh YS. Polarization diversity system for mobile radio. *IEEE Trans. Commun.* Oct. 1972; 20: 912-922.

48. Brennan DG. Linear diversity combining techniques. *Proc. IRE*. June 1959: 1075-1102.

49. Sakamoto M, Kozono S, and Hattori T. Basic study on portable radio telephone design. *IEEE Veh. Technol. Conf.,* May 1982: 279-284.

50. Kozono S, Tsuruhara T, Sakatamoto M. Base Station Polarization Diversity Reception for Mobile Radio. *IEEE Transactions on Vech. Technology*. Nov. 1984; 33(4)